

Dissertation

zur Erlangung des Doktorgrades der Fakultät für Chemie und
Pharmazie der Ludwig-Maximilians-Universität München



A proteomic and genomic approach to in vivo chemoresistance
using spheroid and xenograft cancer models

vorgelegt von

Lilja Thoenes

aus Starnberg

2009

Erklärung

Diese Dissertation wurde im Sinne von § 13 Abs. 3 der Promotionsordnung vom 29. Januar 1998 von Herrn Prof. Dr. Ernst Wagner betreut.

Ehrenwörtliche Versicherung

Diese Dissertation wurde selbständig, ohne unerlaubte Hilfe erarbeitet.

München, am 23.6.2009

.....
(Lilja Thoenes)

Dissertation eingereicht am 23.6.2009

1. Gutachter: Prof Dr. Ernst Wagner
2. Gutachter: Prof Dr. Christian Wahl-Schott

Mündliche Prüfung am 21.07.2009

Table of Contents

1. Introduction.....	1
1.1. Colon cancer	1
1.1.1. Low passage colon cancer cell lines	1
1.1.2. Threedimensional culture systems	1
1.1.3. Proteomic profiling of multicellular spheroids of low passage colon carcinoma cells	2
1.1.4. Chemoresistance to 5-fluorouracil in colon cancer	4
1.1.5. Chemoresistance of low passage colon carcinoma cells towards 5-fluorouracil treatment in vitro	4
1.2. Prostate Cancer	6
1.2.1. Metronomic Cyclophosphamide Therapy.....	6
1.2.2. Chemoresistance to antiangiogenic therapy	7
1.2.3. Proteomics and genomics in drug resistance	9
1.2.4. In vivo resistance of prostate cancer xenografts towards metronomic cyclophosphamide therapy.....	10
1.3. Aim of this thesis	12
2. Materials and Methods.....	14
2.1. Cell Biology Methods.....	14
2.1.1. Cell culture	14
2.1.2. Multicellular spheroid culture	14
2.1.3. Oxygen and serum deprivation.....	15
2.1.4. In vitro chemotherapy	15
2.1.5. Cell viability, Apoptosis and Proliferation	15
2.1.6. TUNEL Assay	16
2.1.7. Transfections	16
2.1.8. Immunocytochemistry.....	17
2.1.9. Flow cytometry and microscopy	18
2.2. Protein analysis	19
2.2.1. Bradford Assay	19
2.2.2. Westernblot.....	19
2.2.3. 2D-DIGE electrophoresis and mass spectrometry	20
2.3. RNA analysis.....	23

2.3.1.	RNA-extraction and concentration measurement for RT-PCR	23
2.3.2.	RT-PCR	23
2.3.3.	Micro Array Analysis	24
2.4.	Ex vivo/ in vivo experiments	27
2.4.1.	Animals	27
2.4.2.	Tumor models	27
2.4.3.	Tumor Measurement	27
2.4.4.	Chemotherapy	28
2.4.5.	Tumor Histology	28
2.4.6.	Isolation of tumor/organs	29
2.4.7.	Reisolation of tumor cells	29
3.	Results	31
3.1.	Colon cancer	31
3.1.1.	Fragmentation of lamin A/C in multicellular spheroid cultures of low passage colon cancer cells	31
3.1.2.	5-FU chemoresistance in low passage colon cancer cells in vitro	35
3.2.	Chemoresistance in metronomic cyclophosphamide therapy of prostate cancer xenografts: an in vivo chemoresistance	39
3.2.1.	Generation of an appropriate in vivo passaged control	39
3.2.2.	Drug efflux activity of reisolated PC3 cells	40
3.2.3.	Proliferation of reisolated cells under hypoxic conditions	41
3.2.4.	Reimplantation of reisolated PC3 cells	41
3.2.5.	Expression of vascular markers and functionality of tumor blood flow in reimplanted tumors	43
3.2.6.	2D-DIGE analysis of reisolated in vivo resistant PC3-D3 and PC3-D4 cells versus PC3-wt cells	44
3.2.7.	Validation of potential protein candidates	50
3.2.8.	Microarray analysis of chemoresistant PC3 xenografts compared to non resistant control tumors	57
4.	Discussion	73
4.1.	Colon cancer	73
4.1.1.	Fragmentation of Lamin A/C in multicellular spheroid of low-passage colon carcinoma cells	73
4.1.2.	Chemoresistance in low passage colon cancer cells	76

4.2. In vivo chemoresistance of prostate cancer in metronomic cyclophosphamide therapy.....	78
4.2.1. A non classical mechanism of chemoresistance in vivo	78
4.2.2. Proteomics and Genomics: two complementary approaches to in vivo resistance	80
5. Summary	92
6. Appendix.....	95
6.1. Tables.....	95
6.2. Abbreviations.....	100
6.3. Publications	104
6.3.1. Original Papers	104
6.3.2. Review Article	104
6.3.3. Poster Presentations	104
7. References	105
8. Acknowledgements	122
9. Curriculum Vitae	125

für Dodo
und
meine Eltern

1. Introduction

1.1. *Colon cancer*

Colorectal cancer is the third leading cause of cancer-related deaths in the United States when men and women are considered separately, and the second leading cause when both sexes are combined. It is expected to cause about 49,960 deaths (24,260 men and 25,700 women) during 2008¹. Despite intensive ongoing research patients show rapid progression and chemoresistance stays one of the major hindrances for successful therapy.

1.1.1. **Low passage colon cancer cell lines**

The appropriate model system is a key implement in cancer research. As cancer is a complex system and an attribute of cancer cells is their genetic instability, in vitro cancer research often does not represent sufficiently the in vivo conditions. In contrast, tissue culture models of colon cancer often do not fulfill all requirements for efficient in vitro research and working with primary cultures is mostly limited by generation of sufficient material for larger screening experiments or e.g. proteomic approaches². Low passage cancer cell lines recapitulate properties of original tumor cells more closely than commonly used standard cell lines that experience artificial selection processes and mutations over years of passaging. Therefore eight human low passage colon cancer cell lines originating directly from the clinic have been generated in the lab of Prof. Wagner. These cells still closely resemble the phenotypes of their corresponding tumor cells and have been extensively characterized concerning their morphology, different cellular marker expressions and their molecular caryotype³.

1.1.2. **Threedimensional culture systems**

Even if low passage cancer cell lines provide already a better in vitro model than classical well established cancer cell lines, loss of tissue-specific properties is common for cells grown in twodimensional (2D) monolayer cultures. 2D in vitro cultures do not reflect aspects of cell proliferation, differentiation and cell environment, i.e. cell-cell contacts and different growth areas of tumors in vivo concerning microenvironmental properties. However, these parameters as well as paracrine and autocrine communication play an important role in cancer therapy of

solid tumors and the failure of many therapeutic approaches is due to structural properties of tumors in vivo. Threedimensional (3D) cultures are widely used as avascular tumor models for metastasis, invasion and for therapeutic screening. In the past 10 years a variety of 3D in vitro culture systems has been established^{4;5}.

One possibility to model 3D cell growth in vitro is the generation of multicellular spheroids (MCS)^{6;7}. Similar to tissue morphogenesis in vivo, complex cell adhesion and differentiation processes contribute to the formation of spheroids. Especially adhesion factors such as integrins and cadherins play a pivotal role in formation of loose aggregates and their maturation towards compact spheroids⁸. Regarding transport of nutrients, oxygen or waste and penetration of therapeutic agents, MCS can simulate the situation of avascular tumors with diffusion limitation of about 150-200 μm ⁹. MCS with a diameter > 500 μm commonly displays a layer-like structure comprising a necrotic core, surrounded by a layer of quiescent cells which is finally surrounded by a proliferating rim¹⁰. Several cell types can recapitulate their polarization and form differentiated tissue like structures e.g. lumen containing spheres¹¹ and adaptation processes of tumor cells to low oxygen and nutrition supply as well as acidic pH can be observed in inner layers of many spheroids^{12;13}. MCS can be generated by different methods often based on prevention of cell adhesion to the culture surface or by individualizing of cells. Popular techniques include the hanging drop method, surface coating with non-adhesive material (liquid overlay technique), spinner flask cultivation or monoclonal growth in agarose⁴.

1.1.3. Proteomic profiling of multicellular spheroids of low passage colon carcinoma cells

Lars Gaedtker established spheroid cultures of the low passage colon cancer cell line COGA-5 and COGA-12 by liquid overlay technique⁶ in his PhD work (**Figure 1**).

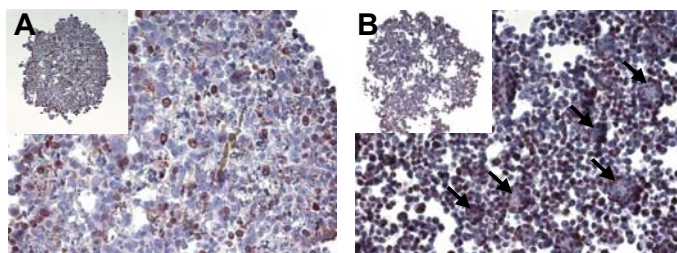


Figure 1: Multicellular spheroids of (A) COGA-5 and (B) COGA-12 cells¹⁴.

He analyzed the proteome of both 3D cultures versus their corresponding 2D cultures. 2D gel electrophoresis (2DE) followed by peptide mass fingerprinting

identified three differently expressed proteins in COGA-5 spheroids (acidic calponin, hydroxyprostaglandin dehydrogenase, lamin A/C) and two in COGA-12 partly compact aggregates (two isoelectric variants of acidic ribosomal protein P0) compared to the respective monolayer cultures (**Table 1**). The lamin A/C spot showed a lower molecular weight in the 2D gel (30 kDa) than expected for full length lamin (**Figure 2**). Purpose of the current work was to clarify the role of lamin A/C fragmentation in MSC of low passage colon cancer cells.

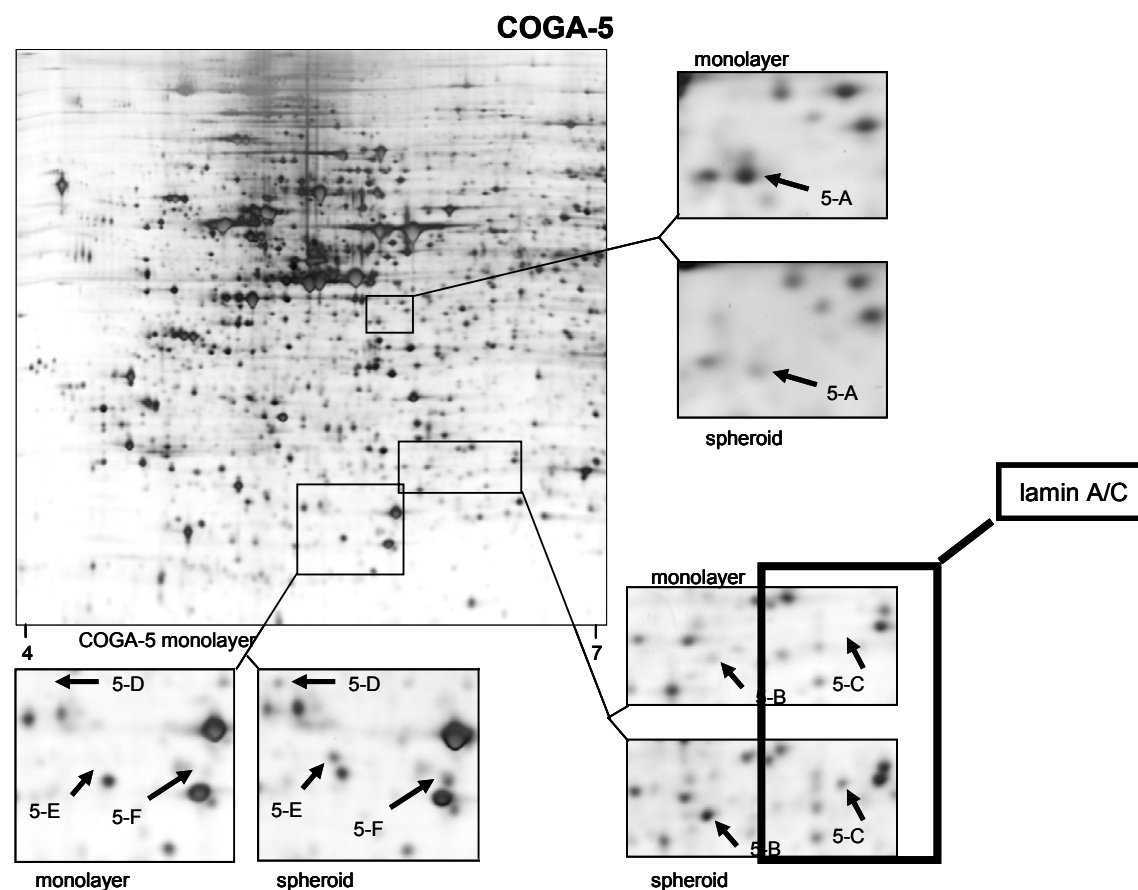


Figure 2: 2D gel of multicellular spheroids versus monolayer cultures of COGA-5 cells. Differentially regulated spots are marked by an arrow. The spot representing the fragmented lamin A/C is highlighted¹⁵.

Spot no.	Identified protein	protein regulation
5-A	Acidic calponin	down
5-B	15-hydroxyprostaglandin dehydrogenase	up
5-C	Lamin A/C	up
12-A	Acidic ribosomal protein P0	up
12-B	Acidic ribosomal protein P0	up

Table 1: Proteins differentially expressed between multicellular spheroids of cell lines COGA-5, COGA-5L, COGA-12 and corresponding monolayers¹⁵

1.1.4. Chemoresistance to 5-fluorouracil in colon cancer

5-Fluorouracil (5-FU)-based chemotherapy regimens are still the standard treatment for colon cancer in both adjuvant and palliative disease settings¹⁶. 5-FU is a fluorinated pyrimidine that acts primarily through inhibition of thymidylate synthase (TS), which is the rate-limiting enzyme in pyrimidine nucleotide synthesis¹⁷. As a pyrimidine analogue, 5-FU is converted to fluorodeoxyuridine monophosphate (FdUMP), which builds a stable complex with TS, and thus inhibits deoxythymidine monophosphate (dTMP) production¹⁸. As dTMP is essential for DNA replication and repair, its depletion finally induces cell cycle arrest and apoptosis^{19;20}. Despite inhibition of TS, 5-FU can also be miss-incorporated into RNA and DNA instead of the nucleotides uracil or thymidine. Following accumulation of 5-FU in the genome causes cytotoxicity in mammalian cells²¹. Recent studies have demonstrated that also RNA-based effects of 5-FU, especially in rRNA maturation and mRNA splicing play a role in the cytotoxic effect of the drug^{22;23}.

Major hindrance in successful chemotherapy is the occurrence of drug resistance. This is responsible for treatment failure in >90% of patients with metastatic cancer²⁴. Overcoming drug resistance is one of the main challenges in cancer research today. Meanwhile, understanding the mechanisms by which tumors become resistant to 5-FU is an essential step towards predicting or overcoming the resistance. Several mechanisms such as high-level expression of TS²⁵, increased activity of deoxyuridine triphosphatase²⁶, methylation of the MLH1 gene²⁷, and overexpression of Bcl-2, Bcl-XL, and Mcl-1 proteins have all been described to be possible mediators of 5-FU resistance²⁸. This leads to the suggestion that resistance is a complex process often composed of multiple pathways playing together.

Therefore appropriate cancer models and more global approaches such as microarray and proteomics techniques might lead to better understanding of the underlying mechanisms.

1.1.5. Chemoresistance of low passage colon carcinoma cells towards 5-fluorouracil treatment in vitro

In order to study protein expression profiles in chemoresistant colon cancer cells compared to corresponding non resistant control cells Lars Gaedtker had established in vitro 5-FU resistant monolayer clones of low passage colon cancer cell line COGA 12 (**Figure 3**).

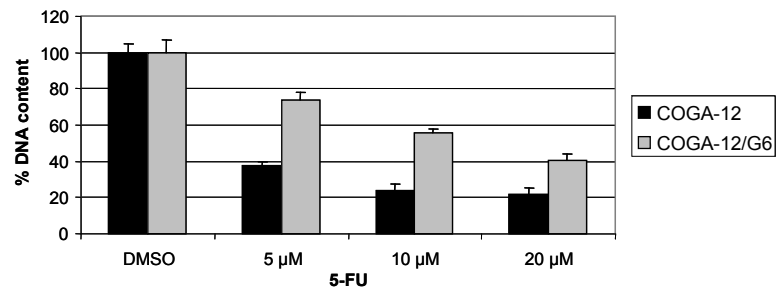


Figure 3: Chemosensitivity of three month 5-FU pretreated COGA-12/G6 cells towards 5-FU in comparison to wildtyp COGA-12 cells¹⁵.

He compared the protein expression profile of these cells (COGA-12/G6 cells) with the non resistant COGA-12 cells and long term passaged non-resistant COGA-12/NO cell by 2DE (**Figure 4**).

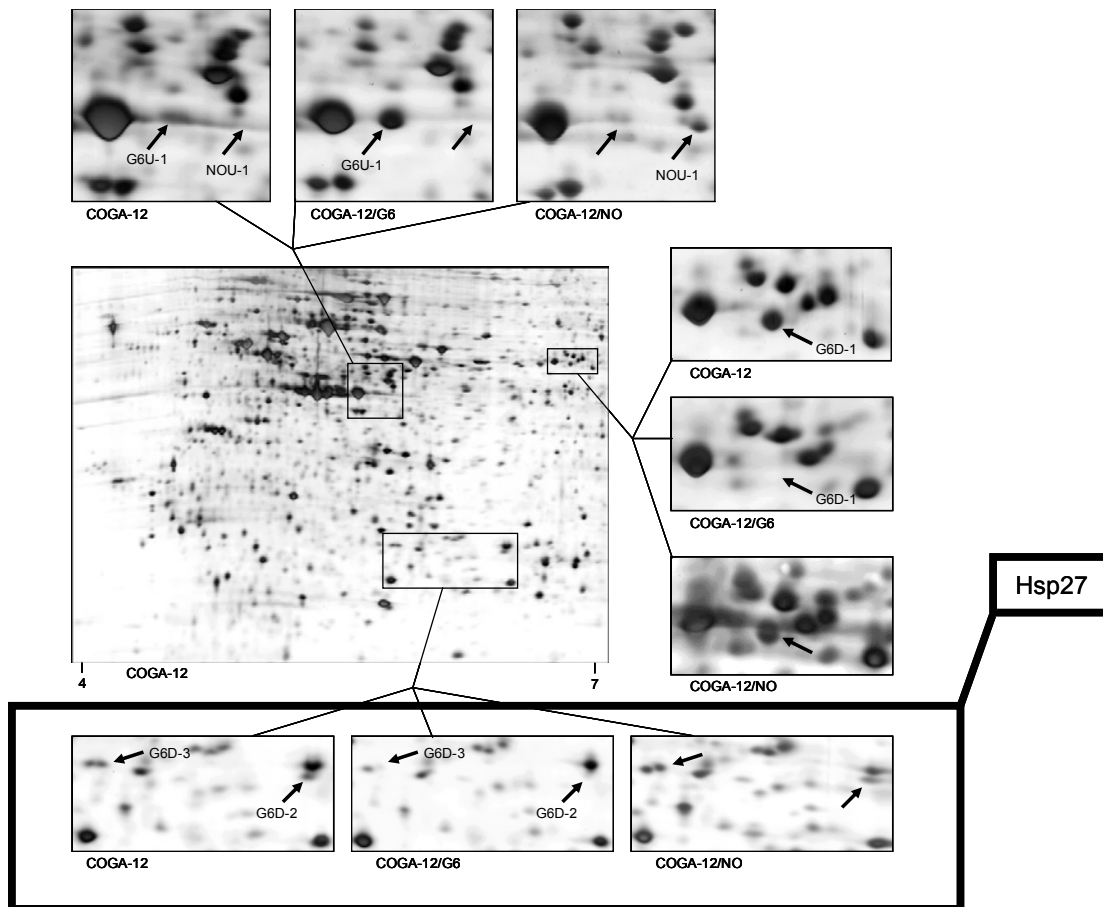


Figure 4: 2D gel of 5-FU resistant COGA-12 cells (COGA-12/G6) compared to non resistant COGA-12 cells¹⁵.

The differential regulated spots have been identified by MALDI-TOF MS (**Table 2**). Hsp27 is not expressed in resistant COGA-12/G6 cells compared to corresponding

non resistant COGA-12 cells. The current work further focused on the role of Hsp27 in 5-FU chemoresistance.

Spot no.	identified protein	protein regulation
G6U-1	Cytokeratin 18	up
G6D-1	Aldehyde Dehydrogenase 1B1	down
G6D-2	Heat shock protein 27	down
G6D-3	Heat shock protein 27	down
NOU-1	Maspin	up

Table 2: Protein identification of differential expressed spots in COGA-12/G6 versus COGA-12 cells

1.2. Prostate Cancer

Prostate cancer is the second leading cause of cancer related death in the United States in 2008 (Cancer Statistics ACS) and the most common newly diagnosed malignancy in the western world²⁹. Angiogenesis is a key requirement for tumor growth and metastasis formation in prostate cancer and anti-angiogenic therapy regimens have been used in several clinical trials especially in hormone resistant prostate carcinoma (HRPC) where the prognosis for patients is poor and patients typically show rapid tumor progression³⁰⁻³²

1.2.1. Metronomic Cyclophosphamide Therapy

The maximum tolerated dose (MTD) is the classical administration regimen of cyclophosphamide (CPA) and other chemotherapeutic drugs in order to exert cytotoxicity to fast dividing cells including the tumor cells and tumor vasculature endothelial cells. This administration schedule requires long treatment-free intervals as it is characterized by high toxic side effects. During treatment-free periods the risk for selection of resistant tumor cells due to genetic instability of cancer cells persists and furthermore vascular endothelial cell in the tumor area have the ability to recover and promote tumor angiogenesis of eventually surviving tumor mass resulting in fast re-growth of tumors leading to therapy failure^{33;34}. Beside these risks, MTD always has severe side effects on the whole organism.

In the last decade administration of chemotherapeutics has been developed towards a more compressed schedule using much lower doses enabling shorter treatment gaps³⁵. Browder et al showed that weekly applied low dose cyclophosphamide could improve antitumoral activity of CPA due to cytotoxic effects on tumor endothelial cells³⁴. Hanahan and co-workers introduced the term “metronomic” for this kind of

longterm low-dose treatment regimen and demonstrated its antiangiogenic properties³⁶. Even if the mechanism of antiangiogenic impact of this therapeutic scheme is not fully understood yet, several aspects may be involved: 1) due to the dosing dividing tumor endothelial cells are affected more direct and selectively compared to other cell types³⁷; 2) metronomic chemotherapy seems to directly target bone marrow derived endothelial progenitor cells^{38;39} preventing their attraction to the tumor; and 3) this therapy scheme modulates the level of angiogenic cytokines and therefore indirectly influences the balance of pro-and anti-angiogenic factors⁴⁰⁻⁴². In vitro evaluation showed decreased proliferation and migration capability of cultured endothelial cells in the presence of activated CPA³⁴. Further studies confirmed decreased angiogenesis in matrigel plug studies⁴³, increased apoptosis of proliferating endothelial cells in the tumor bed and significantly influence of functional tumor blood flow⁴⁴. Currently, metronomic CPA therapy is a promising approach in the clinic for docetaxel-resistant HRPC. Even as follow up therapy for already docetaxel-resistant HRPC, metronomically scheduled CPA reveals encouraging therapeutic response and has the potential to increase patients' life quality and survival⁴².

1.2.2. Chemoresistance to antiangiogenic therapy

Nevertheless recent studies have demonstrated that this therapeutic approach does not come up to its expectations. The effectiveness of antiangiogenic schedules as single agents was low in the clinic and resistance towards this therapeutic scheme also shapes up as a problem^{45;46}.

As tumor angiogenesis is a complex process based on the interplay between tumor cells and endothelial cells, resistance mechanisms towards antiangiogenic therapy can be multifaceted and at different levels of interaction⁴⁷. As the therapy regimen is not designed to kill the tumor cells directly, classical detoxification based resistance mechanism such as upregulation of ATP- binding cassette (ABC) transporters become less relevant⁴⁸.

More complex mechanisms based on cell-cell communications, such as cytokine expression, or survival mechanisms of tumor cells based on metabolic adaptation processes, e.g. tolerance towards hypoxia, may be important in this kind of resistance⁴⁹⁻⁵¹. The phenomenon that tumor cells can imitate endothelial cells which results in functional vessel structures and tumor blood supply without any endothelial cells involved is described as vasculogenic mimicry. Vascular mimicry was first

discovered in melanoma and has been observed in many other types of tumors such as breast, prostate^{52;53}. Tumor cells can also become independently of angiogenesis by growing along existing vessels without evoking an angiogenic response. This process has been defined as vessel co-option. First evidences for this phenomenon have been described by Holash et al in 1999 in a C6 glioma model in rat brain and it has been shown that tumors can evade anti-angiogenic therapy with a vascular endothelial growth factor receptor 2 (VEGFR2) antibody by increased vessel co-option^{54;55}.

Hypoxia induced by anti-angiogenic therapy can also lead to recruitment of bone-marrow derived cells (BMDC). BMDCs are a heterogeneous population including e.g. vascular progenitor cells and pro-angiogenic monocytes which participate in resistance to antiangiogenic treatment either by direct incorporation into functional vasculature or by secreting cytokines, growth factors or proteases. Clinical investigations with anti-VEGF therapy in patients having glioblastoma multiform (GBM) showed that in therapy evasive tumors accumulation of endothelial progenitor cells at the tumor margins occurred and enabled tumor revascularization⁵⁶.

Furthermore pericytes can be recruited to the tumor in case of anti-angiogenic therapy either by a kind of SOS-signal of endothelial cells or by tumor cells themselves. It could be observed that vessels tightly covered with pericytes are less sensitive towards antiangiogenic treatment. Even tumors which stay with only few vessels left can survive as pericytes protected endothelial cells in these vessels resist the antiangiogenic treatment. Beside a mechanical shielding effect on endothelial cells probably secreted cytokines of the pericytes such as e.g. VEGF or survival factors can protect the endothelial cells towards the therapy^{57;58}.

Hypoxia plays a major role in a variety of drug resistance mechanisms in solid tumors. It plays an important role on tumor microenvironment but also on tumor cells themselves. Otto Warburg has described already in the 1920s that tumor cells mainly gain their energy from glycolysis instead of the oxidative respiration which enable these cells to better tolerate hypoxic conditions in solid tumors⁵⁹.

In last few years, cancer stem cells (CSCs) have been identified in almost all types of cancers⁶⁰. CSCs have the ability to generate tumors that recapitulate the original tumor when xenotransplanted into animals, whereas the remaining non-CSC tumor bulk often can not^{61;62}. These cells have also been linked to chemoresistance in several aspects⁶³.

In respect to cyclophosphamide therapy these cells have shown overexpression of ALDH1 an enzyme involved in the detoxification process of cyclophosphamide⁶⁴. The role of CSCs in antiangiogenic therapy is not well understood yet, but a positive feedback loop between CSCs and the vasculature has been observed. CSCs often express high levels of VEGF and can thus initiate angiogenesis⁶⁵. Stem cell factor can activate microvascular endothelial cells in vitro and induce angiogenesis in vivo⁶⁶. Hypoxia can enrich the CSC fraction in tumor which then leads to a more aggressive and resistant tumor phenotype⁶⁷.

1.2.3. Proteomics and genomics in drug resistance

In the pre-proteomic era mostly one protein was identified to play a role in chemoresistance and was declared to be responsible for the phenomenon of the resistance towards a special drug e.g. thymidylate synthase in 5-FU resistance. However, failure of many anti-resistance strategies in the clinics have demonstrated that resistance in vivo is a far more complex phenomenon than modification of e.g. single drug metabolizing pathways⁶⁸. Especially resistance towards antiangiogenic therapy where tumor/ host interaction becomes important a more global approach e.g. by proteomics or genomics, or even combination of both techniques, could reveal novel resistance mechanisms and their interplay in mediating the drug resistant phenotype^{69,70}. In the last few years several lists of proteins related to different cellular pathways such as stress response, cell metabolism, protein biosynthesis, cell cycle and apoptosis have been related to drug resistance by proteomics and genomics⁷¹⁻⁷³. Different proteomics techniques as well as the bioinformatic platforms have been optimized over the last decade and can be combined to obtain maximum output of information. Most prominent techniques are 2D-electrophoresis (2DE) or its optimized form the 2D-differential in Gel electrophoresis (DIGE) and mass spectrometry based techniques such as MALDI-TOF and LC-MS.

In parallel the analysis of gene expression has also been optimized and microarray based gene expression profiling has become a standard technique applied in all areas of biomedical research⁷⁴. The key point of informative output from gene expression as well as proteomics is bioinformatic processing of the data. During the last year many bioinformatic applications for so called “data mining” have been developed which enable the combination of different data sets, pathway analysis of the obtained data and their integration in literature database searching⁷⁵.

However, relevance of the data obtained by proteomics and genomics for their involvement in disease associated pathways in vivo has come more in the focus of attention. In the field of cancer chemoresistance, clinical data provide disappointing results in case of in vitro identified protein candidates for their relevance in vivo^{76;77}. Therefore it has gained importance to create chemoresistance model system which better reflect the situation in vivo and to validate candidates obtained from in vitro studies in the appropriate tissue material.

1.2.4. In vivo resistance of prostate cancer xenografts towards metronomic cyclophosphamide therapy

In order to address this question of a better model of chemoresistance, Dr. Guenther has established an in vivo resistant prostate cancer xenograft model towards metronomic CPA therapy in SCID mice⁷⁸. Male SCID mice bearing subcutaneously implanted PC3 human prostate carcinoma tumors were treated with metronomically scheduled CPA (120 mg/kg every six days). CPA treatment was started on day 11 after tumor implantation when tumors reached an average volume of 37 mm³. Metronomic scheduled CPA treatment resulted in a significant tumor growth delay. Tumor volume of treated mice was constant at <100 mm³ up to day 50 after the tumor cell implantation, whereas tumors in the control group exhibited a tumor volume doubling time of 2.5 days. Around day 50 after tumor implantation tumor volume began to increase in the CPA treated group with a tumor doubling time of 9 days despite ongoing treatment (**Figure 5A, B**). Metronomic scheduled CPA therapy was well tolerated indicated by constant animal body weight up to day 67 after tumor cell implantation. Further CPA treatment resulted in significant loss of body weight observed in all CPA treated animals (data not shown). Treatment was stopped and animals were sacrificed when average loss in body weight reached 20 %.

For further investigation tumors were collected and subject to histological analysis. Further on, tumor cells were extracted in viable form from tumor tissue for characterization and cell culture experiments (**Figure 5A**).

For further investigation of the drug resistance mechanism, the effect of 4-hydroperoxy-cyclophosphamide (4-HOO-CPA) on survival of parental PC3 cells and reisolated PC3-D3 and PC3-D4 tumor cells was investigated in vitro. 4-HOO-CPA is rapidly converted to 4-hydroxy-CPA (4-HO-CPA) in aqueous solution and can be considered equivalent to 4-HO-CPA under experimental conditions⁷⁹. Incubation of parental PC3 cells (PC3-wt) and reisolated tumor cells (PC3-D3 and PC3-D4) at 20

to 50 μM 4-HOO-CPA significantly reduced cell survival after a three days treatment. The reisolated PC3-D3 and PC3-D4 cells exhibited comparable sensitivity to the PC3-wt cells in the monolayer system (**Figure 5C**). Reisolated cells were not able to manifest their acquired *in vivo* chemoresistance in an *in vitro* monolayer cell culture model.

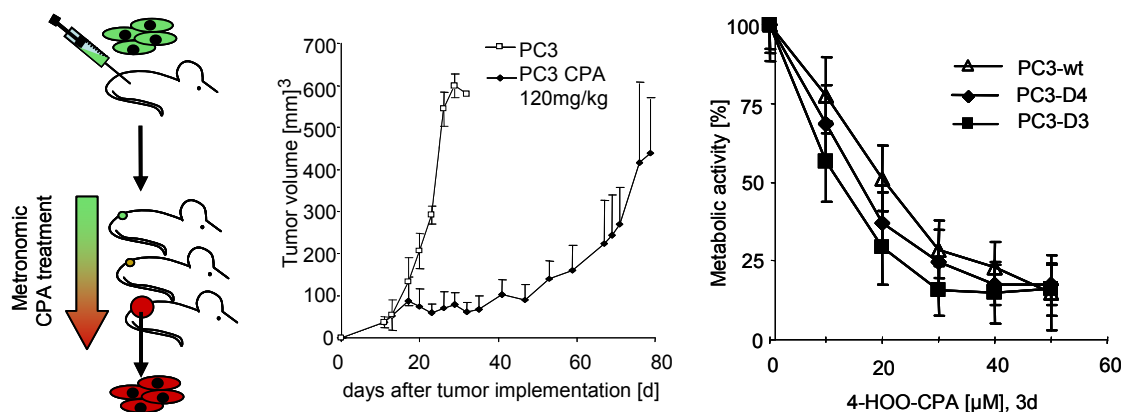


Figure 5: The PC3 chemoresistance mode: (A) Schematic view. (B) *In vivo* resistance of PC3 xenografts in SCID mice. (C) Chemosensitivity of reisolated PC3 cells *in vitro*

In order to analyze the influence of CPA therapy on tumor histology, expression of vascular markers and functional blood flow at the first therapy end point, Dr. Guenther characterized PC3 tumors in terms of histology and immunohistochemistry with focus on vascular markers (**Figure 6**) The tissue structure in untreated PC3 xenografts was compact and only small areas of condensed and fragmented cell nuclei could be detected (**Figure 6A**). In contrast, CPA treated tumors exhibited larger areas of condensed and fragmented cell nuclei, indicating cell death (**Figure 6B**). To evaluate possible reasons for acquired resistance towards CPA treatment, PC3 tumors were analyzed for immunohistological changes. Considering the antiangiogenic metronomic schedule of the CPA treatment, immunostaining was focused on vascular markers such as CD31 and mouse specific laminin. Additionally, tumor blood flow was visualized by intravenously applied Hoechst 33258 dye as a tracer. Antibody staining for murine CD31 was performed to detect mouse endothelial cells and combined with staining for laminin, which is the major component of the vascular basement membrane. Co-localisation of laminin and CD31 positive endothelial cells remained unchanged (**Figure 6C, D**). No statistically significant changes in total count rate for CD31 positive events, representing functional as well as not functional vessel structures, could be detected in CPA treated tumors in

comparison to non treated control tumors (**Figure 6E**). However, long term treatment resulted in increased number of vessel structures without a detectable capillary lumen attended by decreased Hoechst 33258 fluorescence signal within the tumor tissue (**Figure 6C** versus **6D**; **6E**). Decreased tumor blood flow indicates antiangiogenic activity of the treatment regimen at this time point.

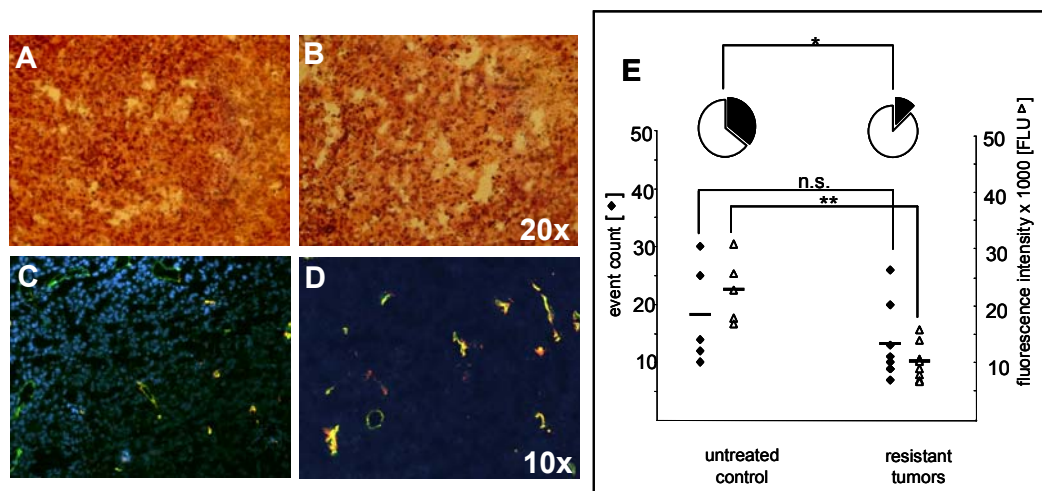


Figure 6: Histology of subcutaneous (A) untreated versus (B) CPA treated PC3 xenografts (H/E stain) Vascular marker expression in untreated (C) and CPA treated tumors (D). CD31 (green) and laminin (red). Hoechst 33258 dye (blue). Vessel structures with detectable lumen are indicated by filled areas of the circular diagram (E). Quantification of functional blood flow by Hoechst 33258 fluorescence at the treatment endpoint (open symbols) (E). For quantification of CD31 count, lumen containing vessel fraction and blood flow (four sections per tumor) were examined and three areas per section were randomly selected for image analysis⁷⁸.

1.3. Aim of this thesis

Drug resistance is still the major drawback for successful cancer therapy in various types of tumors and mechanisms of resistance in vivo are poorly understood. A better understanding of biological pathways of chemoresistance in combination with well evaluated biomarkers for resistance would provide a better basis for the design of suitable therapeutic approaches to overcome tumor resistance in future. Therefore main focus of this thesis will be to address the complex issue of chemoresistance in vivo by a proteomic and genomic approach in order to identify new relevant biomarkers. Furthermore the role of selected candidates for their involvement in chemoresistance and 3D tumor growth should be specified. In detail this question should be addressed by the following steps:

The implication of 3D tumor growth in cancer resistance of solid tumors has been described in various studies⁸⁰⁻⁸². Lamin A/C fragmentation has been previously identified in our group to be specific for 3D cultures of low passage colon cancer cell

in comparison to 2D monolayer cultures. In order to better understand biological mechanisms behind 3D tumor growth, the specific aim of this work should be to clarify the role of Lamin A/C fragmentation in 3D tumor growth.

In parallel siRNA technology should provide information about the functional role of Hsp27 in chemoresistance of low passage colon cancer cells (COGA-12) towards 5-FU¹⁵.

In order to identify biomarkers with high impact for in vivo relevance proteomics and genomics technology should be combined for the analysis of in vivo relevant resistance mechanisms in a xenograft model of prostate cancer cells manifesting their resistant phenotype only in vivo. Therefore protein expression of reisolated cells from resistant tumors towards metronomic cyclophosphamide therapy in vivo⁷⁸ should be compared to their non resistant wild type as well as to in vivo passaged control cells (reisolated from sensitive tumor, which have not been treated with CPA in vivo). Furthermore, to address the complexity of in vivo resistance proteomics data should be supplemented by gene expression profiling of corresponding tumors by microarray analysis (**Figure 7**).

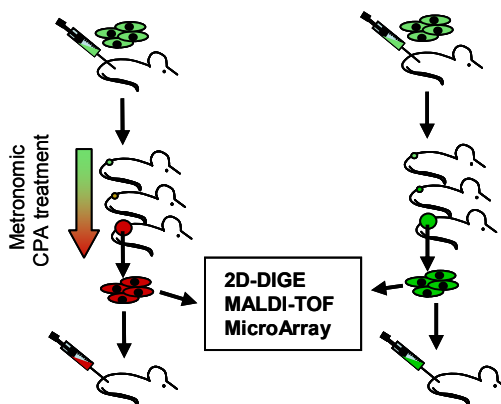


Figure 7: A proteomic and genomic approach to in vivo chemoresistance in metronomic cyclophosphamide therapy

2. Materials and Methods

2.1. Cell Biology Methods

2.1.1. Cell culture

Cell culture media, antibiotics, fetal bovine serum (FBS) and trypsin/EDTA solution were purchased from Invitrogen GmbH (Karlsruhe, Germany).

Human low passage cell lines COGA-1, COGA-2, COGA-3, COGA-5, COGA-5L, COGA-10 and COGA-12 were obtained from colorectal cancer patients and resemble the phenotype of the original tumors as previously described³. Cell lines COGA-1, COGA-5 and COGA-10 exhibited epithelial-like, COGA-5L and COGA-12 piled-up, and COGA-2 and COGA-3 rounded-up morphology. Only 5 - 10 passages after harvesting the primary tumor cells from the patients were required for the generation of such low passage cell lines. The cell lines were grown in RPMI 1640 medium containing 10 % serum (Invitrogen, Karlsruhe, Germany) at 37° C in 5 % CO₂ humidified atmosphere.

PC3 human prostate carcinoma cells (CRL1435) were cultured in RPMI 1640 medium supplemented with 10% FBS. Cells were grown at 37°C in 5% CO₂ in humidified atmosphere.

2.1.2. Multicellular spheroid culture

Multicellular spheroids were generated using the liquid overlay technique as described previously⁸³. Briefly, 24-well culture plates (Nalge Nunc International, Naperville, IL, USA) were coated with 300 µl of 1 % SeaPlaque agarose (Biozym, Hess, Germany) in serum-free growth medium. In each well 10⁵ cells from a single-cell suspension were added to total volume of 1 ml growth medium containing 10 % serum, and multicellular spheroids were allowed to form over 24 to 96 h. In order to inhibit caspases-6 induced lamin A cleavage in spheroids, the caspases-6-specific inhibitor Z-VEID-fmk (50 µM) was added to the media previous to spheroid formation. Spheroids were grown 24h before cell lysis followed by western blot analysis. Controls were grown in media containing appropriate amounts of DMSO.

2.1.3. Oxygen and serum deprivation

For oxygen deprivation cells were incubated in an oxygen-free N₂/CO₂ (95%/5%) atmosphere for 24 h. For serum deprivation cells were incubated in RPMI 1640 containing different percentages of fetal calf serum (0%, 2%) for 24 h. In order to block lamin cleavage by inhibition of caspases, cells were preincubated 30 minutes prior to hypoxia with the inhibitors z-VAD-fmk (10 or 50 µM) the specific caspase 6 inhibitor z-VEID-fmk (50 µM). Control cultures were grown in RPMI containing 10% fetal calf serum.

2.1.4. In vitro chemotherapy

COGA cells were treated with either Camptothecin (Sigma-Aldrich, Taufkirchen, Germany), (1-25 µM) or 5-fluorouracil (Sigma-Aldrich, Taufkirchen, Germany), (5-20 µM) for three days before cell lysates were subject to western blot analysis, MTT or Hoechst assay. Controls were treated with the appropriate amounts of DMSO.

2.1.5. Cell viability, Apoptosis and Proliferation

2.1.5.1. MTT Assay

In order to determine metabolic activity of the cells the (3-(4,5-Dimethylthiazol-2-yl)-2,5-diphenyltetrazolium bromide (MTT) assay was used. Therefore the culture medium in each well was replaced by 300 µl of fresh culture medium containing 0.25% MTT (w/v) followed by incubation for 3 h at 37°C. MTT is converted to a colored, water insoluble formazan salt by the metabolic activity of viable cells. The culture medium was then removed and cells were frozen at -80°C. After thawing the cells, 300 µl of DMSO was added to dissolve the insoluble formazan salt and absorbance at 590 nm was measured using a SPECTRAFluor Plus plate reader (Tecan, Grödig, Austria). Reference absorbance at 630 nm was subtracted from the absorbance at 590 nm for each well.

2.1.5.2. Hoechst Assay

In order to determine cell proliferation, DNA content of cells was measured by staining DNA with Hoechst 33258 dye. Culture medium was removed and cells were washed with PBS. After washing, cells were harvested with Trypsin-EDTA (100 µl) and lysed with Millipore water (100 µl) followed by freeze-thaw-cycle. 200 µl of cell lyses buffer (20 mM Tris, 2 mM EDTA 5 mM NaCl, pH 7.4) containing 2 µg/ml

Hoechst 33258 dye were applied to each well, followed by another freeze-thaw-cycle. 200 μ l of cell suspension were transferred to a black bottom 96 well plate (Greiner-Bio One, Frickenhausen, Germany). DNA content was determined by quantifying fluorescence signal using a SPECTRAFluor Plus plate reader (Tecan, Grödig, Austria), using excitation and emission filters centered at 360 nm (excitation) and 465 nm (emission), respectively.

2.1.6. TUNEL Assay

Apoptotic cells were detected on paraffin embedded section of multicellular spheroids at different time points 24 h and up to 120 h after spheroids formation using a TUNEL assay (Roche, Penzberg, Germany) according to manufacturer instructions. Briefly: After dewaxing and rehydration according to standard protocols the spheroid sections were treated with proteinase K working solution (Roche, Penzberg, Germany) for 10 min. The TUNEL reaction mixture was added and incubated for 60 min at 37°C in a humidified atmosphere. After intensive washing with PBS the sections were mounted with antifade and analyzed using a fluorescence microscope at 488 nm excitation (530 nm emission).

2.1.7. Transfections

2.1.7.1. Hsp27 siRNA transfection

For siRNA applications, cells were seeded at a density of 6×10^4 cells/well in antibiotic-free medium in 24-well plates and incubated at 37° C for 24 hours before transfection. Lipofectamine 2000 (Invitrogen, Karlsruhe, Germany) and siRNA (and nonfunctional mut-siRNA) were dissolved separately in Opti-MEM I (Invitrogen, Karlsruhe, Germany). After 5 min of equilibration at room temperature, each siRNA solution was combined with the respective volume of the Lipofectamine 2000 solution, mixed gently, and allowed to form siRNA liposome complexes for 20 min at room temperature. The transfection mixture was added to the cells at a final concentration of 20-100 nM and 2 μ l/ml Lipofectamine. Controls were treated with 100 μ l/ml Opti-MEM I, and vehicle controls with 2 μ l/ml Lipofectamine 2000. The HSP27 siRNA sequence 5'-AAG-CUG-CAA-AAU-CCG-AUG-AGA-C-3' was reported to be effective in prostate cancer cells. Non functional control siRNA (mut-siRNA. 5'-AUU-GUA-UGC-GAU-CGC-AGA-C-3') was purchased from MWG Biotech (Ebersberg, Germany).

2.1.8. Immunocytochemistry

2.1.8.1. Immunostaining of lamin A/C in multicellular spheroids

After 4 d in culture multicellular spheroids were transferred to tissue freezing medium (Leica Microsystems, Nussloch, Germany) and frozen at -80°C. Cryosections (5 µm) were obtained with a Leica CM3050S cryostat (Leica Microsystems, Nussloch, Germany). Sections were transferred to microscope slides (SuperFrost, Menzel, Braunschweig, Germany), fixed in 4% paraformaldehyde, and subsequently treated with 0.2% Triton-X for 5 min. After blocking with 3% goat serum in PBS for 1 h the sections were incubated with rabbit anti-lamin A/C (1:100, cell signaling technology, Danvers, USA) or anti-cleaved lamin A antibody (1:100, cell signaling technology, Danvers, USA) in 3% goat serum in PBS at 4°C over night. Afterwards the sections were exposed to biotinylated goat anti-rabbit antibody (1:200, Vector Laboratories, Burlingame, USA) in 3% goat serum in PBS for 2 h at RT followed by incubation with Oregon Green streptavidin (Invitrogen, Karlsruhe, Germany) for 40 min in PBS. For counterstaining of the nuclei the slides were incubated with DAPI (4',6-Diamidino-2-phenylindole) at a concentration of 1 µg/ml in PBS for 15 min.

2.1.8.2. Immunostaining of Ki67 in multicellular spheroids

Immunostaining was performed by the avidin–biotin–peroxidase complex staining method according to standard protocols. Briefly, paraffin sections were dewaxed and rehydrated. Antigen retrieval was performed by heat induction incubating the sections in 0.1 M citrate buffer (pH 6.0) for 60 min in the microwave. Sections were incubated with the primary antibody for 60 minutes at room temperature in a moist chamber. The proliferation antigen Ki67 was detected with mab MIB-1 (0.8 µg/ml, IgG1, Dako, Germany). After washing in PBS sections were incubated with a biotinylated antibody diluted (1:4000) in PBS for 30 minutes. Slides were incubated with peroxidase conjugated streptavidin (MIB-1). Peroxidase reaction was developed in AEC for eight minutes at room temperature. The sections were counterstained and mounted.

2.1.8.3. Immunostaining for FACS analysis

Cells were harvested with trypsin/EDTA solution and washed 1x with PBS prior to immunostaining. Primary antibodies were diluted 1:200 in PBS containing 5% FCS and staining was performed by incubating the cell with the antibody dilution for 1h on ice followed by 2 x washing with PBS containing 5% PBS. The secondary antibody

was diluted 1:400 in PBS containing 5% FCS for 45 min followed by 1 x washing with PBS containing 5% FBS resuspension of the cells in 700-100 μ l of PBS containing 5% FBS. Cells were kept on ice until analysis.

2.1.9. Flow cytometry and microscopy

2.1.9.1. FACS analysis

FACS analysis was performed using a CYAN LX High Performance Flow Cytometer (DakoCytomation, Copenhagen, Denmark). Before analysis 1 μ l of DAPI solution (1mg/ml) was added and the cell suspension was passed through a filter to prevent occlusion of the machine. Alexa 488 fluorescence was excited at 488nm and DAPI fluorescence at 360nm. The fluorescence emission was detected using 530/40 nm band pass filter for Alexa 488 and 450/40 nm for DAPI. To exclude cell debris and doublets, cells were appropriately gated by forward versus sideward scatter. At least 20 000 gated events were collected.

2.1.9.2. Transmission light and epifluorescence microscopy

Transmission light microscopy of living cells growing as monolayer cultures or multicellular spheroids was performed using an Axiovert 200 microscope (Carl Zeiss, Jena, Germany) equipped with a infinity2-C3 digital camera (Lumenera, Ontario, Canada). Light was collected through a 5 x 0.12 NA, 10 x 0.25 NA or 32 x 0.40 NA objectives (Carl Zeiss, Jena, Germany). Images were collected using phase contrast. Immunofluorescently stained cells were analyzed using an Axiovert 200 microscope (Carl Zeiss, Jena, Germany) equipped with a Zeiss AxioCam camera. Light was collected through a 10 x 0.25 NA, 20 x 0.3 NA or a 63 x 1.4 NA objective (Carl Zeiss, Jena, Germany). Fluorescence was excited using either a 470 \pm 20 nm band pass filter for Alexa 488. Emission was collected using a 540 \pm 25 nm band pass filter. Digital image recording and image analysis was performed with Axiovision software (Carl Zeiss, Jena, Germany)

2.1.9.3. Confocal laser scanning microscopy

Detection of Oregon Green indicating lamin A/C or fragmented lamin A was performed using a fluorescent confocal laser scanning microscope (LSM 510 Meta, Carl Zeiss, Jena, Germany) at 488 nm excitation (530 nm emission), and DAPI fluorescence was detected at 364 nm excitation (385 nm long-pass emission). Image

recording was performed with the LSM 5 software, version 3.0 (Carl Zeiss, Jena, Germany).

2.2. Protein analysis

2.2.1. Bradford Assay

Protein concentration was determined using the Bradford protein assay (BIORAD, Munich, Germany) according to manufacturer's instructions. Samples for 2D-DIGE analysis were diluted at least 1:2 as the assay only tolerates 6 M urea. Bovine serum albumin (BSA) was used for the protein standard curve and was therefore diluted in the appropriate lysis buffer (Promega lysis buffer for western blotting, DIGE urea lysis buffer for 2DE)

2.2.2. Westernblot

2.2.2.1. Antibodies

In order to detect the protein targets of interest the following antibodies were used in the corresponding western blot analyses: rabbit monoclonal antibody detecting full length lamin A/C and cleaved lamin A (1:1000, cell signaling technology, Danvers, USA), goat polyclonal antibody detecting acidic calponin (1:500, Santa Cruz Biotechnology, Heidelberg, Germany), mouse monoclonal antibody detecting keratin 18 (1:500, cell signaling technology, Danvers, USA), mouse monoclonal anti- α -Tubulin antibody (1:5000; Santa Cruz Biotechnology, Heidelberg, Germany), rabbit polyclonal antibody detecting annexin A3 (1:1000, Abcam, Cambridge, UK), mouse monoclonal antibody detecting cathepsin B (1:1000, Calbiochem, Darmstadt, Germany), mouse monoclonal antibody detecting cytokeratin 19 (1:1000, Exbio, Praha, Czech Republic), goat polyclonal antibody detecting thioredoxin domain containing protein 5 (1:2000, Abcam, Cambridge, UK). The corresponding secondary antibodies were used as following: goat anti-rabbit HRP-conjugated secondary antibody (1:5000; Vector Laboratories, Burlingame, USA) or a rabbit anti-mouse HRP-conjugated secondary antibody (1:5000; Vector Laboratories, Burlingame, USA).

2.2.2.2. Blotting procedure

After SDS-PAGE using the Protean MiniGel system (BioRAD, Munich, Germany) and transfer to a PVDF membrane (Macharey Nagel, Düren, Germany) using a Trans

Blot SD semidry blotting machine (BioRAD, Munich, Germany) the blot was probed with the appropriate antibody binding the protein target of interest in Tris buffered saline containing 0.5 % Tween (TBST) and 5% non fat milk powder at 4°C overnight. After washing with TBST and PBS membranes were exposed to the corresponding secondary antibody followed by chemiluminescence detection (ECL; Amersham Biosciences, Arlington Heights, IL). Equal protein loading was controlled by reprobing the membrane with an antibody detecting a house keeping protein like α -Tubulin or GAPDH.

2.2.2.3. Imaging and quantitative analysis

X-ray films were scanned using an Image Scanner (GE Healthcare, Munich, Germany) and quantitative analysis of the protein bands was performed by densitometry using ImageJ (Sun Microsystems GmbH, Heimstetten, Germany). The house keepers GAPDH and α -tubulin provided the basis for normalization. For western blot analysis of ex vivo tumor tissue, the fraction of mouse protein within each sample has been determined using an appropriate anti-MHC antibody. Therefore western blots from tumor tissue have been compared to different amounts of SCID mouse proteins (**Figure 8**). The content of mouse protein within the tumor samples was below 3% (data not shown).

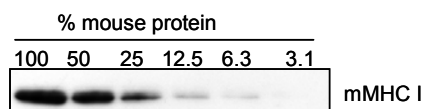


Figure 8: Western blot analysis of different amounts of SCID mouse protein probed with an appropriate MHC antibody detecting SCID mouse MHC I.

2.2.3. 2D-DIGE electrophoresis and mass spectrometry

2D-DIGE electrophoresis was performed as described in the following passage. A schematic view is presented in **Figure 9**.

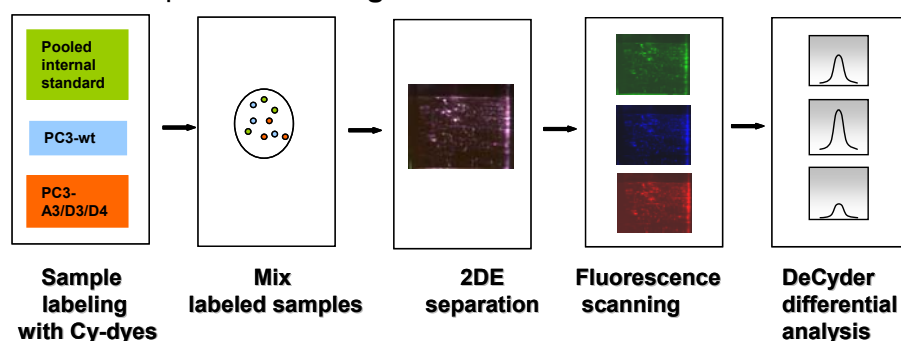


Figure 9: Schematic view of 2D-DIGE experimental setup.

2.2.3.1. Sample preparation

Cells grown as monolayers were harvested with trypsin/EDTA, washed 2 x with PBS and transferred to an Eppendorf tube. Washing solution was quantitatively removed before adding 500 µl of DIGE sample buffer (7 M urea, 2 M thioruea, 30 mM Tris, 4 % CHAPS). Cells were shock frozen in liquid nitrogen before storage at -80°C until further processing. All centrifugation steps were carried out at 500 g for 5 minutes. Cell lysates were homogenized by centrifugation at 17500 g in a Qiashredder Homogenizer (Qiagen, Hilden, Germany) for 2 minutes. After the following centrifugation at 17600 g for 30 minutes supernatants were transferred into fresh Eppendorf tubes and protein concentration was determined by Bradford assay as described earlier (see 2.2.1). Samples were stored at -80°C.

2.2.3.2. Protein labeling with DIGE dye

Labeling with DIGE dyes (GE healthcare Bio-Science, Amersham plc, UK) was performed according to manufacturer's instructions. The internal pooled standard (IPS) was prepared from equal protein amounts of each biological sample and labeled with the Cy2 fluorophore. Three biological and two technical replicates were performed. For each gel 50 µg aliquots of Cy2-,Cy3-,Cy5-labeled samples were combined and diluted with an equal volume of sample buffer (8 M urea, 4 % CHAPS, 2 % dithioerythritol DTE, 2 % Pharmalyte™ pH 3-10). Whenever required, labeled samples were stored at -80°C.

2.2.3.3. 2-DE

For Isoelectric focusing (IEF), the 24 cm gel strips with a gradient of pH 4-7 (Immobiline™ Dry Strips, GE Healthcare Bio-Science, Amersham plc, UK) were used. Labeled samples were applied to the strips by in gel rehydration followed by focusing in an Ettan IPGphor Isoelectric Focusing System (GE Healthcare Biosciences, Uppsala, Sweden; focusing time: 90 000 Vhs). IEF gels were stored at -80°C until further processing. Prior to SDS-PAGE, gel strips were equilibrated for 15 min in 10 ml equilibration buffer (50 mM Tris-HCl pH 6.8, 6 M urea, 30 % glycerin , 2 % SDS) containing 1 % DTE, followed by a second 15 min equilibration step in 10 ml equilibration buffer with 2.5 % iodacetamide and 200 µl saturated bromophenolblue solution.

SDS-PAGE (overall gel size 24cm x 18 cm x 1mm) was performed using a 11% separation gel [1.5 M Tris-HCL pH 8.8, 11 % acrylamide/ bisacrylamide (37.5:1), 0.1

% SDS, 0.05 % APS, 0:05 % TEMED] using a Ettan Dalt Twelve System (GE Healthcare Bio-Science, Uppsala, Sweden). IEF strips were placed onto the second dimension SDS polyacrylamide gels and fixed with 0.5 % agarose in SDS running buffer (25 mM Tris, 192 mM glycine, 0.1 % SDS). Gels were run for 45 min at 2.5 W/gel followed by 4 h at 18 W/gel in SDS running buffer at 20°C.

2.2.3.4. Imaging and quantitative analysis

Gels were scanned with a Typhoon 9400 fluorescence scanning device (GE Healthcare Bioscience) using the parameters suggested by the manufacturer for 2D DIGE experiments. Image analysis was performed with DeCyder™ Differential Software version v6.5 (GE Healthcare BioScience). Parameters for the spot detection algorithm were optimized manually and “estimated number of spots” was set to 3200. Only proteins, where the average normalized signals of all spots were increased respectively decreased more than 1.6 fold were taken into account in order to keep the false discovery rate low. In order to obtain significant data, three biological and two technical replicates of each group (6 replicates in total) were used for quantification.

2.2.3.5. Excision and tryptic in gel hydrolysis of 2-D gel spots

2D Gels were CBB-stained overnight (50 % Methanol, 0.05 % CBB R-250, 10 % acetic acid) and de-stained for 8 h (5 % methanol, 7 % acetic acid). Spots of interest were excised manually and transferred into 96-well reaction plates (Intavis, Köln, Germany). Digests were performed using a Digest- Pro MS digest robot (Intavis, Köln, Germany) with the following protocol: (i) wash step with 60 µl 50 mM NH₄HCO₃, (ii) wash step with 90 µl 50 % Acetonitril (ACN), 25 mM NH₄HCO₃, (iii) 20 min wash with 60 µl ACN, (iv) 20 min wash with 60 µl 50 mM NH₄HCO₃ (v) 20 min wash with 60 µl ACN (vi) 15 min wash with 60 µl ACN (vii) addition of 90 ng porcine trypsin (Promega, Madison, WI, USA) in 15 µl 50 mM NH₄HCO₃ and incubation at 37°C for 6 h, (viii) addition of 15 µl 2.5 % formic acid, and (ix) collection of the supernatant in 96-well collection plates (Intavis, Köln, Germany)

2.2.3.6. MALDI target preparation and MALDI-TOF-TOF analysis

MALDI target preparation was performed with a DigestPro MS robot (Intavis) using the following protocol: (i) wetting of ZipTip C-18 reversed phase tips (Millipore, MA, USA) with 20 µl 50 % ACN, 0.1 % trifluoroacetic acid (TFA); (ii) equilibration with 20

μl 0.1 % TFA; (iii) loading of the tryptic peptides; (iv) washing with 20 μl 0.1 % TFA, and (v) elution of peptides onto the MALDI target plate with 1-2 μl 8 ml/ml cinnamic acid solution, 65 % ACN , 0.1 % TFA.

MS and MS/MS spectra were acquired with 2500 laser shots (ND:Yag laser, 355 nm, N2 collision in the MS/MS mode) on a 4800 MALDI-TOF-TOF mass spectrometer (Applied Biosystems, CA, USA). Peak lists for MS spectra were generated with the 4000 Series Explorer software using minimum S/N of 10 within the window of 50 m/z and cluster area S/N of 50. The peak lists for MS/MS spectra were generated using minimum S/N of 2 within the window of 500 m/z and cluster area S/N of 10. The PMF data subset was searched with Mascot against the human IPI v348 database with the following parameters: (i) fixed modifications: carbamidomethyl (C), (ii) variable modifications: oxidation (M), (iii) cleavage enzyme: trypsin (*KR), (iv) max missed cleavage:1, (v) Peptide mass tolerance mono: 0.5 Da, and (vi) Fragment mass tolerance mono 0.5 Da. Only proteins with a protein score > 90 were taken into account and every spot was identified by at least 2 MS/MS Spectra with a ions score > 30.

2.3. RNA analysis

2.3.1. RNA-extraction and concentration measurement for RT-PCR

For RNA extraction 5 million cells were lysed in 350 μL of lysate buffer containing SDS and β-mercaptoethanol (Merck, Darmstadt, Germany) according to the manufacturer's protocol (NucleoSpin RNA II Kit; Macherey and Nagel, Düren, Germany). After elution from the spin columns the RNA samples were stored at -80°C until further use. RNA concentrations were determined at a wavelength of 260/280 nm using a Biophotometer (Eppendorf, Hamburg, Germany).

2.3.2. RT-PCR

2.3.2.1. Primers

Thymidylate synthase: forward, 5'-ATC-AAG-GGA-TCC-ACA-AAT-GC-3' and reverse, 5'-GGT-CAA-CTC-CCT-GTC-CTG-AA-3'

Hsp27: forward, 5'-TTT-CTG-AGC-AGA-CGT-CCA-GA-3' and reverse, 5'-CTT-TAC-TTG-GCG-GCA-GTC-TC-3'

Glyceraldehyde-3-phosphatedehydrogenase (GAPDH): forward, 5'-CGT CTT CACCAC CAT GGA GAA GGC-3' and reverse, 5'-AAG GCC ATG CCA GTG AGC TTC CC-3'

2.3.2.2. Procedure

Reverse transcription (RT) was performed using M-MLV-reverse transcriptase (Promega, Mannheim, Germany) and oligo-dT-primers (MWG Biotech, Ederberg, Germany) to generate cDNA from 5 µg total RNA. The primers for Hsp27 and thymidylate synthase (TS) were used as described under 3.2.1. As a control, cDNA of the housekeeping gene glyceraldehyde-3-phosphatedehydrogenase (GAPDH) was amplified. The resulting specific PCR products had a length of 865 base pairs (bp) (HSP27), 205 bp (TS) and 400 bp (GAPDH), respectively. In a PX2 Thermal Cycler (Thermo electron corporation, Karlsruhe, Germany) the PCR was initiated with denaturation at 95°C for 2 min followed by addition of 5µl Thermoprime Plus polymerase 0.2 U/µl (Abgene, Hamburg, Germany) and 25-32 cycles (Hsp27), 26 cycles (TS) and 23 cycles (GAPDH) of 30 s 95°C, 1 min 48°C (HSP27), 50°C (TS) or 57°C (GAPDH), and 2 min 70°C, and final extension at 70°C for 10 min. PCR products were detected by ethidium bromide staining after 1.5% agarose gel electrophoresis and documented in a UV chamber (Raytest, Straubehardt, Germany) equipped with a CCD Camera (Raytest, Straubehardt, Germany).

2.3.3. Micro Array Analysis

Tumors were isolated and dissected as described in 2.4.6.2. The conserved tumor pieces were transferred to the laboratory of Dr. Helmut Blum where the RNA isolation and micro array analysis was performed according to the following protocol (**Figure 10**).

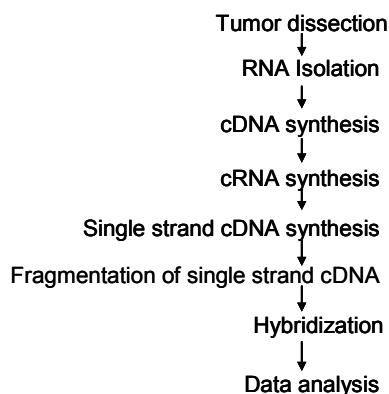


Figure 10: Schematic view of microarray analysis of RNA derived from PC3 xenografts in SCID mice.

2.3.3.1. RNA Isolation

Trizol/chlorophorm extraction

Tumor pieces were weighed and transferred to 2ml reaction tubes, shock frozen in liquid nitrogen and stored at -80°C for further processing. Frozen samples were homogenised in 1ml Trizol using a tissue homogenizer (Heidolph, Schwabach, Germany) and vortexed for 5 min. After each sample the homogenizer was cleaned by washing with 0.5N NaOH and RNasefree water. In a second step phase separation was induced by adding 0.2 ml chlorophorm to each sample followed by the transfer of the aqueous phase containing the RNA into a new tube. After adding 0.5 ml isopropanol the RNA was precipitated by centrifugation at 12 000g, 4°C for 45 min. The pelleted RNA was washed two times with 75% EtOH followed each time by centrifugation (12 000g) for 10 min at 4° . After the second washing step the EtOH was removed and the pellet was dried at the unshielded flame. The dried pellet was dissolved in 53 μl RNasefree H_2O , first incubated with casual vortexing for 20 min at RT than at 42°C on the thermomixer for 15 min. After that samples were put on ice, vortexed and spun down. 1.5 μl RNA-solution were used to determine the concentration at the nanodrop ND-100 (NanoDrop Technologies LLC, Wilmington, DE, USA). The RNA quality was tested on a 1% agarose gel.

Ammonium acetate (NH_4Ac) precipitation

The samples were incubated with equal amounts (50 μl) of a 5M NH_4Ac solution and incubated for 30 min on ice followed by 45 min centrifugation at 25 000g (4°C). Thereafter the supernatant was removed and 250 μl of a 2.5 M NH_4Ac solution was added followed by 10 min centrifugation at 25 000g (4°C). After removal of the supernatant the pellet was resuspended in 500 μl 75% EtOH previous to centrifugation for 5 min at 25 000g (4°C) and removal of 450 μl of the supernatant. Storage of the samples at this stage at -20°C is possible. For further processing the supernatant was discarded completely and the pellet was dried at the unshielded flame before dissolving it in 102 μl RNasefree H_2O for 15 min at 30°C in the thermomixer. Further on the concentration was monitored again using the nanodrop and RNA quality was tested by 1% agarose gel electrophoresis followed by EtBr staining of RNA.

Natrium acetate (NaAc) precipitation of the RNA

For long-term storage an equal volume of isopropanol and 1/10th volume of NaAc were added to each sample, followed by shaking and spinning down previous to storage at -20°C.

2.3.3.2. Control cDNA Synthesis

The precipitated samples were thawed for 15 min at RT previous to 30 min centrifugation at 25000 g (18°C). Subsequently the supernatant was removed and stored until the concentration was measured at the nanodrop. Before measuring the concentration the pellet was washed with 500 µl 75% EtOH, centrifuged for 10 min at 25 000 g (18°C) and dried at the unshielded flame. For concentration measurement the pellet was solved in 100 µl RNasefree H₂O. Whenever the concentration is too low the precipitation could be repeated. The quality was analyzed again by agarose gel electrophoresis with 200 ng RNA/ sample. cDNA synthesis was performed using 10 µg RNA per sample in the superscript III kit from invitrogen (Karlsruhe, Germany) following manufacturer's instructions. Finally the remaining RNA was digested and the quality of the cDNA was monitored by agarose gel electrophoresis as described previously.

2.3.3.3. cDNA synthesis and hybridization

Prior to the cRNA synthesis the concentration and quality of the RNA was again monitored as described earlier. The following steps including cDNA synthesis, cRNA synthesis, single strand cDNA synthesis and fragmentation of single strand cDNA for the Affymetrix human Gene Chip® Gene 1.0 ST array (Affymetrix, High Wycombe, UK) was carried out using the Affymetrix cDNA Synthesis & Amplification Kit according to the manufacturer's instruction and all chemicals used were purchased from Affymetrix (High Wycombe, UK). Concentration and quality were monitored after each synthesis step following the procedure described previously. After each synthesis step the product can be shock frozen and stored at -80°C until further processing. After the enzymatic fragmentation of the single strand cDNA the fragments are labelled and final quality control before the hybridisation was performed on a 2% Biozym-Phor agarose gel using 300 ng cDNA of each sample. The hybridization cocktail was prepared and stored at -80°C until further use. Chips and samples were distributed equally into four groups for hybridization. The fragmented labelled cDNA was hybridized onto the human Gene Chip® HuGene 1.0

ST array in the hybridization furnace (Affymetrix, High Wycombe, UK). Staining and washing was performed in the fluidic station (Affymetrix, High Wycombe, UK) using the Affymetrix Gene Chip washing and stain kit (Affymetrix, High Wycombe, UK). Finally the chips were scanned on an affymetrix scanner using the CommandConsole software.

2.3.3.4. Data analysis

Quality control and normalization was performed R- based using the xps package from Bioconductor. Quality control data were visualized using arrayQualityMetrics 1.8.1 under R 2.8.1. Statistical evaluation of the data was performed using the significance analysis of microarrays (SAM) (Tusher et al.2001) and the Spotfire Decision Site® from TIBCO (Munich, Germany) setting the false discovery rate to < 5% and consider expression changes of >1.6-fold to be relevant. Genes have been clustered using the software “cluster” version 2.11 written by Michael Eisen⁸⁴.

2.4. *Ex vivo/ in vivo experiments*

2.4.1. Animals

Male SCID mice (CB17/lcr-Prkdc^{SCID}/CrI) aged 8-10 weeks were housed in individually vented cages under specific pathogen free conditions with a 12h day/night cycle and with food and water ad libitum.

2.4.2. Tumor models

PC3 cells were cultured as described above. Cells were cultured without antibiotics for at least 3-4 passages, before tumor implementation and were harvested when reaching approx. 70% confluence. After washing with PBS 10^6 PC3 cells in 100 μ l PBS were injected subcutaneously with a 25G needle (Braun, Melsungen, Germany) into the flank of the mice.

2.4.3. Tumor Measurement

Animals were controlled regularly for tumor progression. When the tumor volume reached a size of at least 10mm³, tumor progression was monitored with a digital measuring slide (Digi-Met, Preisser, Gammertingen). Each measurement consisted of three diameters each 90° apart and tumor volume was calculated by the formula $axbxc \times 0.4$ (with a, b and c indicating the three diameters).

All animal procedures were approved and controlled by the local ethics committee and carried out according to the guidelines of the German law of protection of animal life.

2.4.4. Chemotherapy

The chemotherapeutical drug CPA (Cyclophosphamide, Sigma, Taufkirchen) was solved in PBS at a concentration of 10mg/ml followed by sterile filtration (0.22 μ m sterile filter, Millex-GV, Millipore Carrigtwohill, Ireland). Application was performed intraperitoneally. The CPA solution was administered with a 25 G needle (Braun, Melsungen). The application of the CPA solution was carried out every 6th day. The single dose of each application was based on animal body weight. Toleration of the treatment with CPA was monitored by regular measurement of body weight. The vehicle group (PBS) and the drug treatment group (CPA dissolved in PBS) were housed separately.

2.4.5. Tumor Histology

2.4.5.1. HE stain

Cryosections of the tissue was fixed with 4% paraformaldehyde and stained with Haematoxilin (Sigma, St. Loius, USA) for 30 min. After a washing step with PBS and aqua dest., sections were incubated with a 1:100 dilution of Eosin (Sigma, St. Louis, USA) for 4 min. Afterwards, sections were washed with aqua dest., embedded with PBS and analyzed by transmission light microscopy. Analysis was performed with an Anxiovert 200 microscope (Zeiss, Jena, Germany).

2.4.5.2. Immunohistochemistry

Cryosections (5 μ m) were transferred to a microscope slide and fixed with 4% paraformaldehyde (in PBS) for 5 min. Afterwards, tissue sections were rehydrated and washed with the blocking solution (PBS containing 5% FBS) prior to antibody incubation.

Simultaneous staining for laminin and endothelial marker CD31:

Staining was performed with the rabbit-anti-laminin antibody (Chemicon Europe, Hampshire, UK) and simultaneous with the rat-anti-mouse CD31 (CALTAG, Burlingame, USA) antibody; both antibodies were used in a 1:200 dilution (in the blocking solution). After an incubation time of 12h at 4°C in a humidified atmosphere, sections were washed repeatedly with the blocking solution followed by secondary

antibody staining. Therefore the sections were incubated with the Texasred labelled goat-anti-rabbit antibody (Vector, Burlingame, UK) and the ALEXA488 labelled goat-anti-rat antibody (Invitrogen, Oregon, USA); the staining was performed with a 1:200 dilution (in blocking solution) of both antibodies for 2h at room temperature in a humidified atmosphere. Before analysis by fluorescence microscopy, sections were washed with the blocking solution repeatedly. Analysis was performed with a Anxiovert 200 microscope (Zeiss, Jena, Germany) using appropriate filter sets.

2.4.6. Isolation of tumor/organs

2.4.6.1. For Histology

Tumors were dissected from the flank of sacrificed mice and embedded into cryo conservation medium (OCT tissue Tak, Sakura, USA) previous to freezing at -20°C , -80°C for long term storage.

2.4.6.2. For Microarray analysis

PC3-wt, PC3-A3, PC3-D3 and PC3-D4 were implanted subcutaneously and were grown as Xenografts for 10 days for the reisolated cells (PC3-A3, PC3-D3 and PC3-wt) respectively for 17 days for the parental PC3-wt cells until they reached a mean volume of 35 mm^3 . At day 9 respectively 16 one group of each subline was treated with 120mg/kg CPA and the other group was used as untreated control. 24h after CPA application tumors were dissected from the flank of sacrificed mice and were divided into two parts. One half was embedded for histology as described in 2.4.6.1 and the other half was cut into small pieces ($\varnothing 0.5\text{ mm}$). Randomly half of the pieces were collected and embedded in RNAlater (Ambion, Darmstadt, Germany) for RNA conservation. The rest of the pieces were prepared for FACS analysis as described in 2.3.3.

2.4.7. Reisolation of tumor cells

2.4.7.1. Isolation of tumor cells for cell culture

For the reisolation of tumor cells, mice were sacrificed with CO_2 . The skin was cleaned and sanitized by isopropanol (70% in water v/v) followed by drying under sterile conditions. Tumors were collected and immediately inserted in the indicated Penstrep (Biochrome, Germany) containing RPMI medium. Tumor tissue was reduced to small pieces under sterile conditions. This procedure was repeated until

tumor tissue was homogenized. The obtained homogenized cell suspension was diluted with fresh medium, followed a centrifugation step (150g/5min). The supernatant was removed and the tumor cells were resuspended in fresh, Penstrep containing medium. The tumor cell containing suspension was transferred to collagen coated (Collagen G, Biochrom) tissue flasks (TPP, Switzerland) and incubated under standard conditions (37°C, 5% CO₂) in a humidified atmosphere for 2-3 days. When cells were attached to the bottom of the flasks, medium was replaced every second day, until cells reached a confluence of about 70%. Obtained cells were cultured for 2 passages before harvested by tyrpsin/EDTA treatment. Reimplantation studies were performed by injection of 10⁶ PC3 tumor cells at a passage number of 4-5.

3. Results

3.1. Colon cancer

3.1.1. Fragmentation of lamin A/C in multicellular spheroid cultures of low passage colon cancer cells

3.1.1.1. Lamin A/C fragmentation in multicellular spheroids

Previous proteomics data obtained from multicellular spheroid cultures compared to the corresponding monolayer cultures of low passage colon cancer cells revealed several differentially regulated protein candidates. In order to characterize these candidates in detail, western blot analysis and immunostaining was performed. Western blot analysis confirmed the down-regulation of acidic calponin in 3D cultures of COGA-5 and COGA-12 cells and revealed the presence of a lamin A/C fragment (approximately 30 kDa) in COGA-5 spheroids in addition to the intact lamins A and C (**Figure 11 A, B**).

The focus of the present work was on the role of the lamin A fragment detected in multicellular spheroids by 2DE. Immunoblot analysis further revealed that the lamin A/C fragment was also detectable in partly compact COGA-12 aggregates (**Figure 11B**). Notably, expression of lamin A/C and lamin A cleavage was less pronounced in COGA-12 aggregates compared to COGA-5 spheroids.

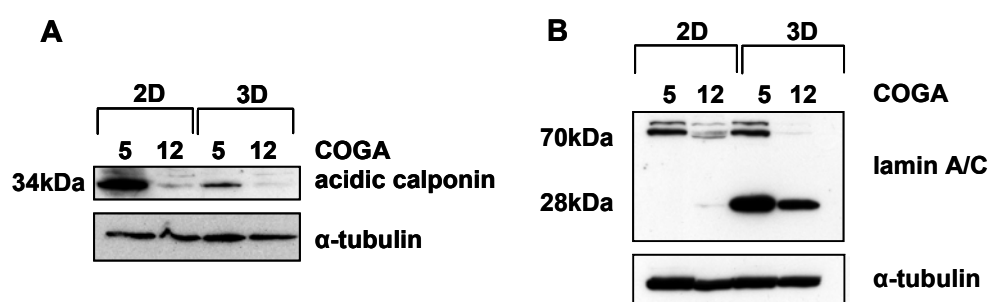


Figure 11: (A) WB of acidic calponin in 2D and 3D cultures of COGA-5 and COGA-12 cells (B) lamin A/C expression in 2D and 3D cultures of COGA-5 and COGA-12 cells

The fragmentation of lamin A was already present after 24 h in COGA-5 spheroids but increased in more compact spheroids, e.g. 96 h after spheroid formation (**Figure 12**).

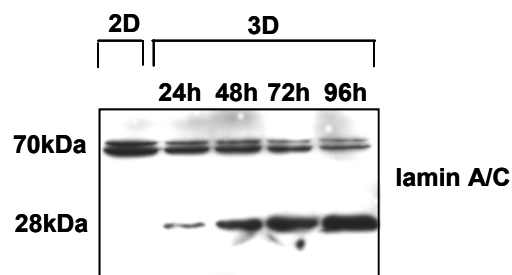


Figure 12: Time course of lamin fragmentation in 3D cultures of COGA-5

TUNEL staining at different time points 24 h and up to 120 h after formation of COGA-5 spheroids revealed that the number of apoptotic cells also increased with time similar to the rising levels of fragmented lamin A in the COGA-5 spheroids (**Figure 13**).

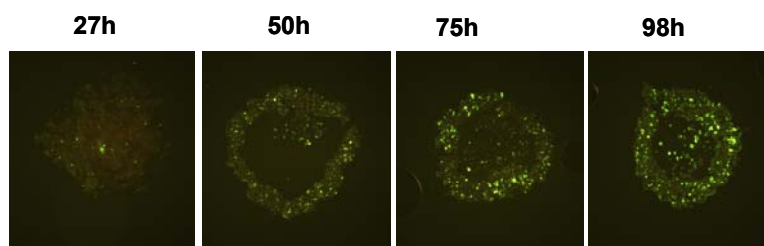


Figure 13: TUNEL stain of COGA-5 spheroids at different time points after spheroid formation

3.1.1.2. Lamin A/C fragmentation in monolayer cultures after serum withdrawal

Since COGA-5 spheroids were more compact and expressed more lamin A/C fragment compared to COGA-12 aggregates, we addressed the question whether the presence of truncated lamin A/C in spheroids could be associated with the lack of oxygen and/or trophic support, conditions known in compact areas of the spheroids⁸⁵. Mimicking these conditions in monolayers western blot analysis revealed that the lamin A/C fragment was detectable in monolayer cells after serum withdrawal (**Figure 14**). Hypoxia further enhanced the level of the protein fragment in cultures deprived of serum, whereas hypoxia alone was not sufficient to induce a lamin A fragmentation in cells cultured with medium containing 10% serum. The fragment was also detected in cells cultivated in medium with reduced serum concentration (2%) when simultaneously exposed to hypoxia (**Figure 14**).

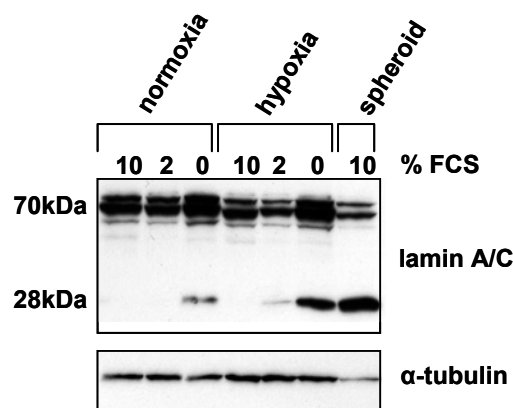


Figure 14: Lamin A/C fragmentation after serum withdrawal and hypoxia

3.1.1.3. Caspase mediated lamin A/C fragmentation

It has been suggested that lamin A/C is cleaved in a caspase-dependent manner during apoptosis⁸⁶. To confirm the involvement of activated caspases in the observed lamin A/C fragmentation in monolayer cultures, we applied the pan caspase inhibitor zVAD-fmk (10 and 50 μ M) during serum deprivation. Caspase inhibition abolished the appearance of the lamin A/C fragment after serum deprivation in a dose-dependent manner (**Figure 15A**). Further, the caspases 6-specific inhibitor zVEID-fmk (50 μ M) significantly attenuated the cleavage of lamin A/C (**Figure 15B**) in spheroid cultures of COGA-5 cells confirming that the observed lamin cleavage was mediated by caspase-6.

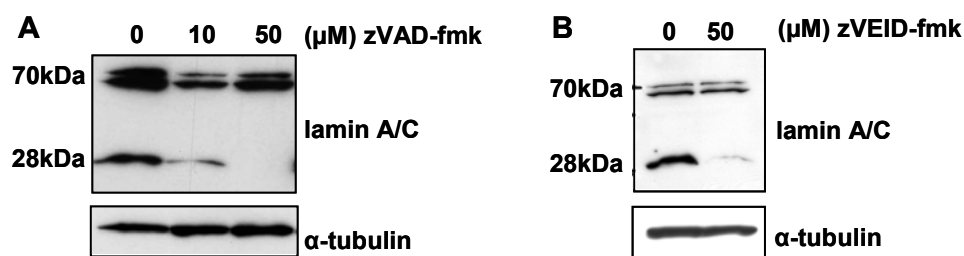


Figure 15: Lamin A/C fragmentation is inhibited by (A) a pan caspases inhibitor (B) a caspases 6 inhibitor.

Western blot analysis using an antibody specific against caspase-cleaved lamin A fragment confirmed the previously observed lamin A/C fragment in monolayer cells challenged by serum withdrawal as a product of caspase cleavage (**Figure 16**). Such stress-induced caspase cleavage product was observed in cells deprived of serum in normoxia as well as in hypoxic conditions.

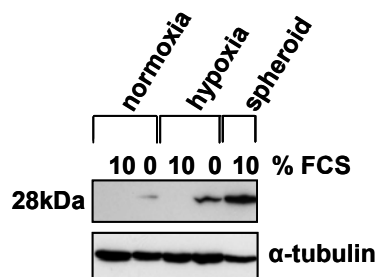


Figure 16: Caspase 6 cleavage product of lamin A in serum-deprived monolayer cultures. COGA-5 cells were incubated for 24 h at hypoxic and normoxic conditions and different amounts of growth factors. Lamin A/C fragment expression was analyzed by Western blot analysis using an antibody specific against the caspase cleavage product of lamin A. Results obtained in spheroid culture are given for comparison.

In COGA-5 spheroids, immunocytochemistry revealed high levels of caspase-cleaved lamin A in individual cells that were distributed throughout spheroid without restriction to inner areas (**Figure 17**). It is important to note that in most cells positive for fragmented lamin A/C the nuclei appeared pyknotic or fragmented, indicating that enhanced lamin cleavage occurred in cells undergoing apoptotic cell death.

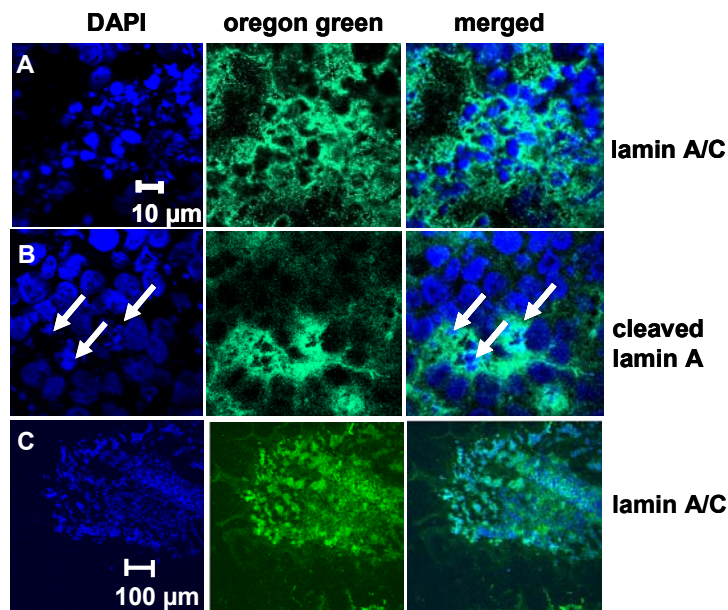


Figure 17: Distribution of lamin A/C and its caspase cleavage product within spheroids. Cryosections of COGA-5 spheroids were incubated with antibodies against full length lamin (A) and cleaved lamin (B) followed by a biotinylated antibody which was visualized by oregon green-streptavidin (green). The sections were analyzed by confocal microscopy. Control sections were only incubated with a biotinylated secondary antibody, counterstaining was performed with DAPI (blue). Arrows mark pyknotic nuclei from apoptotic, cleaved lamin positive cells. Photomicrographs representative for the whole spheroid are shown. (C) Overview of the distribution of lamin A/C and its caspase cleavage product within spheroids. Cryosections of COGA-5 spheroids were incubated with an antibody against full length lamin recognizing also the fragmented lamin of 28 kDa followed by a biotinylated antibody which was visualized by oregon green-streptavidin (green). The sections were analyzed by confocal microscopy. Sections of whole spheroids are shown. Control sections were only incubated with a biotinylated secondary antibody, counterstaining was performed with DAPI (blue).

Since we could observe caspases-6 dependent lamin A cleavage in multicellular spheroids, we further investigated if other caspases-6 substrates, e.g. cytokeratin 18 (CK18), 9 were also cleaved during the apoptotic process in COGA-5 spheroids or COGA-12 aggregates. Western blot analysis revealed CK18 cleavage in both three dimensional cultures (**Figure 18**). Notably, induction of COGA cell apoptosis by 5-fluorouracil (5-FU) or camptothecin was also accompanied by cleavage of lamin A and CK18, suggesting activation of similar caspase-dependent cell death pathways in COGA cells after spheroid formation, by deprivation of trophic support and hypoxia, or after exposure to chemotherapeutics.

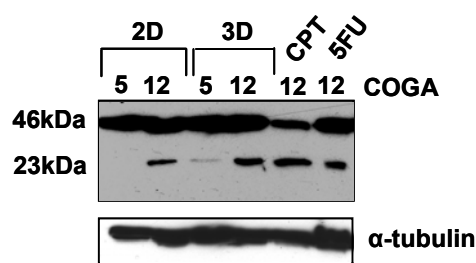


Figure 18: Expression of cytokeratin 18 (CK18) in 96 h old 3D cultures of COGA 5 and COGA 12 compared to corresponding monolayer cultures and after 3 days treatment with chemotherapeutics such as camptothecin (25 μ M) and 5-fluorouracil (5-FU) (20 μ M).

3.1.2. 5-FU chemoresistance in low passage colon cancer cells in vitro

3.1.2.1. HSP27 expression in chemoresistant colon cancer cells

The protein spot identified as Hsp27 on the 2D gel was detected only in chemosensitive COGA-12 cells and not in corresponding 5-FU resistant COGA-12/G6 cells. In order to reveal if this protein regulation is due to decreased mRNA levels a semi-quantitative RT-PCR analysis was performed. It revealed lower levels of HSP27 mRNA in resistant COGA-12/G6 cells compared to 5-FU sensitive COGA12 (**Figure 19A**). Densitometry performed from three independent results confirmed significant HSP27 mRNA down regulation in COGA-12/G6 cells (**Figure 19B**).

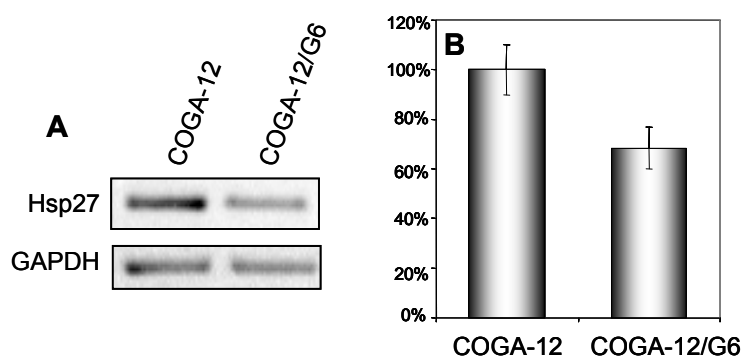


Figure 19: Hsp27 mRNA level in COGA-12 and COGA-12/G6 cells. (A) Gel-electrophoresis of RT-PCR products using HSP27-primer and GAPDH-primer on COGA 12-cells and COGA-12/G6-cells respectively. (B) Grey value analysis of COGA12 and COGA-12/G6 cells from three independent experiments.

Further validation of the 2DE data on protein level was performed by western blot analysis. Down-regulation of Hsp27 in 5-FU resistant COGA-12/G6 cells compared to corresponding parental COGA-12 cells could also be confirmed by western blot analysis. Hsp27 is down-regulated in COGA-12/G6 cells with and without CPA therapy whereas Hsp27 levels are higher in chemosensitive COGA-12 cells when treated with 5-FU (Figure 20).

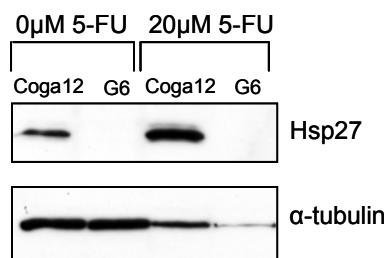


Figure 20: Western blot analysis of Hsp27 in non resistant COGA-12 and chemoresistant COGA-12/G6 cells under influence of 5-FU treatment

In order to determine the functional relationship between the lower Hsp27 expression and the 5-FU resistance in COGA-12/G6 cells, Hsp27 was knocked down in chemosensitive COGA-12 cells by siRNA transfection. Therefore a Hsp27 specific siRNA sequence previously published by Rocchi et al. 2006 as well as a Dicer product established in our lab was used⁸⁷. Hsp27 siRNA transfected cells were re-seeded and treated with 5-FU 24 h after re-seeding. The knockdown of Hsp27 was controlled on mRNA level by RT-PCR 48 hours after transfection with Hsp27 siRNA. A clear knockdown could be detected in all COGA-12 cells transfected with Hsp27 specific siRNA as well as with different concentrations of the Hsp27 Dicer product.

However, scrambled control siRNA did not induce any unspecific knockdown of Hsp27 in COGA-12 cells at the used concentration of 40nM (**Figure 21**).

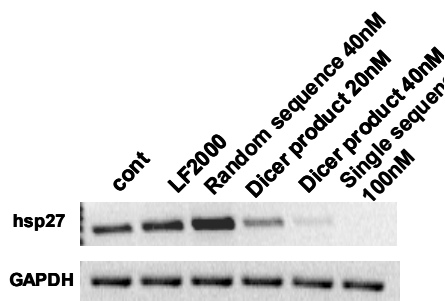


Figure 21: Hsp27 mRNA levels in COGA-12 cells 48 h after siRNA application. Gel-electrophoresis of RT-PCR products of Hsp27 mRNA from COGA12 cells transfected with HSP27 siRNA. Controls received Opti-MEM (-LF), lipofectamine 2000 (LF) or 40 nM non-functional siRNA.

Cell viability was analyzed 72 h after 5-FU treatment by MTT-assay (**Figure 22**). HSP27 siRNA did not increase cell metabolic activity after 5-FU treatment compared to any of the controls.

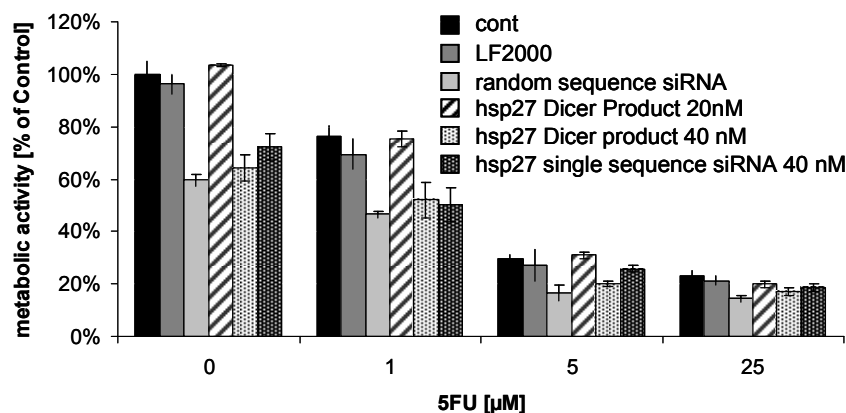


Figure 22: Cell viability of COGA12 transfected with X nM HSP27 siRNA was determined by the MTT assay 3 d after exposure to 5-FU. Controls received lipofectamine 2000 (LF) or 40 nM non-functional siRNA.

3.1.2.2. Thymidylate synthase (TS) mRNA levels in chemoresistant colon cancer cells

Up-regulation of mRNA levels of TS, the main target of 5-FU, is a classical resistance mechanism in 5-FU chemotherapy. As no functional relationship between down-regulation of Hsp27 and 5-FU resistance in COGA-12/G6 cells could be detected, it was tested if any classical 5-FU resistance mechanism which was not obvious by 2DE could be involved in resistance. Therefore the mRNA levels of TS were determined by RT-PCR and normalized to GAPDH levels in COGA-12 and COGA-

12/G6 cells (**Figure 23**). Indeed, RT-PCR revealed higher mRNA levels of TS in COGA-12/G6 cells than in parental COGA-12 cells.

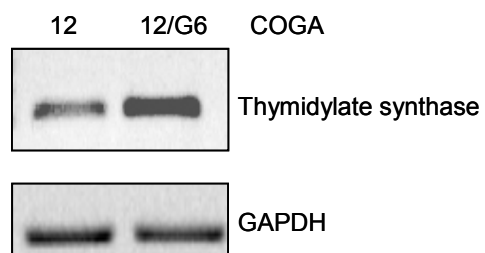


Figure 23: mRNA levels of thymidylate synthase. Gel-electrophoresis of RT-PCR products of thymidylate synthase mRNA from COGA-12 and COGA-12/G6 cells.

3.2. Chemoresistance in metronomic cyclophosphamide therapy of prostate cancer xenografts: an *in vivo* chemoresistance

3.2.1. Generation of an appropriate *in vivo* passaged control

PC3-A3 cells have been reisolated from PC3-wt xenografts which have been grown *in vivo* without metronomic CPA treatment. Reisolation was performed as for the previously reisolated PC3-D3 and PC3-D4 cells (see 2.4.7.1)

3.2.1.1. Morphology

In order to control the identity of the reisolated *in vivo* passaged PC3-A3 cells their morphology after reisolation was examined by transmission light microscopy in comparison to corresponding PC3-wt cells. No major morphological changes compared to the PC3-wt cells could be observed in PC3-A3 cells (**Figure 24**).

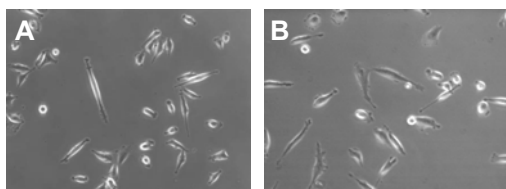


Figure 24: Morphologies of (A) PC3-wt and (B) reisolated *in vivo* passaged PC3 cells (PC3-A3).

3.2.1.2. Receptor status

As PC3-wt cells highly express the human EGF- receptor (EGFR) as well as the human transferrin receptor (CD71) human specific antibodies against these two receptors were used to prove the human origin of reisolated cells and their similarity to PC3-wt cells in terms of characteristic cell surface expression. **Figure 25** displays that 99.9% of PC3-A3 cells show expression of hEGFR and 95.6% expression of human CD71 receptor which is similar to expression levels in PC3-wt and PC3-D3, PC3-D4⁷⁸.

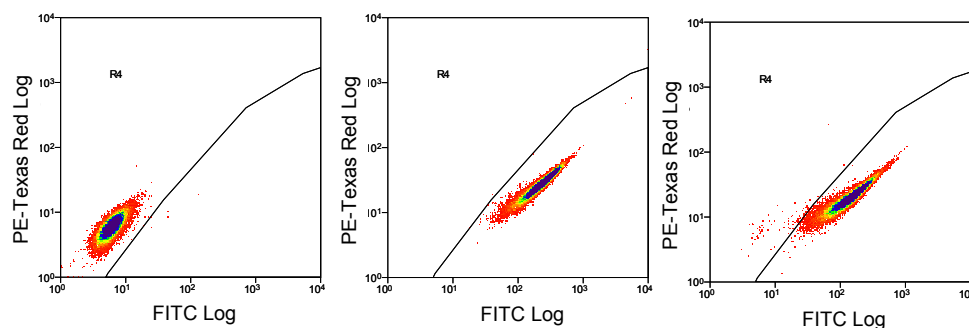


Figure 25: Receptor status for human EGF receptor and human CD71 on reisolated *in vivo* passaged PC3-A3 cells.

3.2.2. Drug efflux activity of reisolated PC3 cells

To consider up-regulation of drug efflux pumps as possible resistance mechanisms, Hoechst dye efflux assay was performed. In none of the tested cell lines PC3-D3, PC3-D4 (resistant) and PC3-A3 (in vivo passaged) a distinctive side population, characterized by higher efflux of the Hoechst 33342, was detected. Co-treatment with Verapamil and Hoechst 33342 confirmed the absence of a Verapamil sensitive side population (Figure 26).

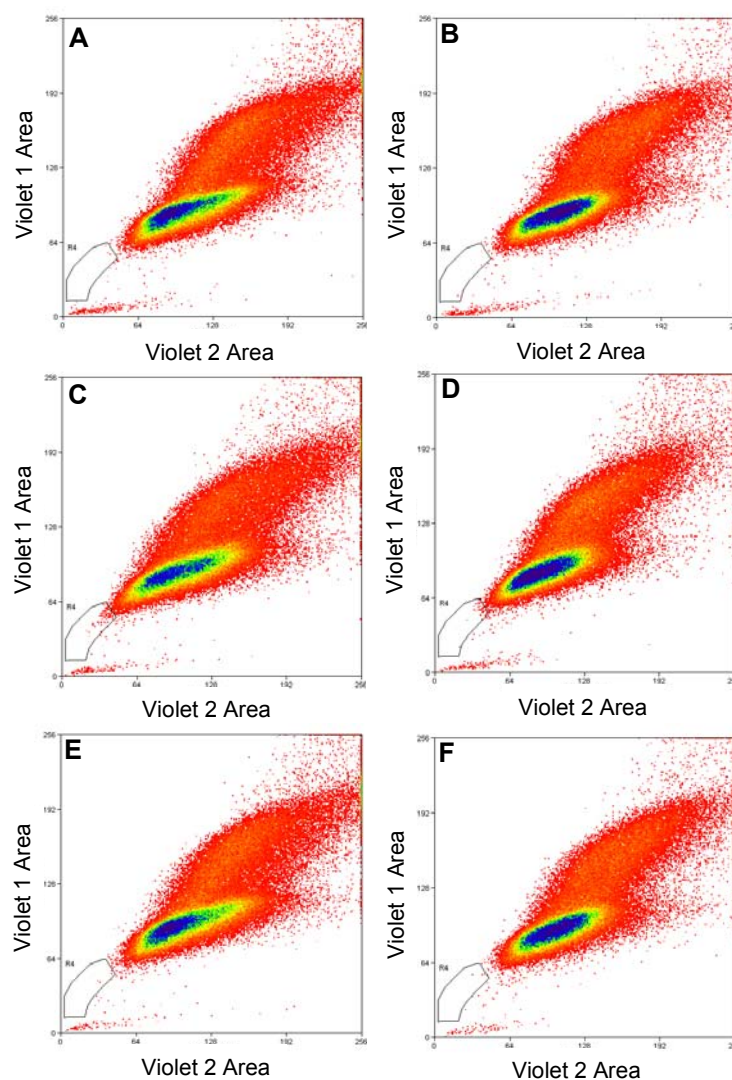


Figure 26: Efflux pump activity was measured for PC3-A3 control cells and resistant variants PC3-D3 and PC3-D4 by incubation with Hoechst 33342 dye in the presence of Verapamil (A, C and E) and in the absence of Verapamil (B, D F). A distinctive population with decreased fluorescent signal, indicating increased pump activity was not detectable for all tested PC3 cell lines. Furthermore, no differences in Hoechst dye uptake were detectable, when Hoechst dye 33342 incubation was performed in the presence of Verapamil compared to samples incubated in the absence of Verapamil. The study was performed in three biological and two technical replicates, respectively.

3.2.3. Proliferation of reisolated cells under hypoxic conditions

5000 cells of each reisolated PC3 cell line (PC3-A3, PC3-D3 and PC3-D4) were seeded into 6-well plates and were cultivated up to seven days at either normoxic or hypoxic (0.1% O₂) conditions. Proliferation was determined by measuring DNA content using Hoechst 33342 based proliferation assay. Under normoxia reisolated PC3 cells from resistant tumors (PC3-D3 and PC3-D4) did not show increased proliferation compared to in vivo passaged PC3-A3 cells. Also hypoxia did not reveal significantly increased proliferation within the resistant PC3 cells. However, PC3-D4 cells showed a tendency of proliferation advantage after seven days of cultivation under hypoxic conditions (**Figure 27**)

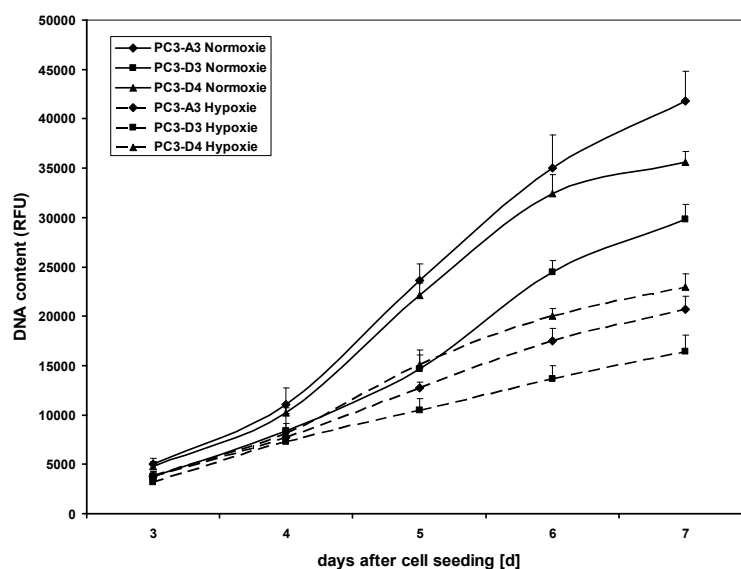


Figure 27: Proliferation of reisolated PC3 cells under normoxic and hypoxic conditions.

3.2.4. Reimplantation of reisolated PC3 cells

3.2.4.1. Resistance of reimplanted PC3 (PC3-D3 and PC3-D4) towards metronomic CPA therapy in vivo

Reisolated PC3 tumor cells PC3-D3 and PC3-D4 derived from tumors resistant towards metronomic CPA therapy in previous studies which did not manifest their resistance in vitro (**Figure 7**) were implanted in the flank of male SCID mice. On day 10 after tumor implantation, when average tumor volume reached 28 mm³, mice were again subject to CPA treatment (120mg/kg, every six days). In contrast to achieved growth delay of parental tumors in the first CPA treatment and in the group with PC3-wt cells (**Figure 7B**), in the case of reimplantated PC3-D3 and PC3-D4 tumors only a

weak growth retardation effect was detectable (**Figure 28**). Control tumors as well as treated D3 and D4 tumors showed an average tumor volume doubling time of approximately three days (**Figure 28**). Metronomic scheduled CPA was again well tolerated, indicated by no significant loss in body weight (data not shown).

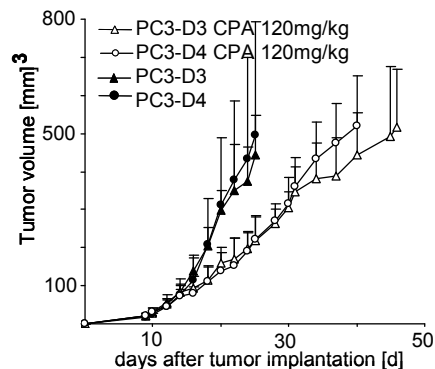


Figure 28: Tumor growth of reimplanted PC3 cancer cells. Resistant CPA treated tumors (PC3-D3 and PC3-D4) were cultured *in vitro* and after several passages implanted again *sc* in male SCID mice. Mice were treated with 120mg/kg every sixth day. (n=5 for control and CPA treated animals).

3.2.4.2. Chemosensitivity of reimplanted *in vivo* passaged PC3 cells (PC3-A3)

In a control experiment 10^6 *in vivo* passaged control tumor cells (PC3-A3) and PC3-wt cells were injected subcutaneously into the flank of SCID mice. Metronomic CPA therapy (120mg/ kg CPA every six days) was started at day 14 after tumor cell implantation. Despite an innate increased proliferation rate *in vivo*, PC3-A3 cells showed similar chemosensitivity towards metronomic CPA therapy as parental PC3 cells (PC3-wt) for a treatment period of 42 days (**Figure 29**).

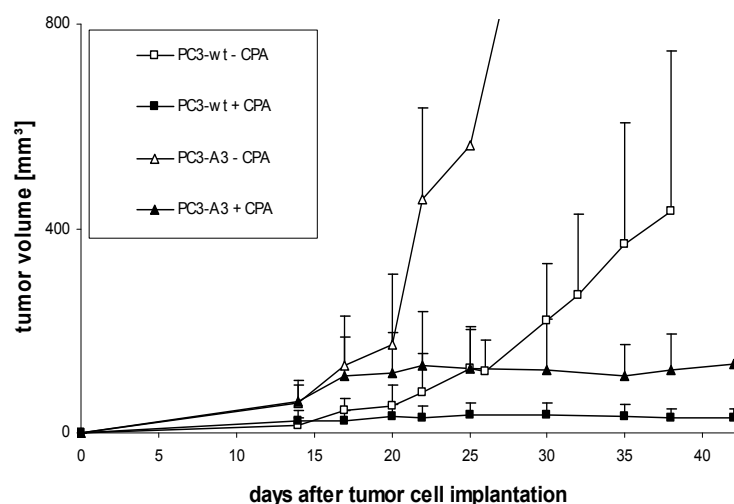


Figure 29: Tumor growth of reimplanted *in vivo* passaged PC3 cancer cells. *In vivo* passaged CPA treated tumors (PC3-A3) were cultured *in vitro* and after several passages implanted again *sc* in male SCID mice. PC3-wt served as control. Mice were treated with 120mg/kg every sixth day. (n=5 for control and CPA treated animals).

3.2.5. Expression of vascular markers and functionality of tumor blood flow in reimplanted tumors

To determine the angiogenic potential of the different reimplanted cell lines PC3-D3, PC3-D4 (resistant) and PC3-A3 (in vivo passaged) and to follow possible antiangiogenic effects of the treatment, quantification of functional tumor blood flow was again determined by using Hoechst dye as a tracer. The initial functional blood flow in the resistant tumors, compared to PC3-A3 did not show any significant differences. The treatment regimen (120mg/kg, every six days) resulted in slightly reduced blood supply for PC3-A3 and the resistant tumors in a similar extent. However, after two cycles of CPA application, blood flow reduction was statistically significant neither in resistant tumors nor in PC3-A3 in comparison to the initial blood flow in untreated animals.

Vasculogenic mimicry was already described in prostate cancer and prostate cancer xenografts and would be a possible escape mechanism from antiangiogenic treatment approaches⁴⁷. Therefore, reimplanted resistant PC3-D3 and PC3-D4 were analyzed for vascular markers in combination with functional blood flow using Hoechst 33258 as a tracer. Analysis was performed before and after two applications of CPA. Vasculogenic mimicry was neither detectable in untreated tumors PC3-D3 and PC3-D4 nor under therapeutic pressure. All functional blood channels within the tumors, indicated by Hoechst fluorescence, were detected to be associated with vascular markers by the host (**Figure 30**). Co-staining of murine and human laminin in combination with staining for murine endothelial cells and functional blood flow confirmed the absence of functional laminin containing structures without participation of murine endothelial cells (**Figure 30**).

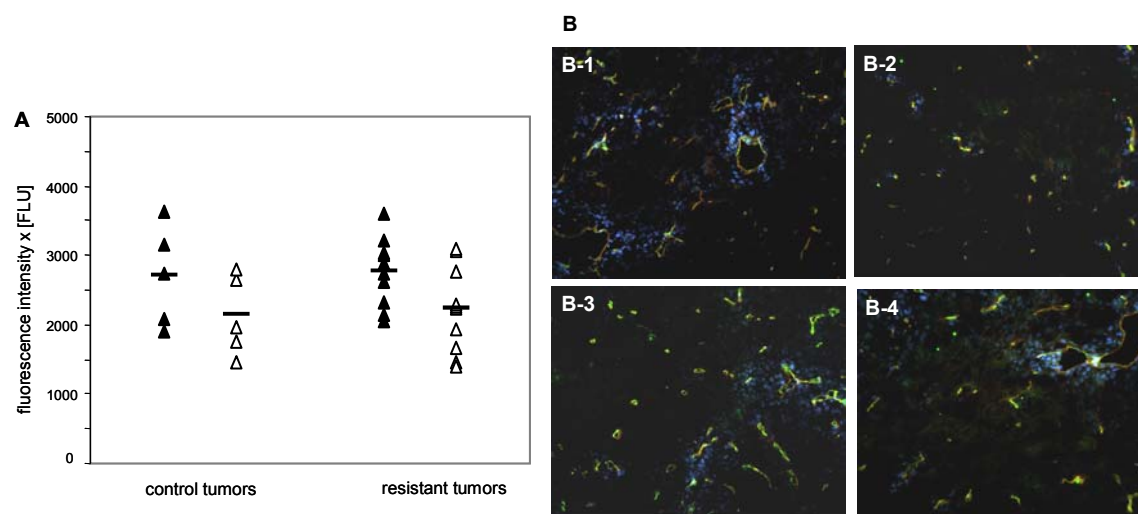


Figure 30: Reimplanted control tumors PC3-A3 and resistant variants PC3-D3 and PC3-D4 were analyzed after a 14 day treatment for functional blood flow (A). Hoechst dye 33258 was used as a tracer. Quantified fluorescence signal in tumors obtained from untreated control animals are represented by filled symbols. Quantified Hoechst fluorescence in tumors obtained from treated animals are represented by open symbols. Twelve sections per tumor were examined and three areas per section were randomly selected for image analysis. Cryosections (5 μ m) of reimplanted, untreated PC3-D3 (B-1) and PC3-D4 (B-3) and CPA treated tumors PC3-D3 (B-2) and PC3-D4 (B-4) were fixed with 4 % PFA and stained with an antibody detecting human and murine laminin (orange) and murine CD31 (green). Functional blood flow was visualized by intravenous application of Hoechst 33258 dye (blue). No functional blood flow was detected in areas without murine CD31 staining. For analysis, antibody staining was performed for two tumors of each group.

3.2.6. 2D-DIGE analysis of reisolated in vivo resistant PC3-D3 and PC3-D4 cells versus PC3-wt cells

3.2.6.1. Different protein expression pattern in resistant versus wt PC3 cultures

PC3-wt, PC3-D3 and PC3-D4 were grown in standard monolayer cultures, and cell extracts of both reisolated PC3 cell lines (PC3-D3 and PC3-D4) and the parental PC3-wt cell line were subject to 2D-DIGE (Figure 31). Proteome analysis revealed different expression of seven protein spots in PC3-D3 cells compared to the PC3-wt (four up- and three down-regulated) (Figure 31A) and altered expression of 18 protein spots in PC3-D4 compared to PC3-wt (nine up- and nine down-regulated) (Figure 31B). Only proteins, where the average normalized signals of all spots were increased respectively decreased more than 1.6 fold were taken into account. Three spots were up-regulated (D3-1/D4-2, D3-3/D4-1, D3-4/ D4-5), one spot (D3-5/D4-14) down-regulated in both reisolated cell lines. The other spots were regulated only in either the PC3-D3 or the PC3-D4 compared to the PC3-wt (Figure 31C).

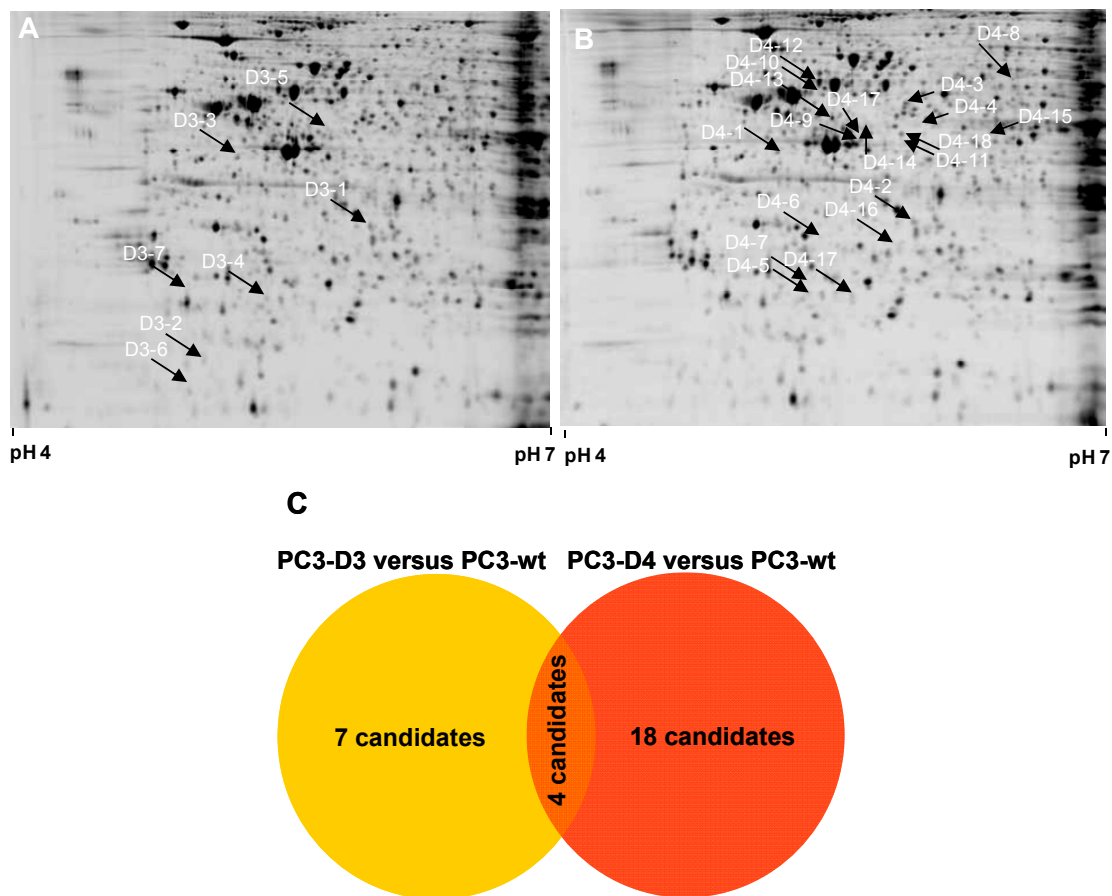


Figure 31: Differences in the expression profiles of resistant and their corresponding wildtype PC3 cells obtained by 2D-DIGE. 2D-DIGE of cell lysates of the cell lines PC3-wt and PC3 resistant were performed with IPG dry strips pH 4 - 7 in the first dimension and 11 % SDS-polyacrylamid gels in the second dimension. Representative DIGE-gels of protein regulations (A) between PC3-D3 and PC3-wt and (B) between PC3-D4 and PC3-wt are shown. (C) Overlap of the differentially expressed protein spots between PC3-D3 and PC3-D4.

3.2.6.2. Protein expression differences in PC3 cells due to in vivo passaging

In order to differentiate between protein regulations caused by in vivo passaging of the reisolated tumor cells the appropriate in vivo passaged control cells PC3-A3 have also been compared to the PC3-wt cells (Figure 32). This control experiment revealed eight differentially expressed protein spots between PC3-A3 and PC3-wt (two up-regulated and six down-regulated in PC3-A3).

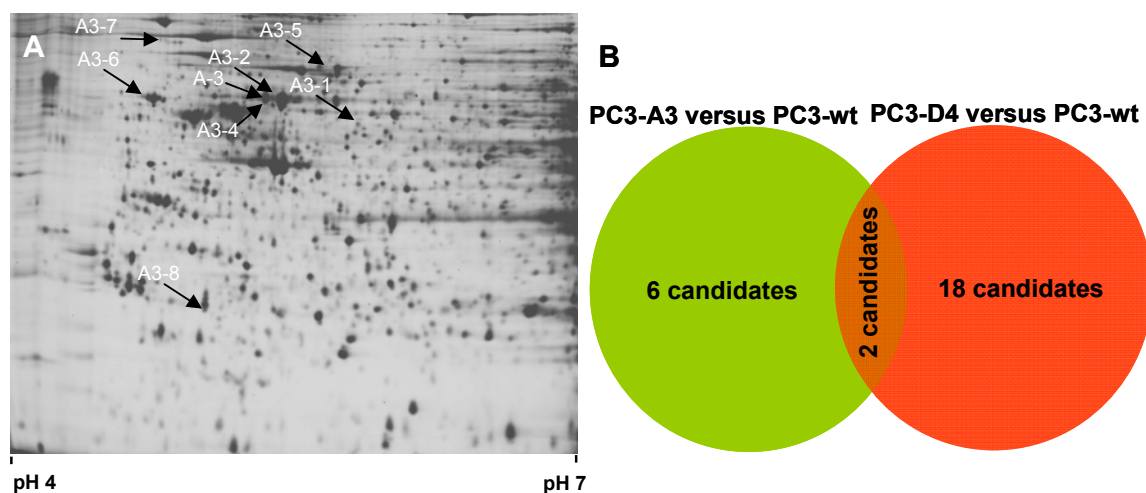


Figure 32: (A) Differences in expression profiles of *in vivo* passaged PC3-A3 cells and their corresponding wildtype PC3 cells obtained by 2D-DIGE. 2D-DIGE of cell lysates of the cell lines PC3-wt and PC3-A3 were performed with IPG dry strips pH 4-7 in the first dimension and 11% SDS-polyacrylamid gels in the second dimension. Representative DIGE-gels of protein regulations between PC3-A3 and PC3-wt are shown. (B) Overlap of the differentially expressed protein spots between PC3-A3 and PC3-D4.

Three spots A-1/D4-3, A-3/D4-12 and A-4/D4-10 showed similar regulations in PC3-A3 and PC3-D4 and also low non significant regulation in PC3-D3 compared to the PC3-wt (**Figure 32B**) but none of the four spots detected in both resistant PC3 cell lines could be detected as differentially expressed in PC3-A3 compared to the corresponding PC3-wt.

3.2.6.3. Mass spectrometry-based identification of differentially expressed proteins

Excised spots were trypsinized and analyzed by MALDI-PMF as well as MS/MS using MALDI-TOF-TOF or LC-MS/MS. MALDI-PMF data as well as MS/MS data were searched with Mascot search against the human IPI v348 database. As minimum criterion for successful identification Mowse protein score > 90 was chosen for PMF data, and in case of MS/MS analysis the presence of at least two spectra with ion score > 30 was mandatory: Using these criteria we succeeded in the identification of 25 spots. The results of the MALDI-MS spot identification are summarized in **Table 3** for the resistant cell line PC3-D3 compared to PC3-wt, in **Table 4** for the resistant cell line PC3-D4 compared to PC3-wt and in **Table 5** for PC3-A3 compared to PC3-wt cells.

spot no.	identified protein	Database	accession no.	T-test	Av. Ratio	theoretical MW (kDa)	exp. MW (kDa)	theoretical pI	exp. pI	protein score	sequence coverage %	no. of matched peaks
D3-1	Annexin A3	IPI human	IPI00024095	0.00032	1.82	36	30-40	5.6	5.7	920	68	33
D3-2	Programmed cell death protein 6 (ALG-2)	IPI human	IPI00025277	1.80E-05	1.75	21	15-20	5.1	4.9	354	46	16
D3-3	Keratin, Type I cytoskeletal 19	IPI human	IPI00479145	4.90E-05	1.75	44	40-45	5.0	5.0	1020	84	48
D3-4	cathepsin B precursor	IPI human	IPI00295741	2.70E-07	1.69	38	20-25	5.8	5.2	194	29	19
D3-5	thioredoxin domain 5 isoform 2	IPI human	IPI00395646	8.70E-06	-1.63	44	50-60	5.7	5.50	229	57	23
D3-6	similar to protein phosphatase 1 regulatory subunit 14B	IPI human	IPI00398922	1.10E-06	-1.77	21	15-20	5.1	4.80	91	12	2
D3-7	Isoform SNAP 23a of synaptosomal associated protein 23	IPI human	IPI00010438	3.00E-06	-1.78	23	20-25	4.9	4.80	311	62	19

Table 3: Differentially expressed proteins in PC3-D3 vs PC3-wt identified by MALDI TOF TOF MS

spot no.	identified protein	Database	accession no.	T-test	Av. Ratio	theor. MW (kDa)	exp. MW (kDa)	theor. pI	exp. pI	protein score	sequence coverage %	no. of matched peaks
D4-1	Keratin, Type I cytoskeletal 19	IPI human	IPI00479145	8.70E-08	2.16	44	40-45	5.0	5.0	882	69	41
D4-2	Annexin A3	IPI human	IPI00024095	9.80E-06	2.15	36.5	30-40	5.6	5.7	703	57	30
D4-3	Keratin, Typ II cytoskeletal 8	IPI human	IPI00554648	1.70E-06	1.90	54	40-50	5.5	5.6	741	59	45
D4-4	Leupaxin	IPI human	IPI00299066	9.60E-06	1.77	45	40-50	5.6	5.8	259	38	18
D4-5	Cathepsin B	IPI human	IPI00295741	2.70E-06	1.75	38	20-25	5.8	5.2	400	23	14
D4-6	Cathepsin B	IPI human	IPI00295741	8.60E-06	1.75	38	25-35	5.8	5.3	364	36	18
D4-7	Cathepsin B	IPI human	IPI00295741	4.50E-06	1.73	38	20-25	5.8	5.2	199	20	13
D4-8	Isoform 3 of UDP-N-acetylhexosamine pyrophosphorylase	IPI human	IPI00607787	2.10E-05	1.72	59	55-65	5.9	6.2	427	49	29
D4-9	Keratin, Type I cytoskeletal 18	IPI human	IPI00554788	2.20E-06	1.64	48	40-50	5.3	5.5	765	72	47
D4-10	HSPD1 60 kDa heat shock protein, mitochondrial	IPI human	IPI00784154	1.10E-08	-1.68	61	50-60	5.7	5.3	949	56	36
D4-11	Protein NDRG1	IPI human	IPI00022078	3.00E-06	-1.70	43	40-50	5.5	5.7	254	40	24
D4-12	HSPD1 60 kDa heat shock protein, mitochondrial	IPI human	IPI00784154	6.70E-09	-1.74	61	50-60	5.7	5.3	1100	67	49
D4-13	Thioredoxin domain-containing protein 5 precursor	IPI human	IPI00171438	4.10E-07	-1.80	44	40-45	5.8	5.4	616	61	29
D4-14	Thioredoxin domain-containing protein 5 precursor	IPI human	IPI00171438	1.20E-06	-1.84	44	40-45	5.8	5.5	240	18	7
D4-15	Pyruvate dehydrogenase E1 component subunit alpha, somatic form, mito (PDHA1)	IPI human	IPI00902645	2.70E-06	-1.93	44	45-50	8.3	6.2	409	50	23
D4-16	Latexin	IPI human	IPI00106687	4.60E-06	-2.29	26	25-30	5.5	5.7	108	13	2
D4-17	Protein NDRG1	IPI human	IPI00022078	6.20E-06	-2.45	43	40-50	5.5	5.6	235	15	6
D4-18	Protein NDRG1	IPI human	IPI00022078	1.10E-06	-2.47	43	40-50	5.5	5.7	371	25	9

Table 4: Differentially expressed proteins in PC3-D4 vs PC3-wt identified by MALDI TOF TOF MS

spot no.	identified protein	Database	accession no.	T-test	Av. Ratio	theor. MW (kDa)	exp. MW (kDa)	theor. pI	exp. pI	protein score	sequence coverage %	no. of matched peaks
A3-1	KRT8 Keratin, type II cytoskeletal 8	IPI human	IPI00554648	0.00019	-1.77	54	50-60	5.5	5.9	265	26	19
A3-2	HSPD1 60 kDa heat shock protein, mitochondrial	IPI human	IPI00784154	1.00E-04	-1.74	61	50-60	5.7	5.5	184	11	10
A3-3	HSPD1 60 kDa heat shock protein, mitochondrial	IPI human	IPI00784154	3.00E-03	-1.69	61	50-60	5.7	5.4	888	35	30
A3-4	HSPD1 60 kDa heat shock protein, mitochondrial	IPI human	IPI00784154	0.00051	-1.67	61	50-60	5.7	5.4	5521	64	221
A3-5	HSPA9 Stress-70 protein, mitochondrial	IPI human	IPI00007765	1.40E-02	-1.63	74	70-80	5.9	5.2	203	19	22
A3-6	P4HB Protein disulfide-isomerase	IPI human	IPI00010796	0.017	-1.62	58	50-60	4.8	5.7	108	10	10
A3-7	HCLS1 Hematopoietic lineage cell-specific protein*	IPI human	IPI00026156	0.0033	1.81	54	70-80	4.7	4.8	534	22	16
A3-8	ARHGDI1 Rho GDP-dissociation inhibitor 1*	IPI human	IPI00003815	1.20E-02	2.62	23	20-30	5.0	5.0	341	32	14

Table 5: Differentially expressed proteins in PC3-A3 vs PC3-wt identified by MALDI TOF TOF MS and LC-MS/MS. * Measured by LC MS/MS.

3.2.7. Validation of potential protein candidates

In order to validate the data obtained by 2DE several protein candidates were analyzed by western blotting in vitro and in vivo. For further validation, the four protein candidates similarly regulated in both resistant PC3 sublines were chosen.

3.2.7.1. CK19: the importance of validation of proteomics data

CK19 expression in vitro

Cytokeratin 19 (CK19), a protein previously associated with chemoresistance in MCF-7 breast cancer cells⁸⁸ was found to be up-regulated in PC3-D3 (1.8-fold) and PC3-D4 cells (2.2-fold) compared to corresponding PC3-wt cells by 2D-DIGE. However up-regulation could not be confirmed by western blot analysis of the corresponding protein extracts (**Figure 33**).

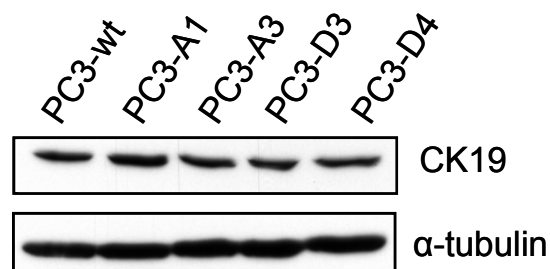


Figure 33: Western blot analysis of CK19 expression in PC3 monolayer cultures in vitro.

CK19 expression in vivo

The up-regulation of CK19 in both resistant PC3 sublines detected by 2D-DIGE could not be confirmed in cell extracts from in vivo tumor tissue. Furthermore, CPA treatment did not show a consistent influence on CK19 levels in PC3-D3 and PC3-D4 cells.

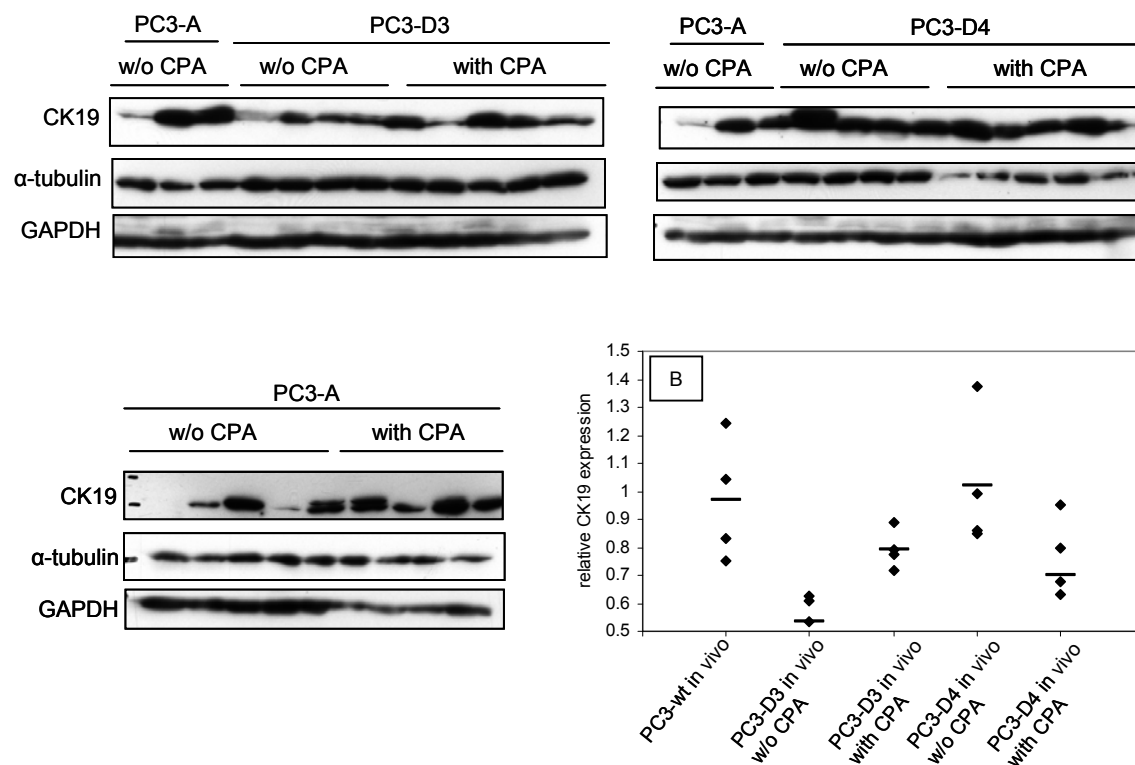


Figure 34: *In vivo* validation of CK19 regulation. Western blot analyses for CK19 of cell extracts from tumor tissue of resistant PC3-D3 and PC3-D4 tumors with and without metronomic cyclophosphamide treatment compared to tumors of PC3-wt with and without treatment. (B) Densitometric quantification of western blot analysis of CK19 from tumor tissue ($n=4$)

3.2.7.2. Mitochondrial localization of truncated Cathepsin B in chemoresistant PC3 cells

Spot D3-4 and D4-5 both of approximately 22 kDa with an isoelectric point (pI) of 5.2 represent cathepsin B, up-regulated in both resistant cell lines. In PC3-D4 cells there are two more spots with a molecular weight of 23 kDa (D4-6) and approximately 32kDa (D4-7) identified as cathepsin B (CatB). Western blot analysis of the corresponding protein extracts confirmed an upregulation of three cleavage products of cathepsin B in the resistant sublines (especially the PC3-D4) compared to the corresponding PC3-wt cells (**Figure 35**).

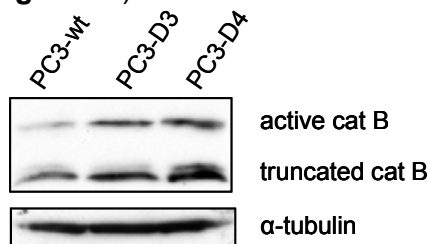


Figure 35: Western blot analysis of Cathepsin B expression in PC3 monolayer cultures *in vitro*.

Furthermore, western blots of isolated mitochondria from PC3-wt, PC3-D3 and PC3-D4 for CatB showed that the 32 kDa protein and a truncated version of the indicated protein (approximately 23 kDa) were localized to the mitochondria in the resistant sublines in contrast to the PC3-wt where it is located in the cytoplasm (**Figure 36**).

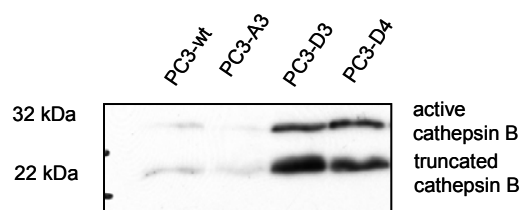


Figure 36: Western blots of isolated mitochondria from PC3-wt, PC3-D3 and PC3-D4 for cathepsin B showed that the 32 kDa protein and a truncated version of the indicated protein (approximately 23 kDa) localizes to the mitochondria in the resistant sublines.

The upregulation of the active form of CatB (32 kDa) and its truncated versions (22 kDa, 23 kDa) in the resistant PC3-D3 and/or PC3-D4 cells which was detected in the 2D-DIGE experiment and western blotting from PC3 monolayer cultures could not be confirmed by western blotting from cell extracts of the corresponding *in vivo* tumor material (**Figure 37**).

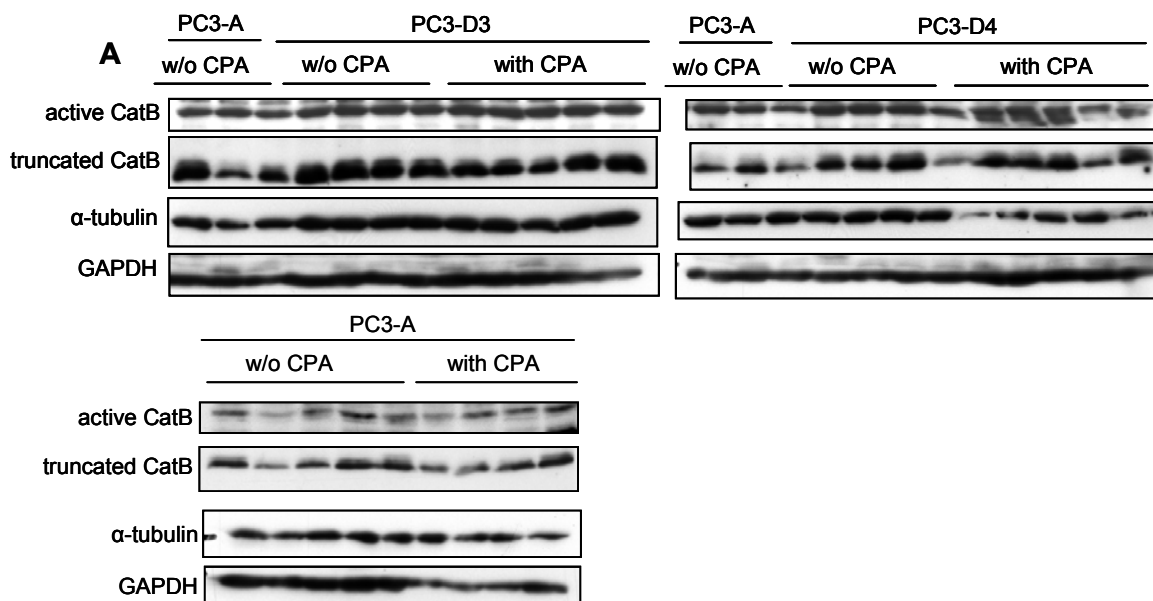


Figure 37A: *In vivo* validation of CatB regulation. Western blot analyses for CatB of cell extracts from tumor tissue of resistant PC3-D3 and PC3-D4 tumors with and without metronomic cyclophosphamide treatment compared to tumors of PC3-wt with and without treatment.

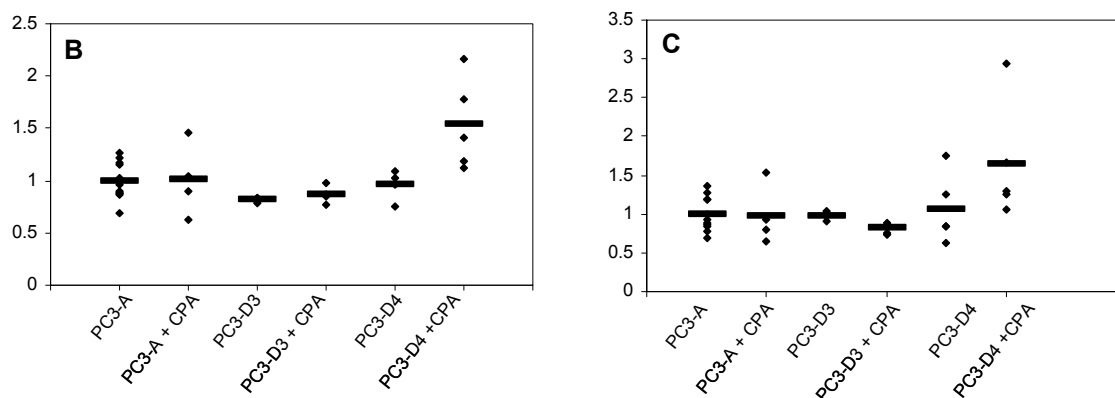


Figure 37B: Densitometric quantification of western blot analysis of protein extracts derived from tumor tissue. (B) quantification of the western blot protein band of active cathepsin (32 kDa). (C) Quantification of the western blot protein band detecting truncated cathepsin B (23k Da)

3.2.7.3. CPA inducible expression of TXNDC5 in chemoresistant PC3 cells

Low levels of TXNDC5 in vitro

Another protein changed in abundance in both resistant sublines was identified as thioredoxin domain containing protein 5 (TXNDC5). This protein was detected to be decreased in PC3-D3 by the factor of 1.6 (spot D3-5) and in PC3-D4 by the factor of 1.8 (spot D4-13 and D4-14) compared to the respective PC3-wt cells. Western blot analysis of the protein extracts in vitro confirmed these results (**Figure 38**).

TXNDC5 expression under hypoxia

Cultivation of reisolated PC3 cells under hypoxic conditions show reduction of TXNDC5 levels in all reisolated cells including the in vivo passaged PC3-A3 cells. This did not correlate with data obtained by 2D-DIGE where down-regulation had been specifically detected in resistant PC3 cells (PC3-D3 and PC3-D4) (**Figure 38**).

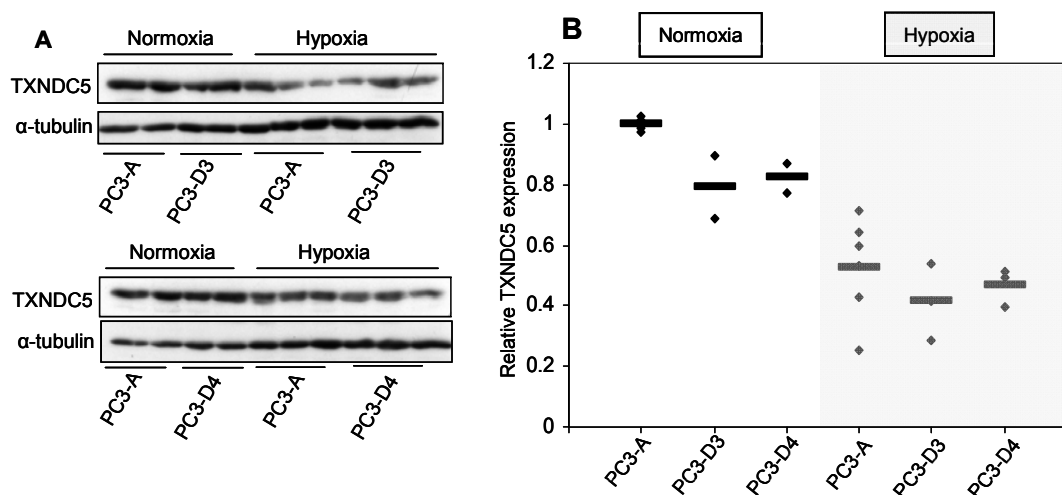


Figure 38: (A) Western blot analysis of TXNDC5 expression in PC3 monolayer cultures in vitro under normoxic versus hypoxic conditions. (B) Densitometric quantification of western blot analysis ($n \geq 4$)

Selective induction of TXNDC5 under metronomic CPA therapy in vivo

Western blot analysis of corresponding tumor tissue from PC3 xenografts confirmed the significant lower levels of TXNDC5 in PC3-D3 and a trend for lower expression of TXNDC5 in PC3-D4 in vivo (**Figure 39**). Metronomic scheduled CPA therapy in vivo increased protein levels of TXNDC5 in the resistant tumors but not in the PC3-wt (**Figure 39**).

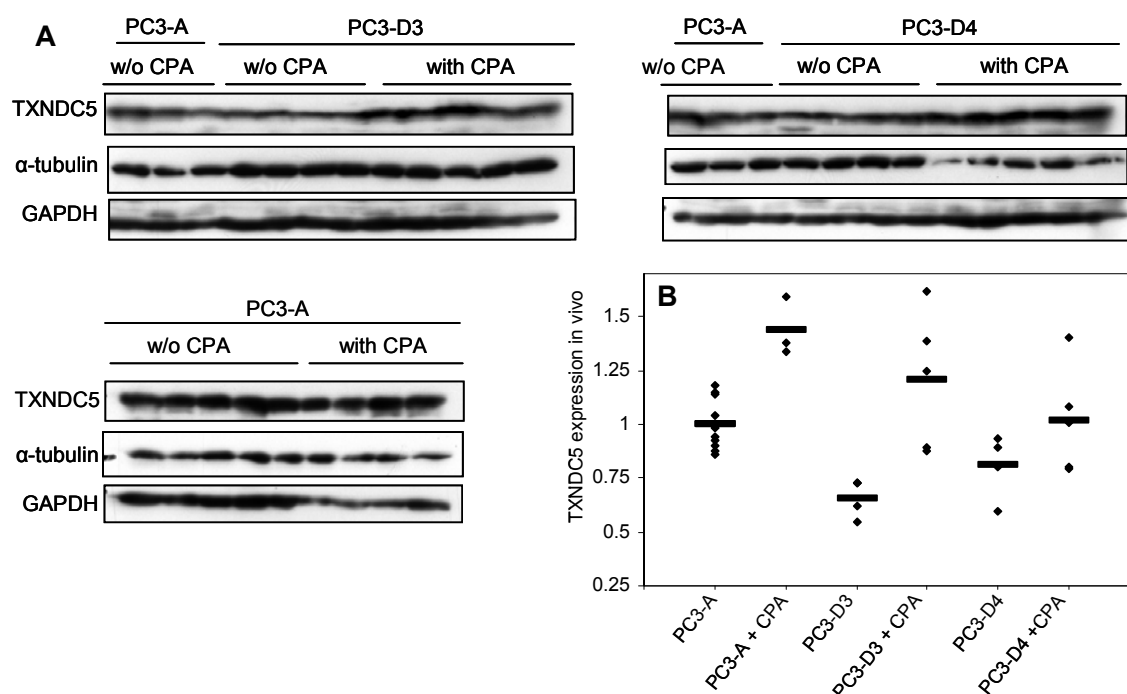


Figure 39: In vivo validation of TXNDC5 regulation. Western blot analyses for TXNDC5 of cell extracts from tumor tissue of resistant PC3-D3 and PC3-D4 tumors with and without metronomic cyclophosphamide treatment compared to tumors of PC3-wt with and without treatment.

3.2.7.4. ANXA3 is up-regulated in prostate cancer chemoresistance in vivo

ANXA3 expression in vitro

The 2D-DIGE analysis of in vitro cultures of the chemoresistant PC3-D3 and PC3-D4 cells revealed a 1.8-fold increase of annexin A3 (ANXA3) in the PC3-D3 cells and a 2.2-fold increase in PC3-D4 cells compared to the chemosensitive PC3-wt cell line. In order to validate these results, protein extracts from different PC3 sublines were analyzed by western blot analysis for the regulation of ANXA3 in vitro. Protein levels were normalized to the house keeping protein α -tubulin and levels were quantified by gray value analysis after the blots were scanned. Western blot analysis also detected an increase in ANXA3 expression in the resistant PC3 cells even if the protein levels in PC3-D4 were only slightly higher than in the PC3-wt cells (**Figure 40**).

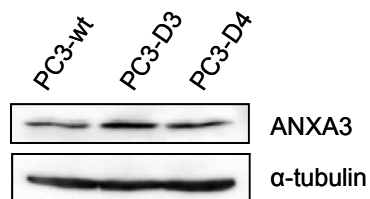


Figure 40: Western blot analysis of ANXA3 expression in PC3 monolayer cultures in vitro.

ANXA3 is induced in response to hypoxia

Cultivation of reisolated PC3 cells for the duration of four days under hypoxic conditions in comparison to normoxic conditions revealed that ANXA3 is up-regulated by hypoxia in all three cell lines independently of their origin from resistant or non resistant tumors (**Figure 41**).

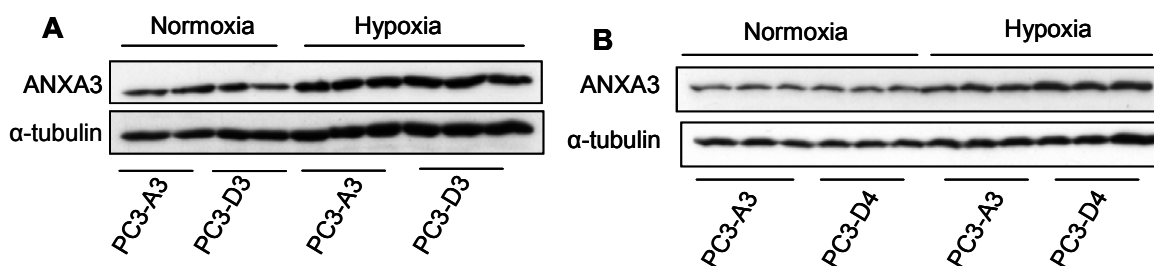


Figure 41: Western blot analysis of ANXA3 expression in (A) PC3-D3 and (B) PC3-D4 compared to PC3-A3 monolayer cultures in vitro under normoxic versus conditions.

ANXA3 up-regulation by resistant tumors in metronomic chemotherapy in vivo

In order to reveal relevance of obtained in vitro data for in vivo chemoresistance, western blot analysis on tumor cell extracts of corresponding xenografts was performed (**Figure 42**). These western blots confirmed an up-regulation of ANXA3 in resistant tumors compared to chemosensitive control tumors. Importantly, the abundance of this protein further increased when tumor-bearing mice were subjected to CPA treatment.

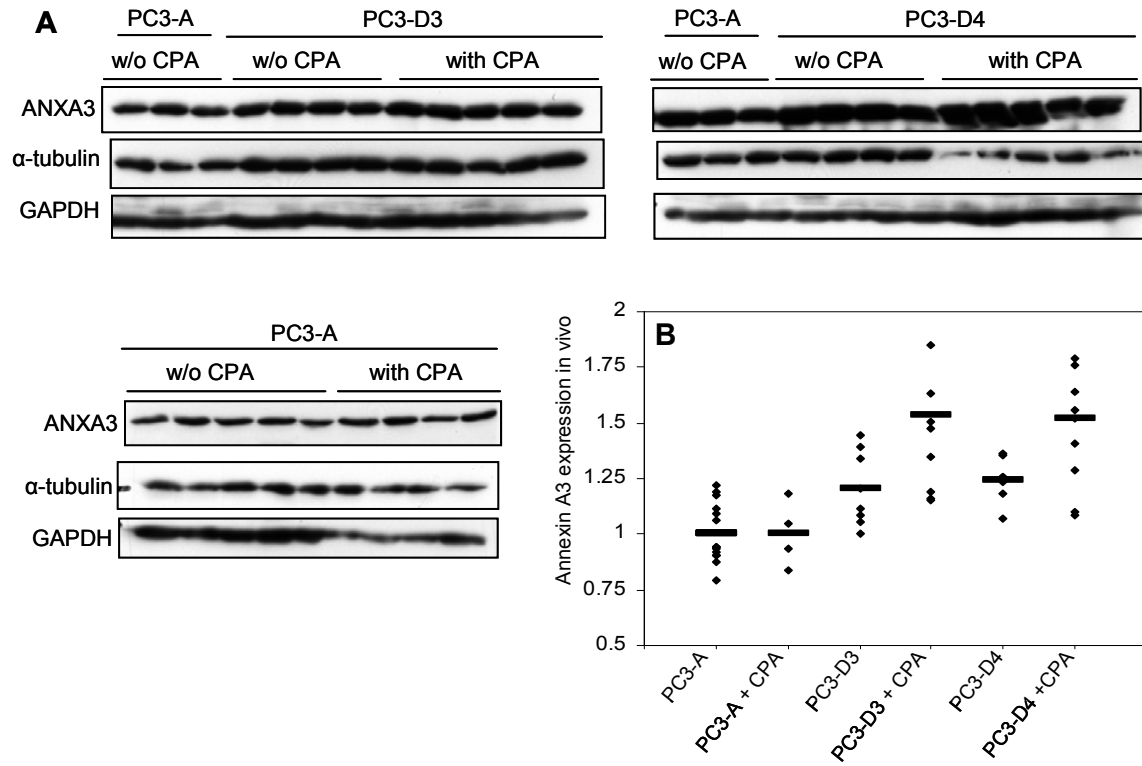


Figure 42: *In vivo* validation of ANXA3 regulation. Western blot analyses for annexin A3 of cell extracts from tumor tissue of resistant PC3-D3 and PC3-D4 tumors with and without metronomic cyclophosphamide treatment compared to tumors of PC3-wt with and without treatment.

3.2.8. Microarray analysis of chemoresistant PC3 xenografts compared to non resistant control tumors

In addition to the proteomics study a microarray analysis was performed to obtain additional information on mRNA level. Microarray was carried out on tumor tissue RNA. Therefore, PC3-wt, PC3-A3, PC3-D3 and PC3-D4 cells were injected subcutaneously and were grown as xenografts until they reached a mean volume of 30 mm³. One group of each PC3 cell line was treated with 120mg/kg CPA, whereas the other group was used as untreated control. 24 h after CPA application tumors were harvested. Microarray analysis of 4 tumors per group using human Gene Chip® gene 1.0 ST array was performed.

3.2.8.1. Sample classification via hierarchical clustering

Robust Multichip Analysis (RMA) can be used to generate normalized expression intensities for a set of Affymetrix GeneChip files. In order to detect distances and similarities between different samples, RMA normalized data were subject to hierarchical clustering analysis. Hierarchical sample clustering compares the different samples to each other in terms of sample to sample variation in total gene expression⁸⁹. The resulting distance matrix was visualized as so called heatmap, where samples which correlate well to each other in terms of their whole gene expression profile appear in red and sample correlate in larger distance are colored in blue (**Figure 43**). This distance matrix revealed that all samples derived from tumors previously passaged in mice (PC3-A3, PC3-D3 and PC3-D4) showed higher similarity to each other than the group of PC3-wt tumor samples which clustered in a different family in larger distance to the rest of the samples, indicating in vivo passaging effects. One PC3-A3 tumor could be identified as outlier by this method and was not included in further analysis.

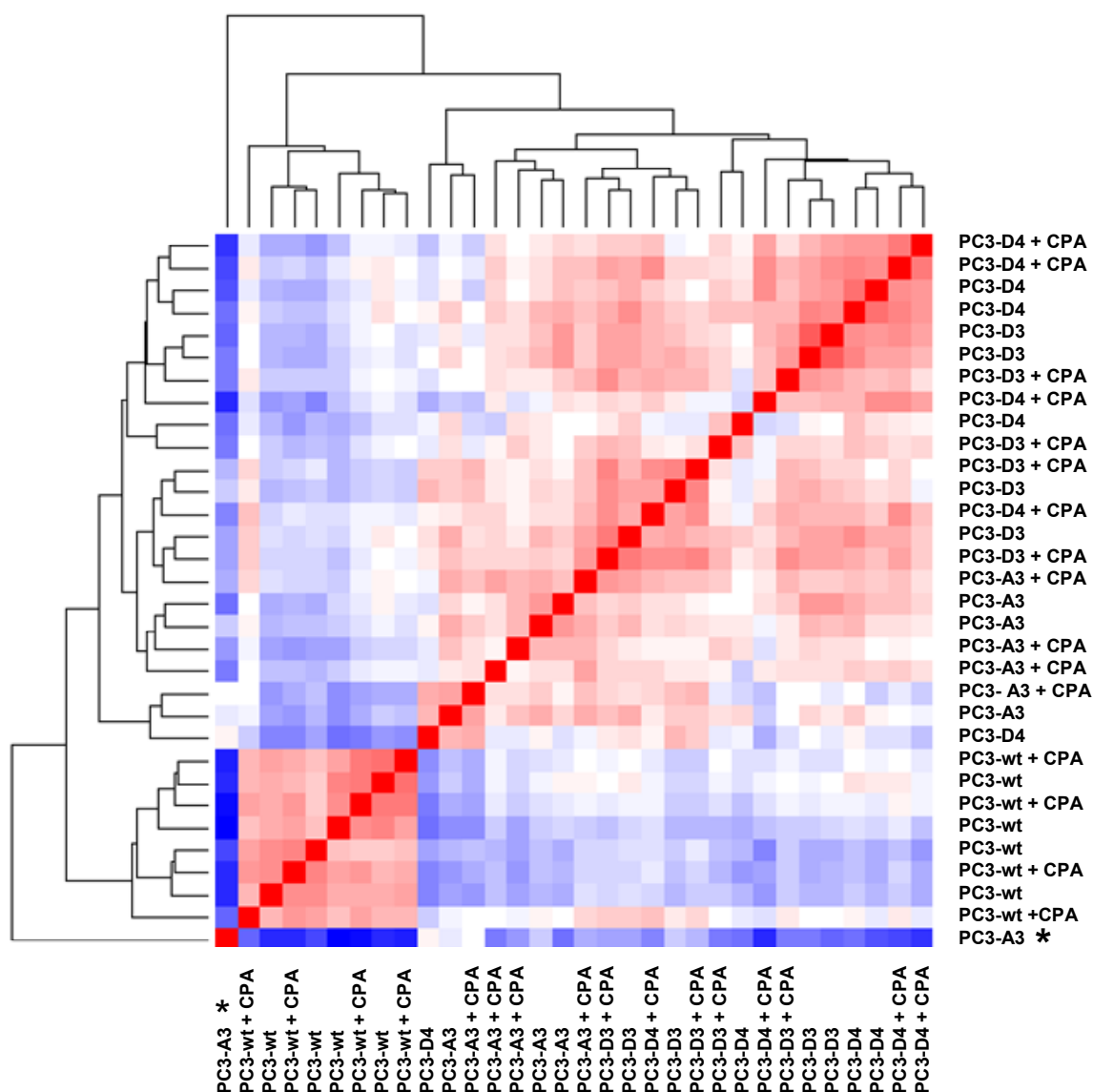


Figure 43: Distance matrix of tumor samples obtained by divisive hierarchical clustering based on robust multichip analysis (RMA) data of microarray analysis from PC3 xenografts. Low distance is visualized in red and high distance is visualized in blue. Outliers are marked by * and are excluded from further data analysis

3.2.8.2. Influence of in vivo passaging on gene expression of PC3 cells

Differentially expressed genes between xenografts of previously in vivo passaged PC3-A3 and corresponding parental PC3-wt were determined using SAM and Spotfire Decision Site®. The corresponding Scatter plots in **Figure 44** display average normalized log₂ values of gene expression levels in PC3-A3 and corresponding PC3-wt tumors. Genes with a total lower expression are colored in red whereas highly abundant genes appear in blue. Genes which show significant

differences between the two groups of PC3 tumors appear in teal blue and are annotated by their gene symbols and are summarized in **Appendix Table 6** (chapter 6.1).

The applied selection criteria (fold change > 2, p-value < 0.05) resulted in 10 genes with higher expression in PC3-A3 compared to parental PC3-wt tumors and in 125 genes with lower expression compared to parental PC3-wt tumors (**Figure 44**, **Appendix Table 6**).

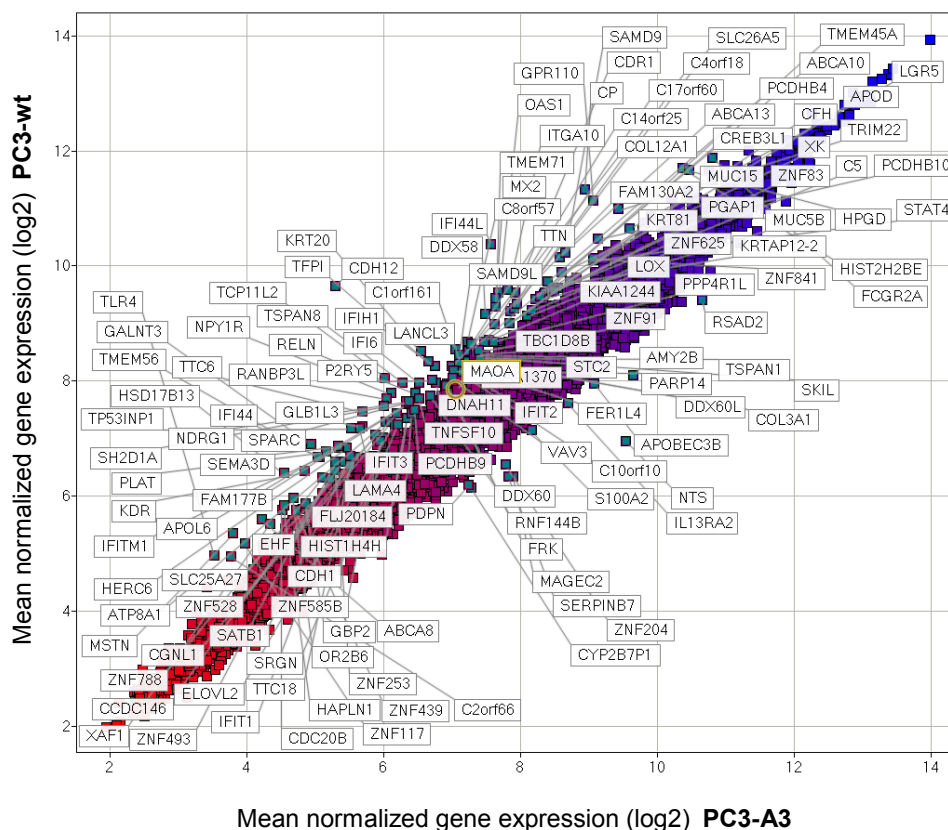


Figure 44: Scatter plot of PC3-wt compared to in vivo passaged PC3-A3 xenografts. The scatter plot display average normalized log₂ values of gene expression levels of PC3-A3 tumors and the corresponding PC3-wt tumors. Genes with a total lower expression are colored in red whereas highly abundant genes appear in blue. Genes, which show significant differences between the two groups of PC3 tumors, are marked in teal blue and are annotated by their gene symbols (2 fold regulation; T-Test: p < 0.05).

3.2.8.3. Differentially expressed genes between resistant and non resistant tumors

In order to detect differences in gene expression between resistant and non resistant PC3 xenografts, tumors from each resistant PC3 cell line (PC3-D3 and PC3-D4) were compared to appropriate control tumors derived from in vivo passaged non

resistant PC3-A3 cells. Due to the fact that PC3-D3 and PC3-D4 cells are derived from resistant tumors of two different animals their gene expression profiles were compared separately to control tumors in order to also incorporate gene expression differences specific for each of the resistant variants.

Resistant PC3-D3 versus in vivo passaged PC3-A3

Differentially expressed genes between in vivo PC3-D3 and PC3-A3 xenografts were determined and the corresponding scatter plot in **Figure 45** displays the detected differences in gene expression profiles between PC3-D3 and PC3-A3 which show regulation >1.6 fold (p -value < 0.05). These selection parameters led to 34 genes with higher expression in resistant PC3-D3 compared to sensitive PC3-A3 tumors and in 12 genes with lower expression compared to PC3-A3 tumors (**Figure 45**, **Appendix Table 7**).

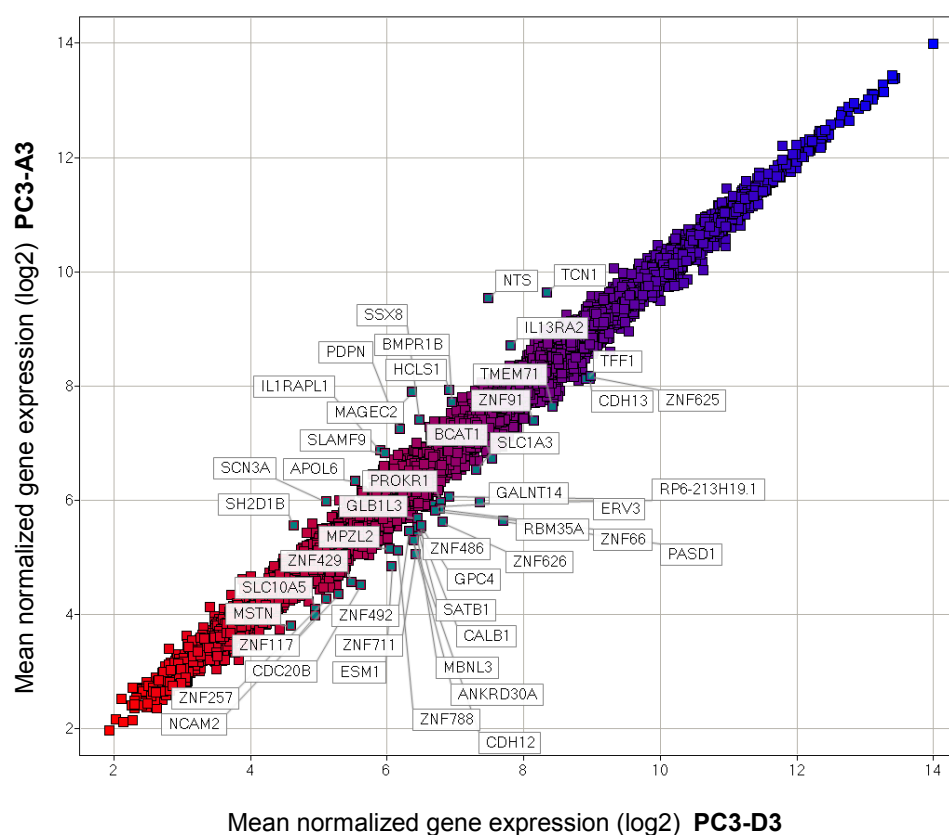


Figure 45: Scatter plot of PC3-D3 (resistant) compared to in vivo passaged PC3-A3 (sensitive) xenografts. The scatter plot displays average normalized \log_2 values of gene expression levels of PC3-D3 tumors and the corresponding PC3-A3 tumors. Genes with a total lower expression are colored in red whereas highly abundant genes appear in blue. Genes, which show significant differences between the two groups of PC3 tumors, are marked in green and are annotated (1.6 fold regulation; T-test: $p < 0.05$).

Resistant PC3-D4 versus in vivo passaged PC3-A3

Figure 46 shows differentially expressed genes (>1.6 fold; p-value < 0.05) between PC3-D4 (resistant) and PC3-A3 (sensitive) xenografts in a scatter plot. Setting selection parameters as described, revealed 26 up- and 30 down-regulated genes in resistant PC3-D4 tumors compared to PC3-A3 control tumors (**Figure 46, Appendix Table 8**).

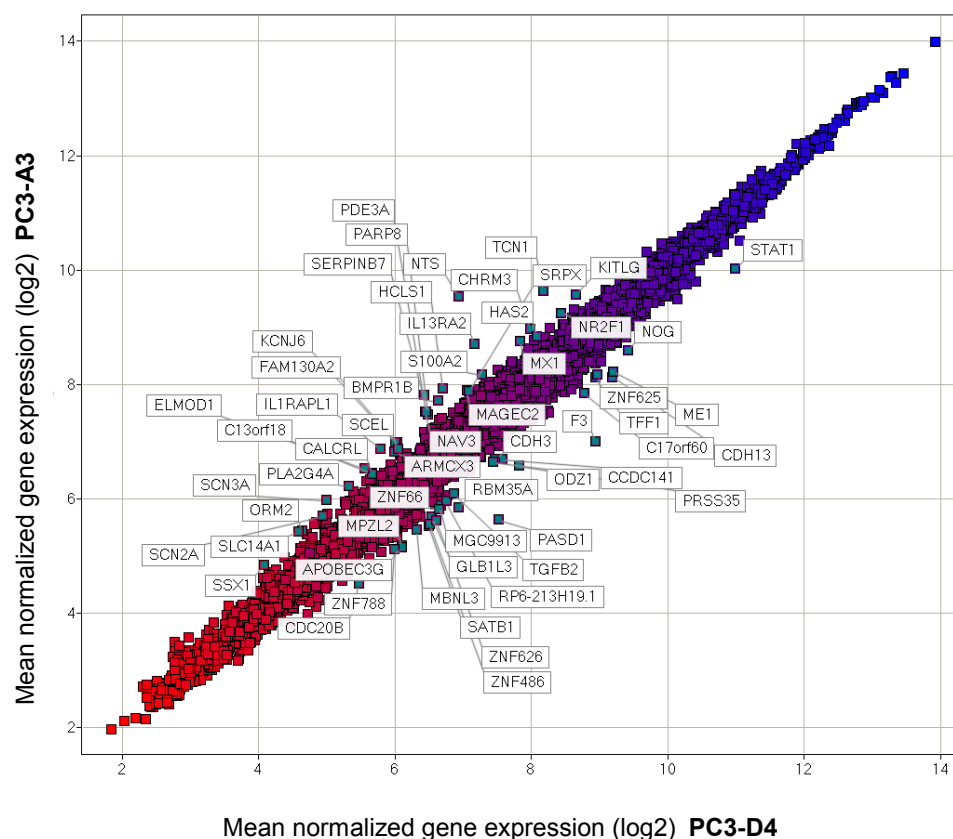


Figure 46: Scatter plot of PC3-D4 compared to in vivo passaged PC3-A3 xenografts. The scatter plot displays average normalized log₂ values of gene expression levels of PC3-D4 tumors and corresponding PC3-A3 tumors. Genes with a total lower expression are colored in red whereas highly abundant genes appear in blue. Genes, which show significant differences between the two groups of PC3 tumors, are marked in green and are annotated (1.6 fold regulation; T-test: p < 0.05).

Differences and similarities between two resistant PC3 cell lines

Comparison of the two different resistant variants revealed that a set of 15 genes is commonly up-regulated in PC3-D3 as well as in PC3-D4 compared to non-resistant PC3-A3 tumors. However, each variant has several genes which are significantly up-regulated only in the respective tumors (19 genes in PC3-D3 and 12 genes in PC3-D4) compared to PC3-A3 tumors (**Figure 47A**). Eight genes are down-regulated in both resistant tumors compared to non-resistant PC3-A3 tumors but a set of 5 genes

(PC3-D3) respectively 23 genes (PC3-D4) is significantly lower expressed only in one of the resistant variants compared to PC3-A3 control tumors (**Figure 47B**).

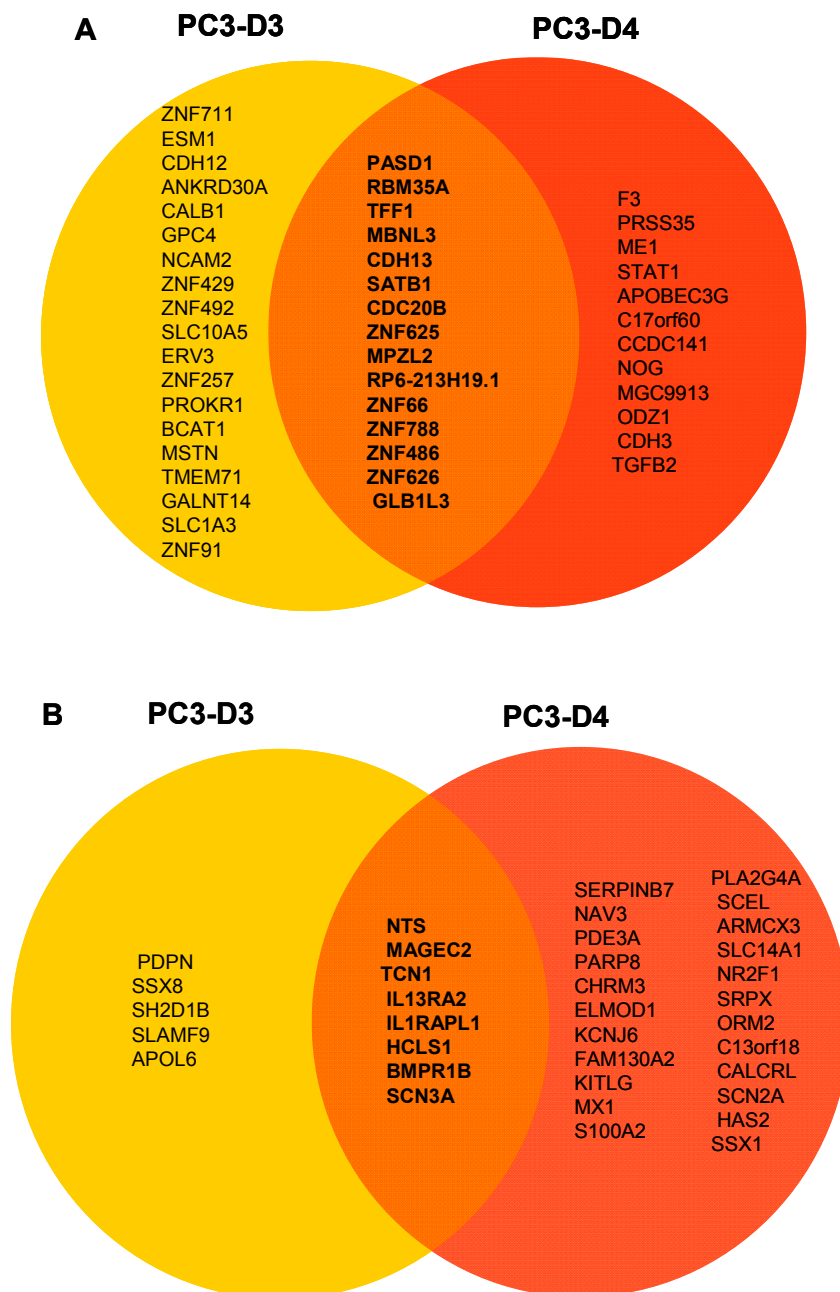


Figure 47: Differences and similarities between gene expression of resistant PC3-D4 and PC3-D3 versus non resistant PC3-A3 tumors. (A) Up-regulated genes in resistant versus non resistant PC3-A3 tumors. (B) Down-regulated genes in resistant versus non resistant PC3-A3 tumors.

3.2.8.4. Influence of CPA on differential gene expression in PC3 tumors

Influence of CPA on differences in gene expression between in vivo passaged PC3-A3 and parental PC3-wt tumors

CPA induced stress provoked similar response in PC3-wt and PC3-A3 tumors towards the drug in terms of gene up-regulation. The only gene, detected to be

specifically up-regulated in PC3-A3 compared to paternal PC3-wt tumors under CPA treatment is GABRE. However, the number of genes down-regulated in PC3-A3 tumors compared to PC3-wt increased significantly in response to CPA treatment (59 specifically down-regulated genes in PC3-A3 compared to PC3-wt in response to CPA) (**Figure 48**).

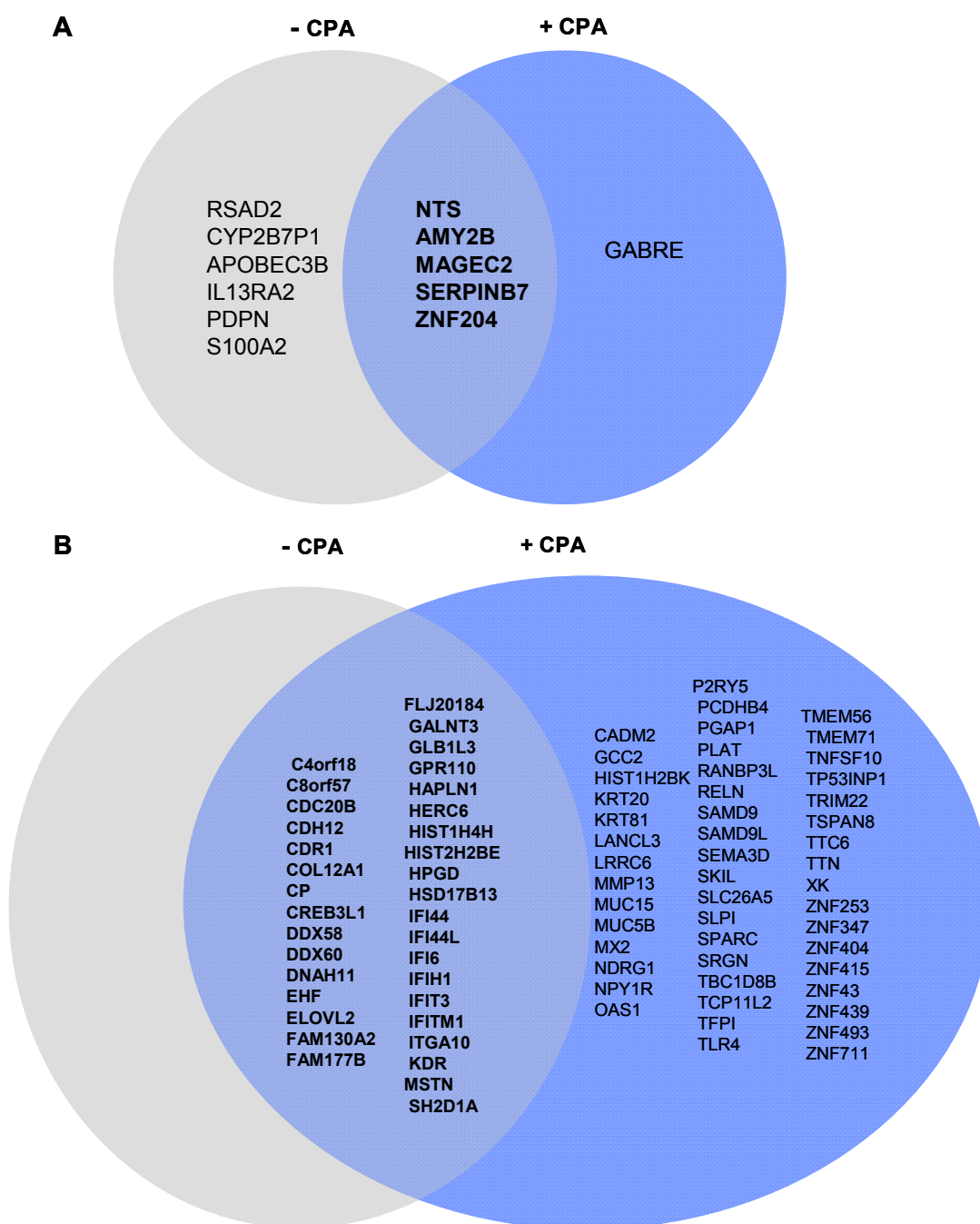


Figure 48: Influence of CPA on differences in gene expression between *in vivo* passaged PC3-A3 and parental PC3-wt tumors. (A) Genes up-regulated in PC3-A3 compared to PC3-wt. (B) Genes down-regulated in PC3-A3 compared to PC3-wt

Influence of CPA treatment on differences in gene expression between resistant and non resistant PC3 tumors

The cytotoxic drug CPA resulted in different effects on gene regulations in PC3-D3 and PC3-D4 tumors 24h after treatment. The influence of CPA on gene expression profiles in PC3-D3 compared to PC3-A3 resulted in specific up-regulation of eight and down-regulation of six genes in PC3-D3 compared to PC3-A3 (**Figure 49**).

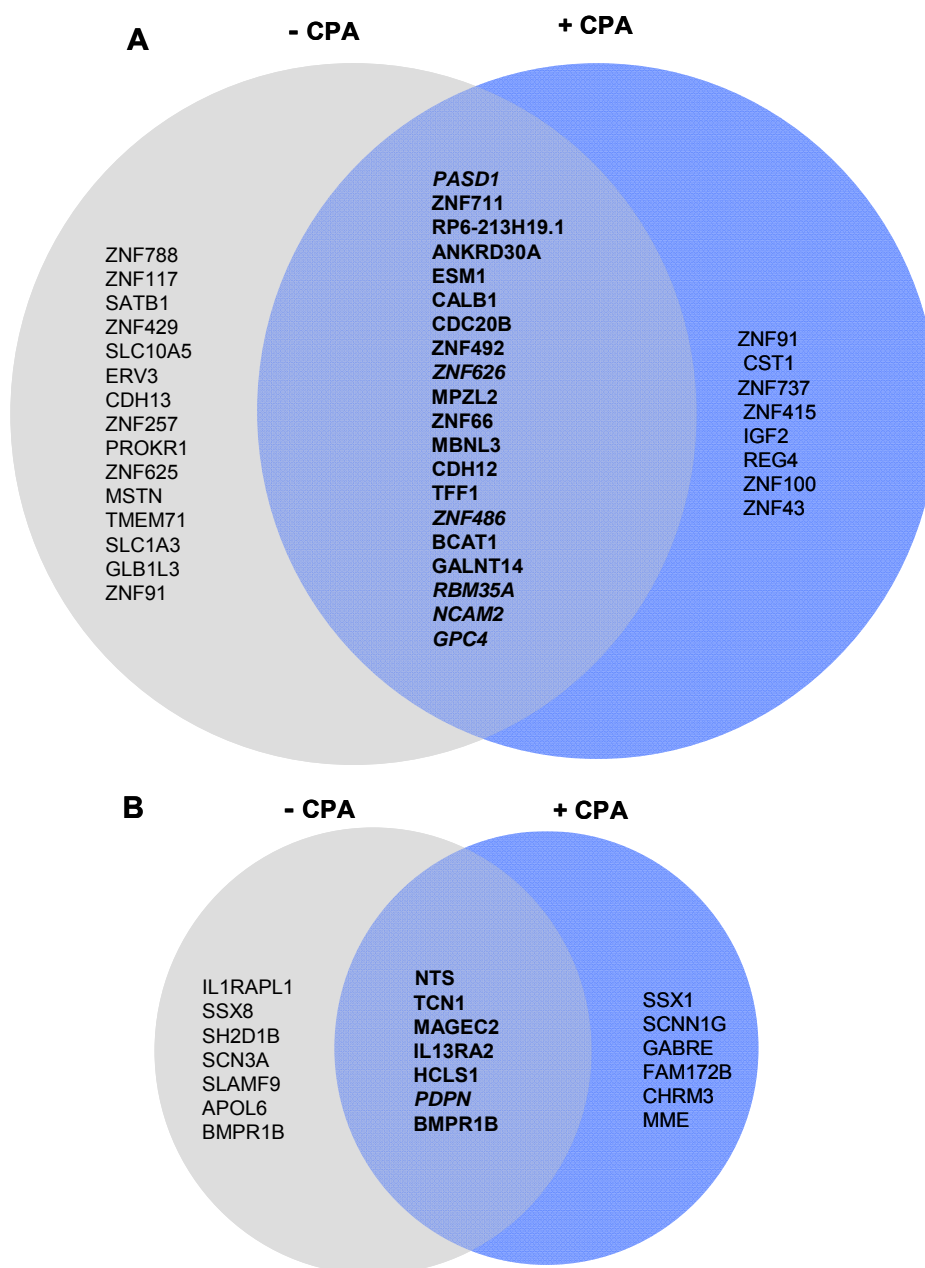


Figure 49: Influence of CPA on differences in gene expression between resistant PC3-D3 and in vivo passaged PC3-A3 tumors. (A) Genes up-regulated in PC3-D3 compared to PC3-A3 tumors. (B) Genes down-regulated in PC3-D3 compared to PC3-A3.

CPA treatment specifically induced overexpression of 98 genes in resistant PC3-D4 compared to PC3-A3 control tumors. Additionally 12 genes were down-regulated in PC3-D4 compared to PC3-A3 xenografts 24 h after CPA application (**Figure 50**).

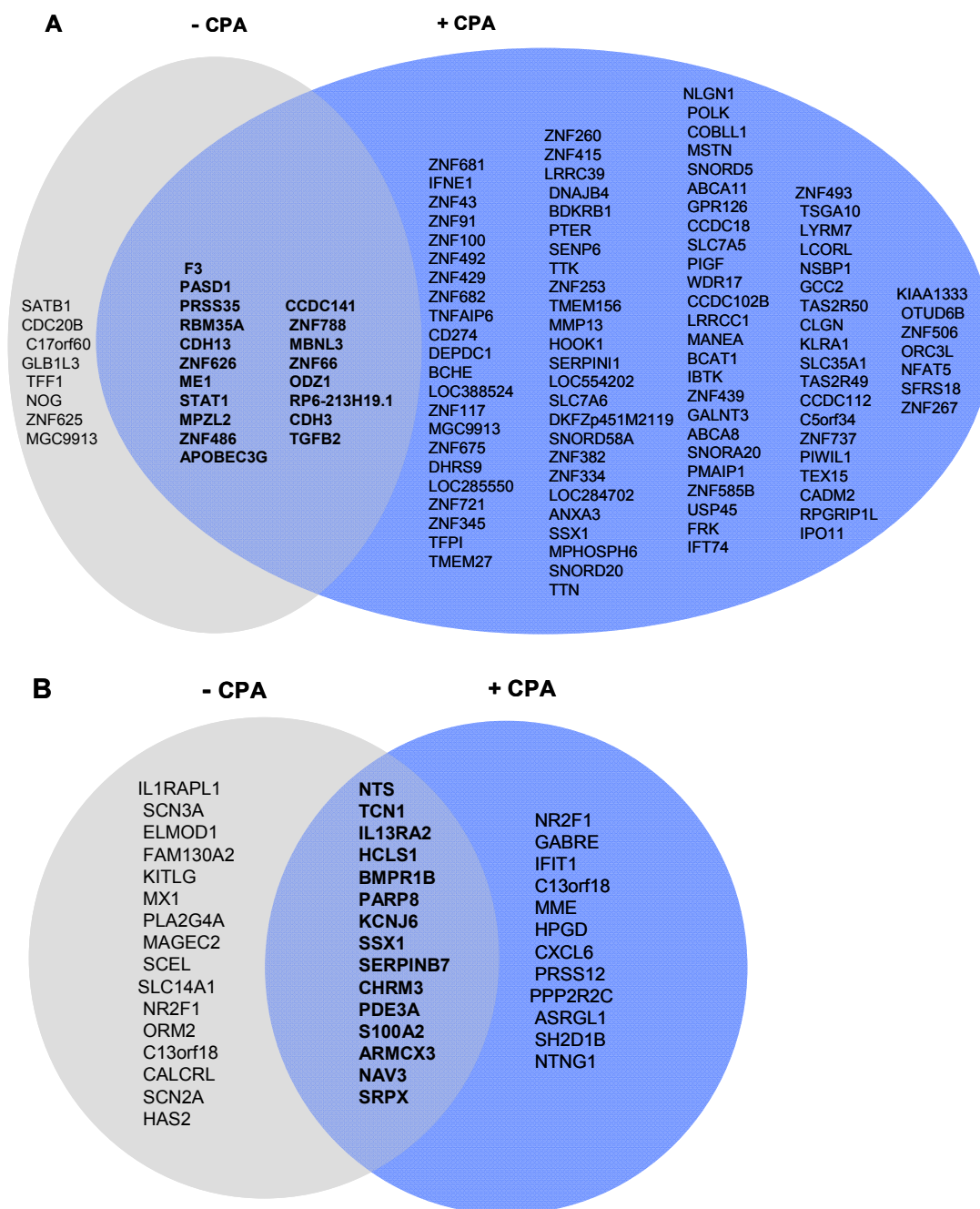


Figure 50: Influence of CPA on differences in gene expression between resistant PC3-D4 and in vivo passaged control PC3-A3 tumors. A) Genes up-regulated in PC3-D4 compared to PC3-A3 tumors. B) Genes down-regulated in PC3-D4 compared to PC3-A3.

Beside the varying numbers of genes specifically regulated in response to CPA there are several genes in each group which are constitutively up- respectively down-regulated in untreated as well as in CPA treated tumors (**Figure 48-50**).

3.2.8.5. Gene Clustering

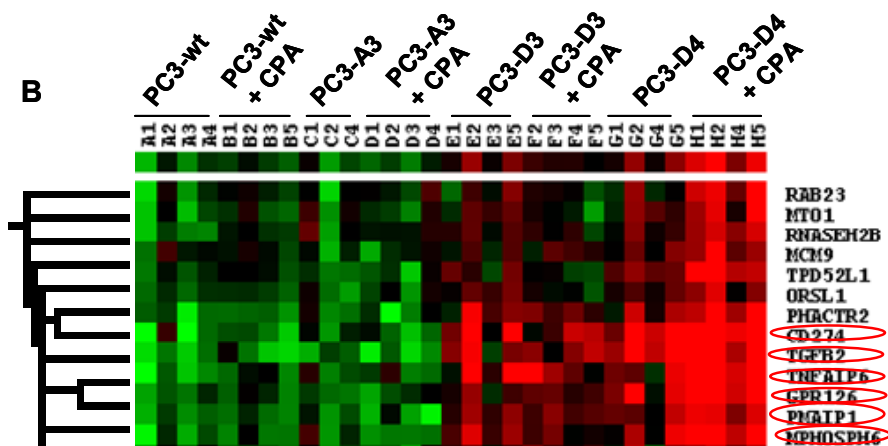
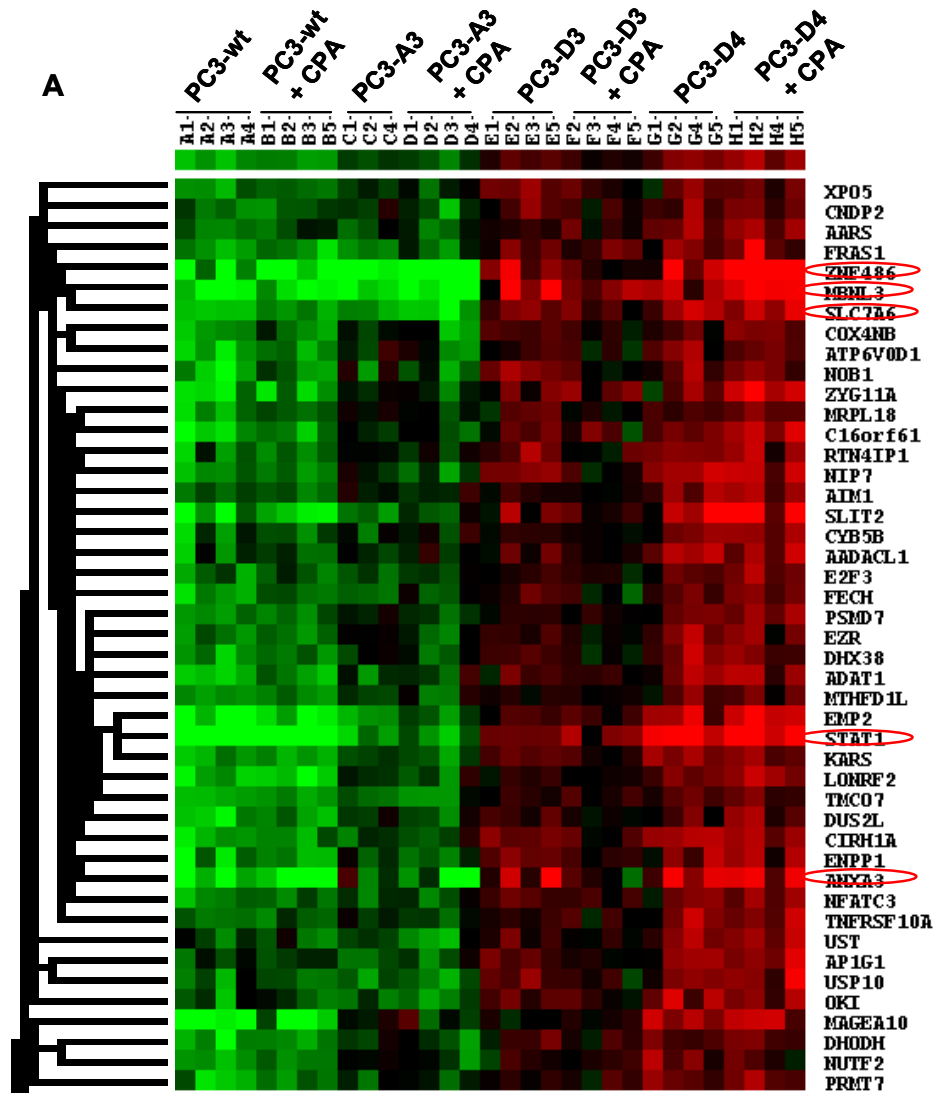
Hierarchical gene clustering is a common method in array data analysis. It is a useful exploratory technique for gene-expression data as it groups similar gene expression pattern together and can hint to potentially meaningful relationships between single genes. In this study hierarchical clustering using open source software of Michael Eisen was applied (Eisen 1998). Selected clusters are presented in the following section. Green color indicates relatively lower gene expression whereas red color stands for relatively increased gene expression compared to the mean expression value.

Gene cluster up-regulated in both resistant variants

Figure 51 shows gene cluster including significantly up-regulated genes (red circle) in at least one resistant variant versus non resistant PC3-A3 tumors and genes with similar gene expression pattern to these selected genes. ANXA3, STAT1, SLC7A6, MBNL3 and ZNF486 are genes with significantly higher expression levels in at least one of the resistant subgroup and cluster in close proximity to a variety of other genes with similar gene expression pattern as indicated in **Figure 51A**.

The genes TGFB2, CD274, TNFAIP6, GPR126, PMAIP1 and MPHOSPH6 all significantly up-regulated in PC3-D4 tumors under CPA treatment, cluster in close proximity. Clustering also revealed that expression levels were also increased in PC3-D3 compared to non resistant tumors however the up-regulation was not significant according to our selection criteria (**Figure 51B**).

The third cluster in Figure 51 includes PASD1 and GALNT4 in the same family tree. Both are significantly higher expressed in resistant tumors than in their non resistant counterparts (**Figure 51C**).



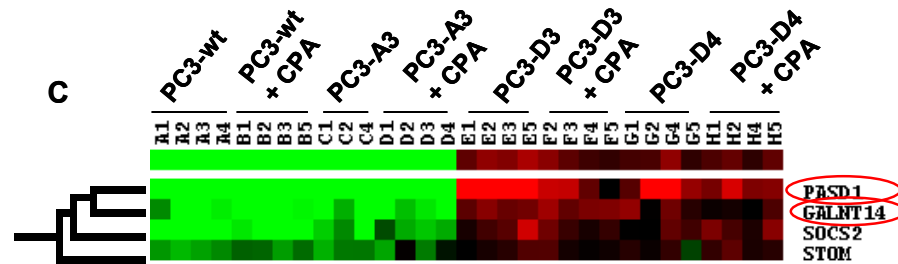
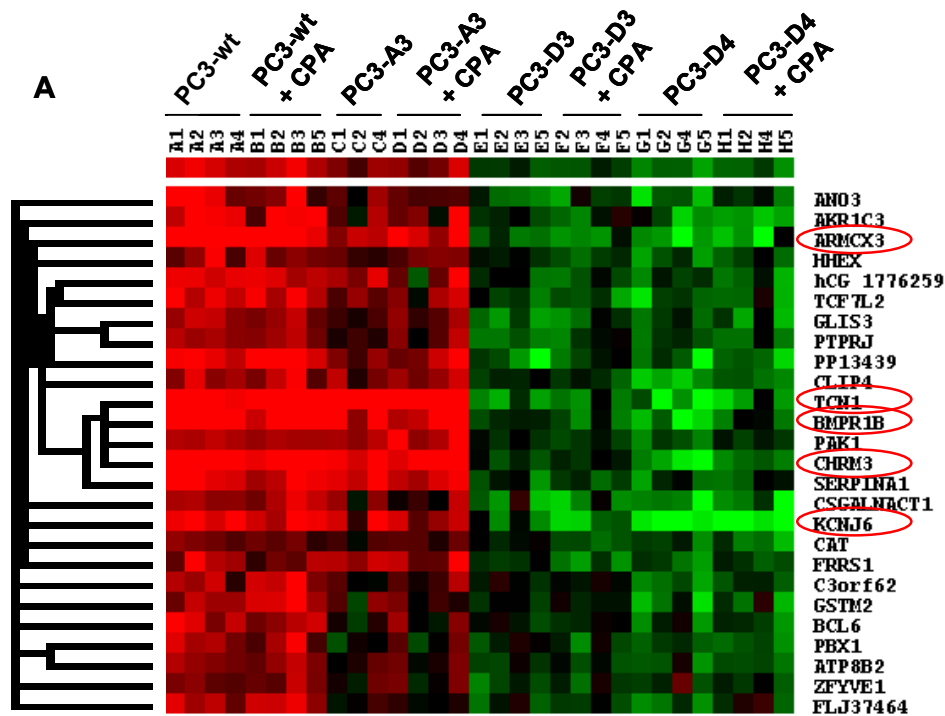


Figure 51: Gene cluster showing higher expression levels in resistant PC3 xenografts than in non resistant PC3 xenografts. (A) Cluster including ANXA3, STAT1 and MBNL3. (B) Cluster including TGFB2 and CD274. (C) Cluster including PASD1 and GALNT4

Gene cluster down-regulated in both resistant variants

Hierarchical gene clustering also revealed gene clusters with relatively lower expression in resistant versus non resistant PC3 tumors. The five candidates ARM CX3, BMPR1, CHRM3, KCNJ6, TCN1 detected to be significantly down-regulated in both resistant variants respectively one of them appear in a common cluster of regulation (**Figure 52A**). Another group of genes including MX1, IFIT1 and PDGFD also showed similar gene expression pattern (**Figure 52B**).



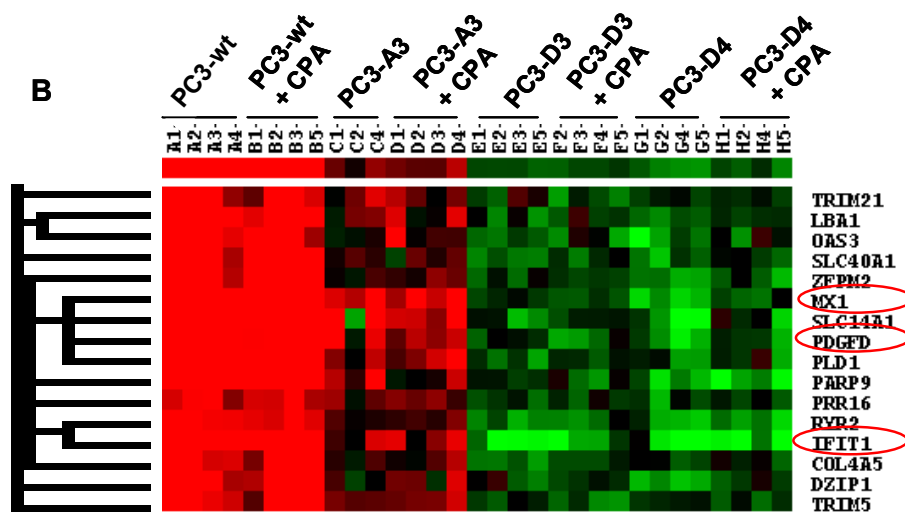


Figure 52: Gene cluster showing lower expression levels in resistant PC3 xenografts than in non resistant PC3 xenografts. (A) Cluster including *ARMCX3*, *TCN1*, *BMPR1B*, *CHRM3* and *KCNJ6*. (B) Cluster including *MX1*, *PDGFD* and *IFIT1*.

3.2.8.6. Tissue Factor (F3) – a candidate for alternative splicing in PC3-D4

The GeneChip® Human Gene 1.0 ST Array offers whole-transcript coverage. Each of the 28,869 genes is represented on the array by approximately 26 probes spread across the full length of the gene covering all exons. Therefore it is possible to use this information in order to detect differentially expression on exon level. As there are only approximately two probes per exon these data have to be confirmed by RT-PCR of the corresponding tumor tissue.

F3 is an example of varying exon expression pattern between different PC3 xenografts. In this case exon 1 showed equal expression between all PC3 xenografts whereas exon 2-6 revealed higher expression in PC3-D4 xenografts compared to all other xenografts (**Figure 53**)

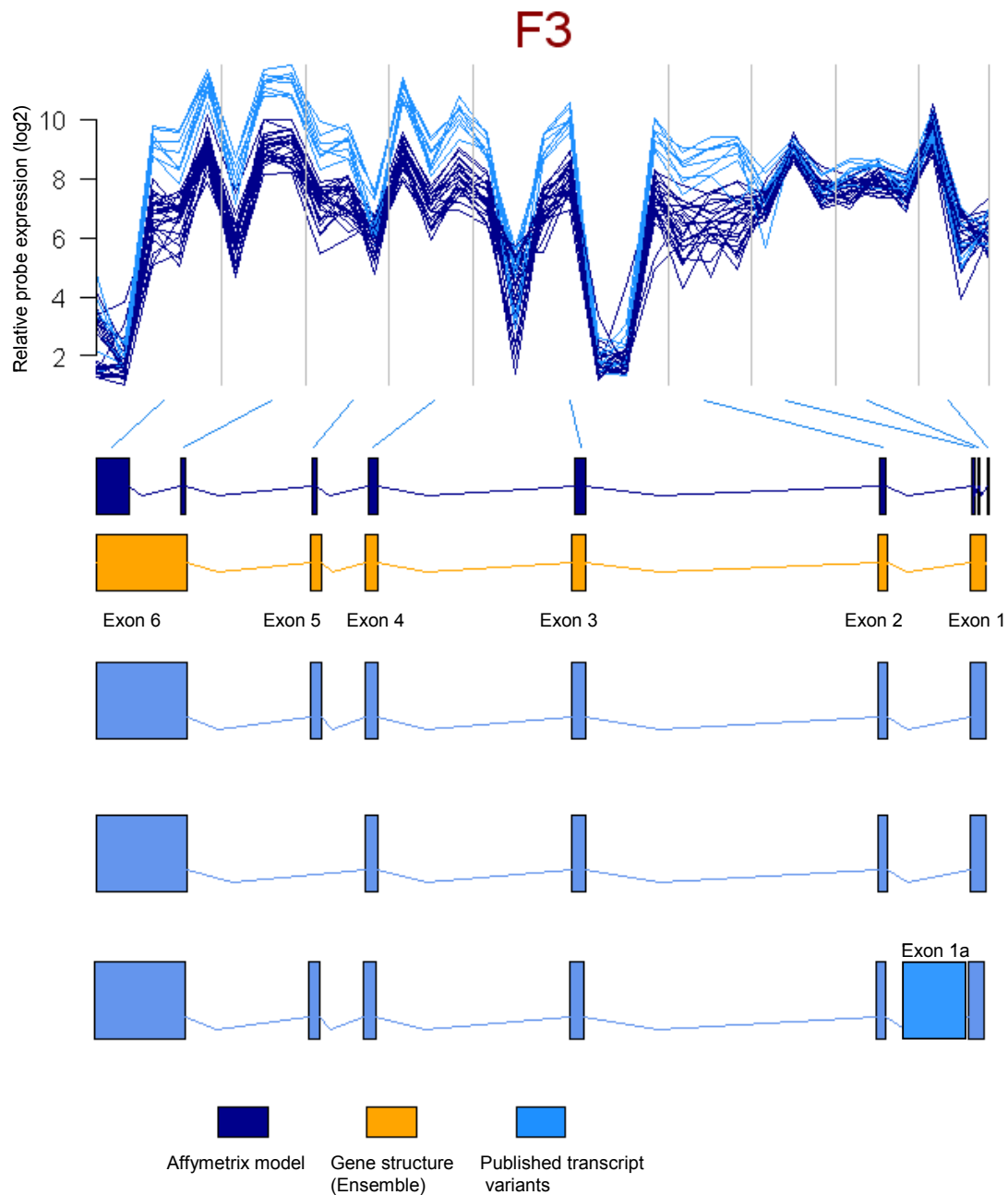


Figure 53: Relative Probe-level expression profile of F3 gene in PC3 xenografts. Expression values of PC3-D4 are presented in clear blue whereas expression values of other PC3 xenografts are presented in dark blue. Assignment of the individuals probes to exons 1 to 6 is indicated by the vertical lines in the expression profile and the gene model as defined by Affymetrix (dark blue) and Ensemble (orange) and the published transcript alternatives (clear blue) in the lower part of the figure.

3.2.8.7. A genomic point of view on candidates obtained by proteomics

Combination of genomic and proteomic approaches provide complementary information about the same problem regarding at two different levels. In order to gain additional information about candidates identified in the proteomics study, gene expression of the three selected proteins ANXA3, TXNDC5, CatB and CK19 differentially regulated in proteomic profiling of resistant (PC3-D3 and PC3-D4) versus non resistant PC3-wt and PC3-A3) cells has been selected for detailed analysis. **Figure 54** shows gene expression profiles of ANXA3, TXNDC5, CatB and CK19 in different PC3 xenografts. CK19 mRNA did not reveal any significant regulation between different PC3 xenografts. The mRNA regulation of CatB reflects western blot data of in vivo tumor tissue where no statistically significant up-regulation in resistant tumors versus non resistant control tumors could be detected. However a tendency of higher CatB levels in PC3-D4 could be detected. TXNDC5 mRNA levels slightly decrease (not statistically significant) in resistant tumors in comparison to their non-resistant counterparts. In contrast, it is obvious that ANXA3 is significantly up-regulated on mRNA level in the resistant PC3 xenografts compared to the non resistant controls. (**Figure 54**, compare **Figures 31, 35-42** for protein expression data).

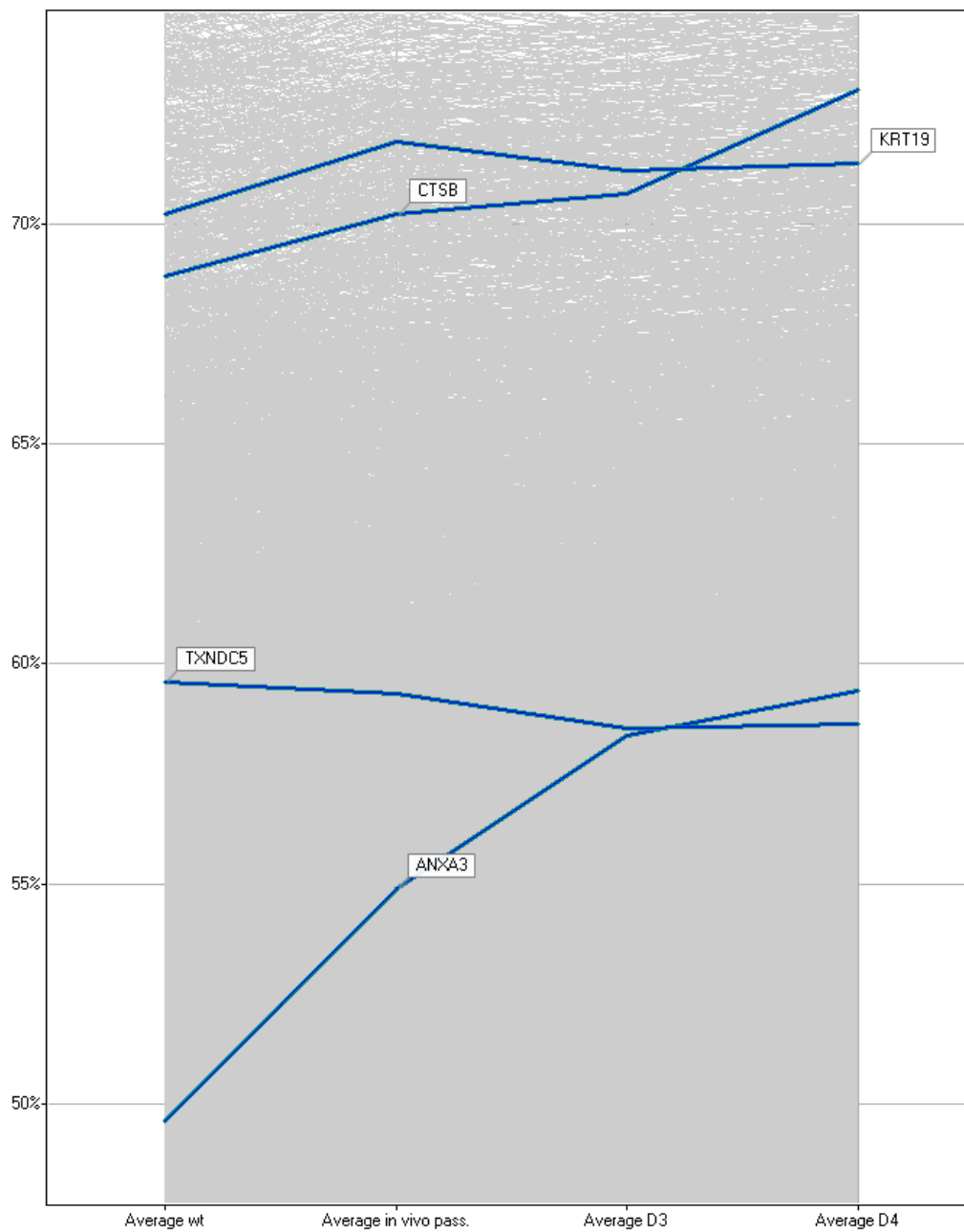


Figure 54: Gene expression profiles of proteomics candidates ANXA3, TXNDC5, CatB and CK19. Average normalized log2 gene expression is visualized over the different sample groups.

4. Discussion

4.1. *Colon cancer*

4.1.1. **Fragmentation of Lamin A/C in multicellular spheroid of low-passage colon carcinoma cells**

In the present work the low passage human colon cancer cells COGA-5³ were cultured as multicellular spheroids to provide a model system that reflects the three-dimensional structure of the respective tumor in vivo. The COGA-5 cell line was the only out of seven tested low passage colon cancer cell lines that generated fully compact multicellular spheroids. Further, the COGA-12 cell line formed partly compact multicellular aggregates with local areas of compaction. The COGA-12 aggregates were additionally investigated in this work as representatives for a three-dimensional cell culture model exhibiting a lower degree of compaction compared to the fully compact multicellular spheroids of cell line COGA-5. Proteome analysis revealed several alterations in the protein expression pattern of the COGA-5 spheroids compared to the corresponding monolayer cultures. Five proteins were found to be up-regulated and one protein was down-regulated in spheroids compared to the monolayer culture. In COGA-12 partly compact aggregates, four proteins were found up-regulated compared to the respective monolayer. In the proteome comparisons between monolayers and the respective spheroids, only two-fold or higher alterations in protein expression were taken into account. This stringent analysis provided a highly reproducible detection of regulated proteins. However, this restriction significantly reduced the number of detected spots. Furthermore, the current analysis was restricted mainly to cytosolic proteins, whereas detection of hydrophobic membrane proteins or basic proteins was limited.

The spots 12-A and 12-B both up-regulated in COGA-12 aggregates were identified as two isoelectric variants of acidic ribosomal protein P0. P0 is highly conserved in vertebrates and forms the lateral stalk of the 60S ribosomal subunit together with two hetero- or homo-dimers of acidic ribosomal proteins P1 and P2; P0 functions as ribosomal core protein for the anchorage of P1 and P2^{90;91}. This stalk is located at the active site of the ribosome particle, where interactions between mRNAs, tRNAs and translation factors take place during protein synthesis. Recently, Wu and Storey reported regulation of P0 depending on oxygen levels in frog brain tissue suggesting

a role of P0 in anoxia resistance⁹². The function of P0 up-regulation under anoxia, however, remains to be clarified. Hence, P0 might be up-regulated in COGA-12 aggregates as a consequence of the lower oxygen supply in compact areas which are restricted from oxygen and serum supply. In addition, it was previously demonstrated that mRNA levels of P0 were increased in hepatocellular and colon carcinoma in accordance with increased biological aggressiveness, i.e. enhanced tumor outgrowth and cancer progression^{93;94}. Overall, these data link altered P0 expression to cellular stress as well as cancer cell proliferation which both are features in three dimensional cultures.

The protein down-regulated in COGA-5 multicellular spheroids was identified as the acidic isoform of calponin, as also confirmed by immunoblot analysis. Calponins are actin-associated proteins and besides acidic calponin two other isoforms are known, namely basic and neutral calponins^{95;96}. Basic calponin is the best studied isoform and is exclusively expressed in smooth muscle cells where it plays a role in the regulation of contraction⁹⁷. Less is known about acidic calponin which is expressed in a wide variety of tissues, including the colon⁹⁸. Acidic calponin is not involved in contraction⁹⁹ but may play a role in cytoskeletal organization, since it binds to actin^{96;100}. The down-regulation of calponin in multicellular spheroids therefore implies differences in cytoskeletal structures compared to monolayer cultures. In fact, changes in the tumor architecture of multicellular spheroids compared to the corresponding monolayers have been reported in a variety of tumor types including renal¹⁰¹, gastric⁶ and colorectal carcinomas^{102;103}. Altered cell and nucleus shapes attributable to changes in cytoskeletal elements and nuclear structures are hallmarks of cancer cell morphology that may contribute to altered properties compared to normal cells¹⁰⁴. It is likely that cells in multicellular spheroids represent such alterations of in vivo tumor cells better than monolayer cells.

Another protein that was up-regulated in multicellular spheroids of COGA-5 cells was identified as 15-hydroxyprostaglandin dehydrogenase (15-PGDH). 15-PGDH mediates prostaglandin degradation¹⁰⁵ and therefore prevents tumor promoting effects of prostaglandins¹⁰⁶. For example, prostaglandins promote growth factor signaling and antagonize apoptosis¹⁰⁶. Therefore, 15-PGDH is considered to expose tumor suppressor activity, since it may antagonize prostaglandin-mediated tumor progression. In multicellular spheroids 15-PGDH may contribute to proliferation inhibition, which is an established feature of multicellular spheroids where

proliferation is restricted to local areas⁸⁵. In addition, the up-regulation of 15-PGDH as a potential tumor suppressor fits well with the observed lamin cleavage as a result of enhanced apoptosis rate in the multicellular spheroids.

Proteome analysis revealed a 28 kDa fragment of the protein lamin A/C in COGA-5 spheroids and low levels of this lamin A/C fragment were also detected in COGA-12 partly compact aggregates but not in the respective monolayer cultures. Lamins are type V intermediate filament proteins that form the nuclear lamina, a filamentous network that connects the inner nuclear envelope membrane with chromatin¹⁰⁷. Lamins form stable structures in the nuclear lamina and the nucleoplasm thereby determining nuclear shape and size, stability, and the position of nuclear pore complexes¹⁰⁸⁻¹¹⁰. Furthermore, it has been suggested that lamins are involved in DNA replication and transcription^{107;111}. In caspase dependent apoptosis lamin A/C is cleaved by caspase-6 which is a requirement for the initiation of the nuclear events of apoptosis, e.g. condensation of chromosomal DNA and formation of apoptotic bodies^{112;113}. Inhibition of caspase-6 and thus inhibition of lamin cleavage enables chromatin to fully condense leading to the suggestion that lamin cleavage frees chromatin from the lamina¹¹². However, additional experiments performed in other studies in neuronal cells showed that caspase-6-dependent lamin A cleavage is not a general phenomenon in apoptotic cell death. For example, in a model of glutamate-induced cell death in neuronal HT-22 cells we could not detect cleaved lamin A in the apoptotic cells¹⁴. In this model system the cells undergo caspase-independent apoptosis that is mediated by mitochondrial release of apoptosis inducing factor AIF¹¹⁴. Thus, the absence of lamin A cleavage serves as additional evidence for the lack of caspase-6 activation after glutamate-induced apoptosis.

The detected truncation of lamin A/C in the spheroids may be a result of apoptotic stress induced by the lack of oxygen and growth factors. Our results clearly show that truncation of lamin A/C was induced in monolayer cultures by withdrawal of trophic support. Serum deprivation alone was sufficient for lamin A/C fragmentation and enhanced by simultaneous hypoxia, whereas hypoxia alone was not sufficient to produce the protein fragment. Using an antibody that only recognizes caspase-cleaved lamin A and by pharmacological inhibition of caspases we could further verify that the detected lamin A fragment was indeed a product of caspase cleavage.

Recent studies demonstrated that lamin A/C is a preferred substrate of caspase-6 in apoptotic cells^{86;115;116}. Consistent with these previous reports, in our studies the pan

caspace inhibitor zVADfmk reduced lamin A/C cleavage in a dose-dependent manner. Furthermore, addition of a caspases-6-specific inhibitor to spheroid cultures of COGA-5 cells confirmed that caspase-6 is responsible for the cleavage of lamin A/C in spheroid cultures of the COGA cells. Thus, the results indicate that apoptosis is a feature of the investigated spheroids of low passage colon cancer cell lines. Similar findings were made with spheroids from other cancer cell lines¹¹⁷. Such apoptotic signaling involves the activation of caspases and cleavage of lamin A/C and may be triggered by reduced trophic support rather than hypoxia. In compact areas of multicellular spheroids, hypoxia may further amplify the apoptotic stress similar to the additive effect of hypoxia on lamin A/C cleavage in serum-deprived monolayer cultures. Interestingly, immunochemical analyses suggest a distribution of caspase-cleaved lamin A throughout the COGA-5 spheroid, not only in compact inner areas but also in cells in the outer layers. This finding correlates with results from the TUNEL assay indicating apoptotic cells in different areas in compact COGA-5 spheroids. This leads to the assumption that apoptosis may take place not only in inner spheroid areas due to reduced trophic support and hypoxia. Another possibility is that apoptotic cells are transferred to outer regions of the spheroid instead of resting encapsulated within the spheroid.

4.1.2. Chemoresistance in low passage colon cancer cells

Differences in protein expression as observed in the 5-FU resistant cells compared to the original COGA-12 cells could result from genetic deletion, altered protein synthesis or increased degradation of the protein. The present results from RT-PCR analysis revealed reduced mRNA levels in 5-FU chemoresistant COGA-12/COGA-12/G6 cells versus COGA-12 cells, strongly indicating that the previously detected down-regulation of Hsp27 protein in COGA-12/G6 cells resulted from altered protein synthesis at the transcriptional level. Hsp27 is subjected to regulation by both heat shock transcription factors (HSFs) and by post-translational modification through phosphorylation at serine-residues of the protein, for example by MAP-kinase activated protein, and protein kinases C or D, after various forms of extracellular stress. Such phosphorylation seems to be very important for structure and function of Hsp27, for example regulating its chaperone function or the quaternary structure of the protein¹¹⁸. However, in the COGA-12/G6 cells down-regulated Hsp27 levels are more likely attributable to the HSFs which can reduce mRNA levels of Hsp27¹¹⁹. The observed mRNA down-regulation hence opens up the possibility that Hsp27 is

involved in the 5-FU resistance mechanism and is not due to long term culturing. Since reduced mRNA levels were detected in COGA-12/G6 cells but not in COGA-12/NO cells which represent corresponding long term passaging control cells without chemotherapeutic stress. As the down-regulation of Hsp27 is still present after several passages in vitro without chemotherapeutic stress, it can also be concluded that down-regulation of Hsp27 seems to be consistent over time in the COGA-12/G6. In order to clarify if the lower levels of Hsp27 have any functional relationship with the observed chemoresistance in COGA-12/G6, a siRNA knockdown approach was chosen. Down-regulation of Hsp27 in the non resistant COGA-12 cells neither with the HSP27 single sequence siRNA⁸⁷ nor with a corresponding Dicer product resulted in higher chemoresistance of these cells towards 5-FU. As the results of the corresponding RT-PCR showed, this could not be due to an insufficient knockdown effect, as both single sequence siRNA and Dicer product showed remarkable knockdown of Hsp27 mRNA level. Therefore it is more probable that HSP27 down-regulation in the COGA-12/G6 cells is at least not one of the causative events relevant for the 5-FU resistance. As it is described that HSP27 up-regulation has a protective role against chemo-induced cell death in many resistant tumor cells it is possible that down-regulation of this protein is just a consequence of other processes in COGA-12/G6 cells and maybe due to lower stress levels in these cells or that alternative proteins have taken over the function of Hsp27¹²⁰.

There are many modes of resistance to 5-FU. 5-FU itself does not have cytotoxic effects, but its metabolites FdUMP, FdUTP, FdUTP and FUTP which compete with the corresponding uracil metabolites for incorporation into RNA. In addition, FdUMP binds to thymidylate synthase and thereby inhibits its enzyme activity, by inhibiting the generation of deoxythymidine triphosphate (dTTP) that is required for DNA-replication¹²¹. One of the most common resistance mechanisms of 5-FU is increased expression of thymidylate synthase^{25;121}.

Therefore the mRNA level of thymidylate synthase was compared between resistant COGA-12/G6 and parental COGA-12 cells. Increased levels of thymidylate synthase mRNA were observed in the 5-FU resistant COGA-12/G6 cells, indicating that this might at least be one key player in the 5-FU resistance of the COGA-12/G6 cells.

4.2. *In vivo chemoresistance of prostate cancer in metronomic cyclophosphamide therapy*

4.2.1. A non classical mechanism of chemoresistance in vivo

In the present work, acquired *in vivo* chemoresistance against metronomic cyclophosphamide treatment was studied in a human prostate cancer xenograft model. The observed tumor growth profile exhibited two phases. In the first phase (response-phase), tumor progression was significantly suppressed by therapy and tumor volume remained constant. After 50 days of tumor cell implantation and about 40 days of treatment, tumor volumes increased despite ongoing CPA therapy (escape-phase) (**Figure 5B**). Two tumor cell lines (PC3-D3) and (PC3-D4) were obtained from two different resistant tumors and one cell line (PC3-A3) was isolated from an untreated non resistant control tumor.

As CPA is a prodrug, which has to be metabolized by liver cytochrome P450 enzymes¹²² and the therapeutic approach reveal antiangiogenic properties several escape mechanisms come into direct consideration. On one hand, prolonged CPA treatment might result in decrease of liver capacity in terms of drug bioactivation, resulting in decrease of systemically available active metabolites. On the other hand, as metronomic CPA therapy exhibits antiangiogenic activity, development of alternative, non-angiogenesis dependent forms of blood supply (vasculogenic mimicry^{52,53}) come into consideration to revoke tumors from efficient therapeutic response⁴⁷. In line with previous studies, tumor blood flow analysis demonstrated a reduced functionality of tumor vessels in CPA treated tumors at the treatment endpoint, indicating still effective conversion of CPA to the cytotoxic active drug after prolonged treatment (**Figure 6C versus D;E**). Analysis of laminin, which is a main compound of the basal lamina of blood vessels, and staining for CD31 positive endothelial cells showed co-localization in treated as well as in untreated tumors (**Figure 6C versus D**). Total count of mouse CD31 positive structures, representing functional as well as non functional vessel structures within tumor tissue, was not significantly reduced by the therapeutic regimen. However, decreased functional blood flow was detected to go along with a reduced number of vessels with detectable lumen (**Figure 6E**). Therefore it seems unlikely that lacking responsiveness in the second period of treatment is due to insufficient CPA biotransformation followed by non effective suppression of angiogenesis. This is

consistent with recently published pharmacodynamic and pharmacokinetic studies of prolonged low-dose CPA therapy¹²² and further suggests that re-growth of tumors is not due to malfunction of antiangiogenic scheduled CPA e.g. by non efficient activation of the pro-drug in the liver. Further histological analyses of collected tumor tissue, comparing relapsing CPA treated tumors and untreated control tumors resulted in a similar tissue structure; however, treated tumors exhibited larger areas of condensed and fragmented cell nuclei, probably resulting from direct cytotoxic effects of CPA and/or by microenvironmental effects resulting from decreased blood supply⁷⁸.

To give further consideration to possible resistance mechanism resulting from metronomic scheduled CPA treatment, immunohistochemistry of tissue from reimplanted tumors was performed in combination with respect to functional blood flow. Blood flow analysis of reimplanted resistant tumors revealed no significant differences in comparison to the in vivo passaged PC3-A3 control tumor, indicating that resistant tumors do not compensate the antiangiogenic treatment by exhibition of increased angiogenic potential (**Figure 30A**). Further on, the following short term treatment for 14 days resulted in a similar response in terms of blood flow in resistant and control tumors. In resistant tumors and in PC3-A3 control tumors two cycles of CPA application were not sufficient for statistically significant changes in tumor blood flow (**Figure 30A**). As therapeutic strategies targeting preferentially endothelial cells would not be effective in tumors whose blood supply is formed in the absence of angiogenesis, tumor microsections were analyzed for the existence of alternative blood supply routes (vasculogenic mimicry). These functional routes are characterized by tumor cells generating microcircular channels composed of extracellular matrix, including laminin and lined by tumor cells in the absence of endothelial cells^{52;53}. The existence of such channels was already described for different Dunning rat prostatic adenocarcinoma cell lines as well as for the human cancer line DU145¹²³. However, in the PC3 xenograft model, CD31/laminin co-staining revealed that all functional vessel structures, indicated by Hoechst fluorescence, showed a positive reaction for CD31 on the lumen internal surface. Functional microvascular channels without participation by endothelial cells could not be detected in the resistant tumors even under therapeutic pressure (**Figure 30B**). Reisolated resistant (PC3-D3 and PC3-D4) and in vivo passaged control tumor cells (PC3-A3) were characterized and identified in terms of cell morphology and their

human receptor status in order to distinguish them from mouse derived cells. No differences in cell morphology or epidermal growth factor (EGF) receptor or transferrin receptor expression were detected by comparing reisolated tumor cells with PC3-wt cells⁷⁸ (**Figure 24, 25**)

In vivo chemoresistant, reisolated tumor cells (PC3-D3 and PC3-D4) did not manifest their drug resistant phenotype in two-dimensional monolayer culture, when treatment was performed with 4-HOO-CPA, indicating the involvement of microenvironmental factors (**Figure 5C**) and suggesting resistance mechanisms which differ from classical mechanisms based on up-regulation of drug efflux pumps⁴⁸. Indeed, Hoechst efflux assay revealed that PC3 cells do not have a side population with increased efflux transporter activity¹²⁴. Further on, the assay did not detect any differences between resistant and non resistant PC3 control cells (**Figure 26**) indicating that increased drug efflux is not relevant for resistance in this case.

Importantly however, resistant tumor cells have an endogenous component crucial for in vivo resistance as the acquired drug resistant phenotype of reisolated tumor cells (PC3-D3 and PC3-D4) was manifested after reimplantation into mice (**Figure 28**) even in the first phase of CPA treatment. Reisolated PC3 control tumor cells passaged in vivo without CPA treatment (PC3-A3) remained sensitive to the treatment regimen (**Figure 29**). Chemosensitivity of PC3-A3 cells exclude that resistance is acquired by unspecific selection processes of the in vivo tumor environment which may change the behavior independently of the applied chemotherapeutic regimen^{125;126}.

4.2.2. Proteomics and Genomics: two complementary approaches to in vivo resistance

As no classical tumor escape mechanism could be detected to be responsible for in vivo resistance of PC3 xenografts towards metronomic CPA therapy, the analysis had to be continued on a more global level to discover new resistance mechanisms.

In order to address the complexity of the system a proteomic as well as a genomic approach have been chosen as two alternating approaches to identify new candidates involved in resistance.

4.2.2.1. Proteomic approach

Proteome analysis by 2D DIGE revealed several alterations in protein expression pattern of reisolated cell lines PC3-D3 and PC3-D4 compared to corresponding

parental PC3-wt. From 25 relevant spots detected by 2D-DIGE, all could be assigned and recovered from preparative CBB-stained gels. All of these proteins could be identified by MALDI-PMF and MS/MS analysis on basis of commonly accepted database search criteria. In proteome comparisons between resistant and respective parental PC3-wt cells, only 1.6-fold or higher alterations in protein expression were taken into account, to keep the false discovery rate low. The identities of all identified spots are shown in **Table 3, 4**. Expression levels of four proteins were found to be increased and three proteins were down-regulated in PC3-D3 cells compared to parental PC3-wt cells (**Figure 31A**). In the PC3-D4 cultures, nine proteins were found up-regulated and nine down-regulated compared to parental PC3-wt (**Figure 31B**). Some alterations such as upregulation of keratin 8 and down-regulation of HSPD1 (60kDa mitochondrial heat shock protein) were also present in in vivo passaged non resistant control cells, indicating regulations by microenvironmental influences. These alterations in protein pattern were excluded from further investigation as their regulations are independent from the therapeutic treatment regimen (**Figure 32, Table 5**). As both resistant sublines PC3-D3 and PC3-D4 are derived from different animals with resistant tumors, they do not have mandatory exactly the same resistance mechanisms activated. We assume that resistance towards antiangiogenic treatment is a complex process not only mediated by one distinctive molecular pathway. Therefore we analyzed two different clones in order to identify some common key proteins regulated in different resistant tumors in response to metronomic CPA therapy. We focused on ANXA3, TXNDC5, CatB and CK19. These candidates were identified by their differential expression profiles in both resistant variants compared to the chemosensitive controls (**Figure 31C**).

Validation: Removal of false friends

One protein detected to be regulated in both chemoresistant PC3 cell lines was identified as cytokeratin 19 (spot D3-3 and D4-1). Cytokeratin 19 is part of one group of intermediate filament proteins responsible for the integrity of cell structure, and have been reported to play a role in conferring a drug resistance phenotype in several types of cancer such as breast and cervical carcinoma^{127;128}. However, in contrast to 2D-DIGE analysis, up regulation of this protein was not evident in the validation experiments by western blot analysis (**Figure 33, 34**)

Cathepsin B: where to B(e)?

The catB spot regulated in both reisolated sub-lines (D3-4 and D4-5) has a molecular weight around 20-25 kDa and a pI value of 5.2 (**Figure 31, Table 4, 5**). Validation experiments by western blot analysis in vitro confirmed increase in catB in resistant compared to non resistant tumor cells detected by 2D-DIGE (**Figure 35**). No significant increase in protein level could be confirmed in corresponding tumor tissues (**Figure 37**). CatB is part of the class of cystein proteases, which belong to the papain family. The cystein proteases are predominantly endopeptidases, which are located intracellularly in endolysosomal vesicles. CatB can act as both endopeptidase and exopeptidase and is expressed constitutively participating in protein turnover. Cystein cathepsins are highly up-regulated in a variety of cancers by mechanisms ranging from gene amplifications to post-transcriptional modification. Their localization within intracellular lysosomes often changes during neoplastic progression, resulting in secretion of both inactive and active forms and association with binding partners on the tumor cell surface. Secreted, cell surface and intracellular cystein cathepsins function in proteolytic pathways that increase neoplastic progression^{129;130}, and are also described to be promising markers for aggressive prostate cancer¹³¹.

The spot up-regulated in PC3-D3 and PC3-D4 has a lower molecular weight and different pI from full length cathepsin b protein representing a variant for catB arising either from the use of alternative promoters or alternative splicing e.g. by exon skipping¹³². Truncation in catB sequence often results in altered localization of the protein to different membraneous organelles¹³³ and several studies describe that exon 2 and 3 can be skipped resulting in a shorter form of catB targeting mitochondria¹³⁴ where it can influence the apoptotic pathway¹³⁵. This finding is consistent with our observation that the two detected cathepsin forms of 32 kDa and 22 kDa translocate to the mitochondria in the reisolated PC3 cells but not in the PC3-wt cells in vitro (**Figure 36**). Nevertheless the role of catB in mitochondria in this case has to be clarified in future studies.

TXNDC5: less is more?

The spot D3-5 (1.6-fold down regulated) in the PC3-D3 cells and the spots D4-13 and D4-14 (both 1.8-fold down regulated) in the PC3-D4 cells were identified as TXNDC5 (**Figure 31, Table 4, 5**). The spot D3-5 and D4-14 have the same position in the gel

whereas the D4-13 has a lower pI and a difference in molecular weight compared to the other spots of approximately 1 kDa. Peptide sequence comparison identified lack of peptides of the signal peptide at the N-terminus of TXNDC5 in the sequence of D4-13, which might explain the lower pI value. Molecular weight difference might be due to posttranslational modification of the protein or represents a different isoform. TXNDC5 belongs to the protein superfamily of thioredoxin proteins. Thioredoxin (Trx) family members play critical roles in regulation of cellular redox homeostasis^{136;137}, their role is widespread. It is described that they play a crucial role in increased proliferation, resistance to cell death and increased angiogenesis¹³⁷. TXNDC5 is a protein disulfide isomerase (PDI) mostly located in the endoplasmic reticulum¹³⁸. TXNDC5 is especially present in endothelial cells where it protects the cells against apoptosis induced e.g. by hypoxia or chemotherapeutics^{139;140}. In cancer cells its up-regulation was associated so far with colon and hepatocellular carcinogenesis^{141;142}. In our study the TXNDC5 protein was found to be down-regulated in both resistant sub-lines compared to PC3-wt cells in vitro. This could also be confirmed by western blot analysis in vitro (**Figure 38**) and in vivo (**Figure 39**). As our findings using hypoxic in vitro conditions do not correlate with the increased levels of TXNDC5 under hypoxia observed by Sullivan et al. in endothelial cells where it is protective against hypoxia-induced apoptosis¹³⁹, TXNDC5 must play a different role in PC3 cells (**Figure 38**). It is described that PDIs can not only have chaperone function but also can exhibit the contrary in case of low concentrations compared to the unfolded substrate. Under these circumstances its role changes from preventing protein aggregation to promoting protein aggregation which finally leads to increased secretion of these proteins¹⁴³. In our case of in vivo resistance where the cross talk between tumor and its microenvironment might be involved in resistance this role of TXNDC5 can be more important than its chaperone function. Chemotherapy resulted in significantly increased levels of TXNDC5 in the PC3-D3 tumor xenografts of the resistant PC3 cell lines whereas its expression was not affected in the chemosensitive tumors (**Figure 39**). As the induction of TXNDC5 under therapy is specific for resistant PC3 tumors it seems to be unlikely that its role is implicated in a general chaperone function under stress but a more specific role in activation/inhibition of resistance mediating signaling proteins by disulfide isomerization¹⁴⁴.

ANXA3: a functional key player in metronomic chemoresistance in vivo?

ANXA3 (D3-1 and D4-3) was up-regulated in both resistant sub-lines (**Figure 31, 40**). Western blot analysis from the corresponding tumor tissues showed that this effect is relevant under in vivo conditions. Additionally performed cross reactivity tests revealed that the detected regulation of ANXA3 is not influenced by potential changes in the content of mouse cells within the tumor tissue (data not shown). The protein levels even increase under therapy in PC3-D3 and PC3-D4 (resistant) but not in PC3-A3 control tumors (in vivo passaged), further indicating the involvement of this candidate in the in vivo resistance mechanism (**Figure 41**). ANXA3 is a member of the annexin family (I-XIII). All annexins have a conserved core domain consisting of four or eight annexin repeats, through which annexins binds to the phospholipids in a Ca^{2+} -dependent manner¹⁴⁵. ANXA3 is one of the least studied members and its function is widely unknown. It can mediate membrane-membrane contact during biological processes (i.e., phagosome-lysosome fusion, vesicular trafficking, plasma membrane binding and degranulation)¹⁴⁶ and can interfere with arachidonic acid inflammation pathway¹⁴⁷. Furthermore it is described as chemoattractant for macrophages¹⁴⁸. Its role in cancer is still not fully understood. However, a proteomic study showed that ANXA3 might be implicated in response of lung cancer cells to the cytotoxic drug OSU03013, a derivative of celecoxib, and overexpression of ANXA3 was detected in platinum-resistant human ovarian cancer cells^{149;150}. With respect to the anti-angiogenic therapeutic schedule of our study ANXA3 could be considered to attribute to regulation of angiogenesis as it is proclaimed by Park et al. in an in vitro model¹⁵¹. However, we could not detect a statistically significant increase in angiogenic potential of resistant tumors. Our in vitro studies under hypoxic conditions showed increased expression of ANXA3 but without any difference between resistant and non resistant PC3 cells (**Figure 42**). This finding does not reflect the protein expression profile of ANXA3 in vivo, leading to the conclusion that resistance in vivo includes mechanisms going beyond direct hypoxia-induced regulations. Regarding at this discrepancy between in vivo and in vitro cell behavior the role of ANXA3 in inflammation and in outward cell signaling attracts notice to its role in tumor host interactions. In this context, the xenograft model provides the required environment for in vivo acquired drug resistance towards metronomic CPA therapy.

4.2.2.2. Genomic approach

Microarray analysis was performed of tumor tissue (4 mice per group) derived from resistant (PC3-D3, PC3-D4) and non resistant PC3 (PC3-A3, PC3-wt) xenografts, either in the absence or presence of CPA therapy (24 h before tumor harvesting).

Data analysis by hierarchical sample clustering revealed major variance in total gene expression between PC3-wt on the one hand and all other *in vivo* passaged tumors (PC3-A3, PC3-D3 and PC3-D4) on the other hand (**Figure 43**). This indicates the large influence of *in vivo* environment on tumor gene expression already previously described in several studies^{126;152;153}. Genes up-regulated by *in vivo* passaging in PC3-A3 compared to PC3-wt include e.g. podoplanin, IL13RA2, S100A2 which have been associated with aggressiveness, increased proliferation and migration of tumor cells¹⁵⁴⁻¹⁵⁶. Down-regulated genes due to *in vivo* passaging include a variety of tumor suppressor genes such as e.g. TP53INP1 and LOX^{157;158} (**Figure 44, Table x**). These observations on genetic level are sustained by our data showing a more aggressive tumor growth of PC3-A3, PC3-D3 and PC3-D4 *in vivo* compared to PC3-wt tumors (**Figure 29**). These genes did not correlate with resistance in PC3 xenografts as PC3-A3 tumors are still chemosensitive towards metronomic CPA *in vivo* (**Figure 29**) and up-regulated genes of aggressive tumor growth such as podoplanin, IL13RA2 and S100A2 did not keep their higher gene expression compared to PC3-wt under CPA treatment (**Figure 48**).

With respect to the *in vivo* passaging effect, gene expression of resistant tumors has been compared to PC3-A3 in order to identify resistance relevant genes. These studies revealed innate alterations in mRNA levels between resistant and non resistant tumors (**Figures 44-46**). Analogue to results obtained by proteomic approach, both resistant tumors showed common alterations in gene expression as well as clone specific ones reflecting their origin from different resistant tumors (**Figure 47**). The majority of genes with constitutive differential expression between resistant and non resistant tumors kept their significant regulation after CPA treatment. Expression levels of several genes further increased respectively decreased after therapy. CPA treatment induced a variety of additional changes in gene expression between resistant and non resistant PC3 tumors (**Figures 48-50, Appendix Tables 6-8**). Especially in PC3-D4 tumors the fraction of candidates selectively up-regulated by CPA therapy exhibited to be outsized (**Figure 50**).

In line with our previous experiments, differentially expressed genes between resistant and non resistant PC3 tumors did not hint directly towards any classical resistance mechanism described so far. However, the gene expression profiles of several gene candidates could be linked to these of other genes with similar expression pattern via hierarchical gene clustering⁸⁴. This could hint to their involvement in common pathways and provides interesting information for further detailed analysis of the candidates.

ANXA3, already detected by proteomics to be up-regulated in resistant tumors, showed similar gene expression pattern to a cluster of genes especially highly expressed in PC3-D4 tumors but also showing higher expression in PC3-D3 tumors compared to non resistant PC3-A3 and PC3-wt tumors (**Figure 51A**). In addition to ANXA3 this cluster includes the significantly regulated candidates STAT1, SLC7A6, MBNL3 and ZNF486. ANXA3 clusters in close vicinity to the transcription factor NFATC3. NFATC3 is involved in Ca^{2+} /calmodulin dependent transcription regulation promoting prostate cancer cell proliferation¹⁵⁹ and its inhibition can lead to apoptosis in retinoblastoma cells¹⁶⁰. STAT1 has been described as key modulator in apoptosis resistance in response e.g. to radiation and cytotoxic stress in renal carcinomas and head and neck cancer cells^{161;162}. It mediates the responsiveness of cells to several cytokines and growth factors and can be induced by INF signaling¹⁶³. The involvement of ANXA3 and STAT1 in Ca^{2+} dependent signaling might be the link between both candidates¹⁶⁴⁻¹⁶⁶. STAT1 clusters in proximity to EMP-2 which has been described to play a role in integrin receptor regulation in endometrium and has been associated with poor outcome of endometrial adenocarcinoma^{167;168}. In mice, inhibition of EMP2 significantly reduced tissue production of inflammatory cytokines, recruitment of polymorphonuclear leukocytes, and local tissue inflammation¹⁶⁹. Despite there is no clear link towards a well known resistance pathway; all these candidates can be associated to cytokine signaling. Thus this clustering can hint to the involvement of cytokine signaling and STAT1 mediated apoptosis resistance mechanisms in PC3 tumor resistance in vivo.

Regarding at a second cluster of genes with up-regulated gene expression pattern in resistant versus non resistant PC3 tumors further hints towards involvement of inflammatory cytokine signaling in the resistance mechanism of PC3 tumors (**Figure**

51B). The cluster which groups around TGFB2, a candidate up-regulated in both resistant PC3 tumors under CPA therapy (especially PC3-D4) includes five other up-regulated genes (significant regulation in PC3-D4) such as CD274, TNFAIP6, GPR126, PMAIP1 and MPHOSPH6. TGF β has been described as a key player in angiogenesis as well as in inflammation and tissue repair¹⁷⁰. Impaired calcium signaling can induce TGF β ¹⁷¹. Secreted TGFB2 has shown to effectively activate NFkappaB mediated apoptosis resistance in PC3 cells which can be overcome by targeting TGFB2 mRNA using siRNA¹⁷². It has been previously described that TGFB directly influences expression of CD274¹⁷³. As these two proteins cluster in direct proximity an involvement of both within the same pathway therefore might be probable. CD274 is involved in inflammatory cytokine signaling¹⁷⁴. Similar to STAT1, CD274 is also involved in interferon signaling¹⁷⁵ and its overexpression is associated with a higher risk of relapse in Wilms Tumors¹⁷⁶. Gene expression profiles of TNFAIP6 and GPR126 also show high similarity to that of TGFB2. GPR126 is a G-protein cell surface receptor mostly described in endothelial cells which has been associated with cell adhesion and inflammation¹⁷⁷. TNFAIP6 encodes TSG-6, a 35 kDa inducible secreted glycoprotein. Activation of the TNFAIP6 gene by pro-inflammatory cytokines, presence of TSG-6 protein in inflammatory lesions and its anti-inflammatory effect suggest a role for TSG-6 in a negative feed-back control of the inflammatory response¹⁷⁸. It was shown that treatment of a murine macrophage cell line with TNFAIP6 protein up-regulates the expression of inducible cyclooxygenase-2 (COX-2), a key enzyme in inflammation and immune responses¹⁷⁹. TSG-6 has been observed to directly interact with BMP-2 a component of the TGFB/BMP pathway in vitro¹⁸⁰.

A third cluster includes the candidates PASD1 and GALNT4 up-regulated in both resistant PC3 variants which cluster together in the same subfamily making them interesting candidates for following pathway analyses (**Figure 51C**). Both candidates are still poorly described in terms of their biological function. However, PASD1 has been previously associated with poor prognosis in B-cell lymphoma. The nuclear localization sequence and leucine zipper domain of PASD1 promotes the presumption that it plays a role as transcription factor¹⁸¹. GALNT4 belongs to the family of N-acetylgalactosaminyltransferases which are key enzymes in O-glycosylation of

different glycoproteins and have been recently shown to be relevant for TGF β signaling¹⁸².

Genes with decreased expression levels in resistant compared to non resistant PC3 xenografts can also be grouped by hierarchical gene clustering. **Figure 52A** shows similar gene expression pattern for ARMCX3, TCN1, BMPR1B, CHRM3 and KCNJ6 along with a set of other genes of similar expression profile. Activated BMP signaling has been described to show reduction in tumor growth of subcutaneous PC3 tumors in mice¹⁸³. Therefore down-regulation of BMPR1B, a receptor involved in the BMP signaling cascade, in resistant PC3 tumors hints towards an inactivation of this growth control pathway. There is no clear link described so far between BMP signaling and other genes within this cluster. ARMCX3 also known as armadillo repeat-containing protein is a member of the outer mitochondrial membrane and interacts with Sox-10 a nuclear cytoplasm shuttle protein and transcription factor¹⁸⁴. CHRM3 codes for an acetylcholine receptor¹⁸⁵ and KCNJ6 codes for a G protein-activated inward rectifier potassium channel 2 (GIRK2). Inhibition of GIRK channels appears to result, at least in part, from activation of phospholipase C (PLC) and the resultant decrease in membrane levels of phosphatidylinositol-4,5-bisphosphate (PIP2), an endogenous co-factor necessary for GIRK channel activity¹⁸⁶. BMP signaling is also associated with intracellular Ca²⁺ pathways such as Ca/Calmodulin pathway and a cross talk of BMP signaling with the JAK/STAT pathway has been described^{187;188}.

The majority of genes included in a second cluster with a profile of lower gene expression in resistant versus non resistant variants can be associated to interferon signaling (**Figure 52B**). MX1, TRIM21, TRIM 5, OAS3 and IFIT1 are all genes which are normally induced by interferons in response to viral infection¹⁸⁹. However, these factors have been shown to modulate not only antiviral response but also to play a role in cellular growth control, protein turnover and induction of apoptosis¹⁹⁰⁻¹⁹². It is not clear yet how PDGFD can be related to these Interferon induced effectors. PDGFD is known to code for platelet-derived growth factor D which is a member of the PDGF/VEGF family of growth factors involved in a variety of cellular processes such as cell proliferation, invasiveness and angiogenesis. PDGFD has been

implicated in macrophage attraction¹⁹³ and endothelial mesenchymal transition of PC3 cells¹⁹⁴.

Even if hierarchical gene clustering did not reveal a clearly defined pathway, it provided first evidence of the involvement of impaired Ca^{2+} and interferon signaling as well as a role of TGFB2 in prostate cancer CPA resistance in vivo. Each of the three pathways has been described independently from each other to be involved in apoptosis resistance of androgen independent prostate cancer^{172;195-197}. However, there are still open questions how they play together in mediating resistance to metronomic CPA therapy in vivo and it will be interesting to further analyze the connection between these three pathways and to clarify their detailed involvement in CPA resistance in vivo (**Figure 55**). As all three pathways are also associated with inflammatory cytokine signaling an involvement of tumor host interaction might also be relevant in this process^{198;199}.

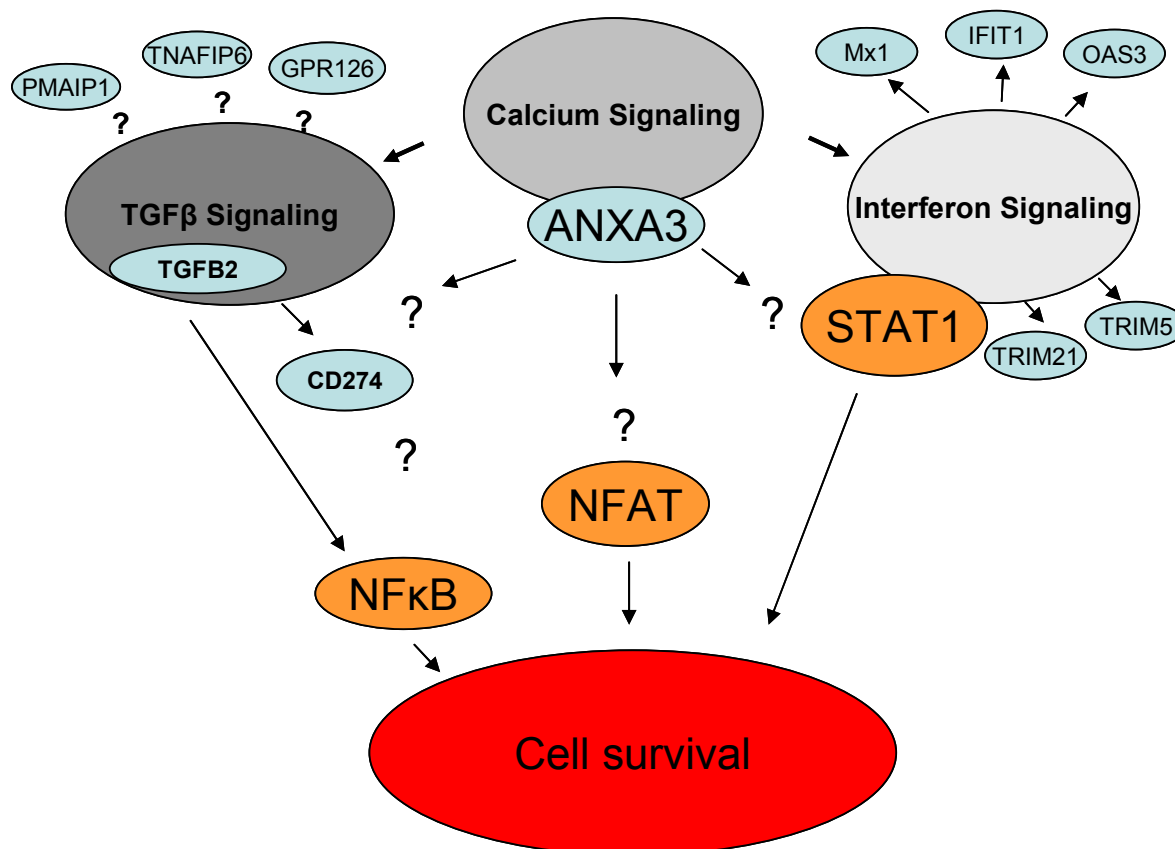


Figure 55: Schematic view of possible mechanisms involved in prostate cancer resistance towards metronomic cyclophosphamide in vivo

Probe design of the Gene 1.0 ST Array System where each of the well-annotated genes is represented by 26 probes on average, spread across the full length of the gene, makes this array suitable also for a more detailed view on transcript level. The information about differences in expression of single exons can hint towards alternative splicing instead of whole gene regulation. F3 was one example where altered expression levels in different exons were detected specifically in resistant PC3-D4 compared to all other tumors. F3 codes for the tissue factor (TF) classically described as anti-coagulation factor. Tissue factor is overexpressed in a variety of cancers including prostate cancer²⁰⁰ and has been associated with tumor growth and angiogenesis²⁰¹. In addition to the normal full length F3 transcript which was constitutively expressed in all PC3 tumors, a transcript variant could be detected to be up-regulated in PC3-D4 which showed only higher expression of sequences binding the probe set spanning exon 2-6 (**Figure 53**). Up to date two variants of alternative splicing have been described. Alternative splicing in terms of exon 5 leading to a soluble form of TF (asTF) has been described to play a role in blood clotting²⁰². More recently a splice variant was discovered to be present especially in solid tumors in addition to the normal full length F3. This variant describes an enlarged F3 transcript due to insertion of an exon 2 flanking sequence of intron 1^{203;204}. However no transcript variant lacking exon 1 has been described in the literature so far. Therefore it would be important to further validate this observation by PCR using an appropriate set of primers.

4.2.2.3. Gene expression of proteomic candidates

ANXA3, TXNDC5, CatB, three candidates for resistance detected by 2D-DIGE were studied in detail regarding their mRNA regulation by microarray analysis. Thus it could be determined if protein regulations were due to posttranslational modifications or to differences in mRNA levels. Gene expression of CK19, a protein also identified by proteomics but which could not be further confirmed as relevant for resistance was also analyzed in comparison to the other candidates.

TXNDC5 which is down-regulated on protein level in resistant tumors shows only a tendency of lower gene expression in resistant variants compared to non resistant ones (**Figure 54**). As the difference in gene expression is not significant, there must be another posttranslational component involved in the lower protein expression of TXNDC5 within the resistant cells. Indeed two separate spots of TXNDC5 appeared

in the proteome of PC3-D4 cells which can hint to a posttranslational modification of this protein (**Figure 31B, Table 4**).

CatB was significantly up-regulated on protein level in resistant PC3 cells compared to non resistant cells in vitro but could not be detected to be significantly increased in vivo by western blot analysis. Gene expression is also not significantly increased in both resistant variants but showed similar pattern to protein expression data of tumor tissue in vivo (**Figure 54** versus **Figure 37**) where a non significant tendency of higher CatB expression in PC3-D4 tumors can be detected. In terms of its role in resistance the mitochondrial localization might be more interesting to investigate in detail than simple up-regulation of the gene.

Figure 54 shows that gene expression of ANXA3 is strongly up-regulated in resistant compared to non resistant PC3 xenografts. This link of mRNA level and protein level makes ANXA3 an interesting candidate for siRNA knockdown in vivo. Interestingly, gene expression of ANXA3 is also increased in the PC3-A3 compared to the PC3-wt tumors however this regulation on mRNA level was not detected by western blot analysis on protein level of corresponding tumors (**Figure 54** versus **Figure 41**).

5. Summary

Resistance in tumor therapy with chemotherapeutic drugs is still a major issue in cancer treatment and escape mechanism behind are far from being clear. Especially cancer resistance in vivo has been identified to be highly complex and not clarified in detail²⁰⁵. Mechanisms behind escape from antiangiogenic treatment approaches, a phenomenon which has been long supposed to be unlikely, are still far from being clear²⁰⁶. In the course of this thesis a proteomic combined with a genomic approach was applied to address chemoresistance in vivo and the involvement of selected proteins was studied in the chemoresistance relevant context of 3D tumor growth and in vitro resistance.

Spheroid cultures of cancer cells better reflect characteristics of tumors than traditional monolayer cultures in terms of cell-cell contact and oxygen as well as nutrient supply. Furthermore, low-passage cancer cell lines recapitulate the properties of the original tumor cells more closely than commonly used standard cell lines that experience artificial selection processes and mutations over years of passaging. Fragmentation of Lamin A/C has been previously detected by 2D electrophoresis to occur in low passage colon cancer spheroids¹⁵. However, its role in 3D versus 2D tumor growth has not been clarified. The present work identified the lamin protein as a caspase-6-cleavage product in apoptotic cells of the spheroid. Similar caspase-dependent lamin cleavage was observed in monolayer cultures after serum withdrawal and further increased under hypoxic conditions, suggesting cleaved lamin as an indicator for apoptotic stress.

A direct functional involvement of Hsp27 down-regulation in 5-FU chemoresistant colon cancer cells could not be detected by siRNA mediated knockdown of Hsp27 in chemosensitive colon cancer cells. However thymidylate synthase, a key enzyme in 5-FU metabolism which has been previously described to be involved in 5-FU resistance was detected to be up-regulated in the 5-FU resistant colon cancer cells in vitro.

Proteomic analysis of in vivo chemoresistance focused on a human prostate cancer (PC3) xenograft model which reflects acquired in vivo resistance towards metronomic cyclophosphamide treatment. Cells from in vivo resistant PC3 tumors were reisolated and reimplanted into SCID mice. Interestingly cells exhibited their resistant phenotyp

only *in vivo* but not *in vitro*⁷⁸ whereas *in vivo* passaged control cells did not show resistance after reimplantation. Several known *in vivo* relevant escape mechanisms were experimentally excluded. Differences in drug efflux or changes in initial angiogenic potential of reimplanted resistant tumors were not detected. Vasculogenic mimicry as a potential escape mechanism was not evident. The sensitive and resistant tumor isolates were subject to 2D-DIGE followed by MALDI-TOF-TOF analysis of differential regulated protein spots. A total of 25 differences in protein expression between resistant and non resistant PC3 cells could be identified from which 4 protein spots were present in both resistant analyzed PC3 clones. Differential *in vivo* expression of these 4 candidates (annexin A3, thioredoxin containing protein 5, cathepsin B, cytokeratin 19) was evaluated by western blot analysis from the corresponding tumor tissue. Cytokeratin 19 regulation was detected not to be associated with resistance by validation experiments. Thioredoxin containing protein 5 was upregulated only in resistant xenografts by *in vivo* treatment. A truncated version of cathepsin B, a third protein spot identified in both resistant clones could be detected to be translocated into mitochondria in resistant clones whereas it stays cytoplasmic in corresponding parental PC3 cells. Annexin A3 was found to be upregulated *in vitro* and *in vivo* and protein levels further increased by metronomic cyclophosphamide treatment *in vivo*.

Microarray analysis was performed of corresponding reimplanted PC3-xenografts derived from resistant and non resistant PC3 cells with and without CPA treatment (tumor harvesting 24h after CPA treatment). Data analysis revealed a strong influence of *in vivo* passaging onto the gene expression of PC3 xenografts. This strengthened the importance of taking *in vivo* environmental conditions into account. Several alterations in gene expression between resistant and non resistant PC3 tumors could be identified. Hierarchical gene clustering led to first evidence that impaired interferon, calcium and TGF β signaling might be involved in PC3 chemoresistance *in vivo*.

Furthermore microarray analysis revealed no significantly increased mRNA levels in case of cathepsin B which is consistent with protein analysis. Thus it would be interesting to focus on the truncated version of CatB which localizes to mitochondria of resistant PC3 cells. The regulation of TXNDC5 was also not reflected to a significant extent on mRNA level which leads to the conclusion that posttranslational mechanisms are involved in the significant protein regulation of TXNDC5 which have

been detected by proteomics and western blot analysis. In contrast, ANXA3 showed significant up-regulation on mRNA level in resistant compared to non resistant tumors. This makes ANXA3 a valid biomarker for prostate cancer resistance in vivo and can make it a potential target for in vivo knockdown studies in resistant PC3 xenografts using siRNA application.

6. Appendix

6.1. Tables

Gene_Symbol	Gene_Name	Average A3	Average wt	fold change A3 vs wt	t-test/Anova A3 vs wt
NTS	neurotensin	9.54	6.96	5.99	0.0002
AMY2B	amylase, alpha 2B (pancreatic)	9.65	8.10	2.93	0.0001
MAGEC2	melanoma antigen family C, 2	7.89	6.34	2.92	0.0003
SERPINB7	serpin peptidase inhibitor, clade B (ovalbumin), member 7	7.82	6.34	2.79	0.0002
RSAD2	radical S-adenosyl methionine domain containing 2	10.66	9.42	2.36	0.0004
ZNF204	zinc finger protein 204 pseudogene	7.78	6.55	2.35	0.0004
CYP2B7P1	cytochrome P450, family 2, subfamily B, polypeptide 7 pseudogene 1	7.28	6.15	2.19	0.0012
APOBEC3B	apolipoprotein B mRNA editing enzyme, catalytic polypeptide- like 3B	9.08	7.96	2.17	0.0006
IL13RA2	interleukin 13 receptor, alpha 2	8.70	7.62	2.11	0.0059
PDPN	podoplanin	7.24	6.20	2.06	0.0000
S100A2	S100 calcium binding protein A2	8.16	7.14	2.03	0.0007
CDH12	cadherin 12, type 2 (N-cadherin 2)	5.29	9.65	-20.45	0.0000
IFI44L	interferon-induced protein 44-like	7.56	10.38	-7.07	0.0001
CP	ceruloplasmin (ferroxidase)	8.95	11.33	-5.21	0.0002
GPR110	G protein-coupled receptor 110	9.07	11.14	-4.21	0.0005
TCP11L2	t-complex 11 (mouse)-like 2	6.02	8.06	-4.12	0.0007
KRT20	keratin 20	6.55	8.51	-3.91	0.0008
GALNT3	UDP-N-acetyl-alpha-D-galactosamine:polypeptide N- acetylgalactosaminyltransferase 3 (GalNAc-T3)	4.95	6.90	-3.88	0.0002
HSD17B13	hydroxysteroid (17-beta) dehydrogenase 13	4.55	6.41	-3.65	0.0045
OAS1	2',5'-oligoadenylate synthetase 1, 40	7.68	9.54	-3.63	0.0004
TMEM71	transmembrane protein 71	7.64	9.45	-3.50	0.0002
ITGA10	integrin, alpha 10	7.82	9.59	-3.43	0.0001
TTC6	tetratricopeptide repeat domain 6	5.69	7.46	-3.42	0.0021
TSPAN8	tetraspanin 8	6.28	7.98	-3.25	0.0003
DDX58	DEAD (Asp-Glu-Ala-Asp) box polypeptide 58	7.48	9.17	-3.23	0.0002
TFPI	tissue factor pathway inhibitor (lipoprotein-associated coagulation inhibitor)	6.65	8.34	-3.21	0.0132
NPY1R	neuropeptide Y receptor Y1	6.11	7.79	-3.21	0.0009
RANBP3L	RAN binding protein 3-like	6.04	7.71	-3.17	0.0006
MX2	myxovirus (influenza virus) resistance 2 (mouse)	7.64	9.30	-3.17	0.0005
TP53INP1	tumor protein p53 inducible nuclear protein 1	5.53	7.18	-3.14	0.0034
TMEM56	transmembrane protein 56	5.04	6.69	-3.13	0.0004
CDR1	cerebellar degeneration-related protein 1, 34kDa	7.92	9.54	-3.08	0.0009
PLAT	plasminogen activator, tissue	5.16	6.77	-3.06	0.0009
IFI44	interferon-induced protein 44	5.07	6.67	-3.04	0.0012
ABCA13	ATP-binding cassette, sub-family A (ABC1), member 13	8.57	10.16	-3.01	0.0007
KDR	kinase insert domain receptor (a type III receptor tyrosine kinase)	4.85	6.43	-3.00	0.0003
SAMD9	sterile alpha motif domain containing 9	8.66	10.23	-2.97	0.0001
SH2D1A	SH2 domain protein 1A	6.01	7.57	-2.95	0.0002
TRIM22	tripartite motif-containing 22	9.43	10.98	-2.94	0.0003
MSTN	myostatin	3.80	5.36	-2.94	0.0011
IFIT3	interferon-induced protein with tetratricopeptide repeats 3	5.65	7.19	-2.90	0.0015
SEMA3D	sema domain, immunoglobulin domain (Ig), short basic domain, secreted, (semaphorin) 3D	5.34	6.87	-2.89	0.0003
GLB1L3	galactosidase, beta 1-like 3	5.69	7.22	-2.89	0.0000
IFIH1	interferon induced with helicase C domain 1	6.75	8.26	-2.85	0.0006
C1orf161	chromosome 1 open reading frame 161	7.05	8.55	-2.83	0.0042
IFITM1	interferon induced transmembrane protein 1 (9-27)	5.36	6.84	-2.79	0.0002
C8orf57	chromosome 8 open reading frame 57	7.22	8.69	-2.75	0.0003
IFI6	interferon, alpha-inducible protein 6	6.52	7.97	-2.72	0.0005
TLR4	toll-like receptor 4	3.52	4.97	-2.72	0.0005

SLC26A5	solute carrier family 26, member 5 (prestin)	7.95	9.34	-2.62	0.0007
C17orf60	chromosome 17 open reading frame 60	7.85	9.22	-2.59	0.0001
TTN	titin	7.28	8.65	-2.59	0.0004
HERC6	hect domain and RLD 6	5.46	6.84	-2.59	0.0041
C4orf18	chromosome 4 open reading frame 18	7.90	9.27	-2.58	0.0017
ABCA8	ATP-binding cassette, sub-family A (ABC1), member 8	4.22	5.59	-2.58	0.0013
C14orf25	chromosome 14 open reading frame 25	7.62	8.99	-2.57	0.0007
SAMD9L	sterile alpha motif domain containing 9-like	7.10	8.46	-2.56	0.0003
PCDHB10	protocadherin beta 10	9.13	10.48	-2.53	0.0007
PCDHB4	protocadherin beta 4	8.40	9.74	-2.53	0.0025
RELN	reelin	6.46	7.80	-2.52	0.0111
HIST2H2BE	histone cluster 2, H2be	10.37	11.71	-2.52	0.0003
COL12A1	collagen, type XII, alpha 1	7.23	8.54	-2.48	0.0004
NDRG1	N-myc downstream regulated gene 1	6.33	7.65	-2.48	0.0002
ZNF493	zinc finger protein 493	5.29	6.59	-2.46	0.0002
HAPLN1	hyaluronan and proteoglycan link protein 1	4.54	5.84	-2.46	0.0003
P2RY5	purinergic receptor P2Y, G-protein coupled, 5	6.72	8.01	-2.46	0.0132
OR2B6	olfactory receptor, family 2, subfamily B, member 6	4.68	5.97	-2.45	0.0004
CREB3L1	cAMP responsive element binding protein 3-like 1	7.24	8.53	-2.44	0.0019
XK	X-linked Kx blood group (McLeod syndrome)	8.60	9.89	-2.44	0.0002
APOL6	apolipoprotein L, 6	6.33	7.61	-2.42	0.0119
SPARC	secreted protein, acidic, cysteine-rich (osteonectin)	6.38	7.65	-2.42	0.0002
FAM130A2	family with sequence similarity 130, member A2	6.99	8.26	-2.41	0.0243
ATP8A1	ATPase, aminophospholipid transporter (APLT), class I, type 8A, member 1	6.03	7.29	-2.40	0.0002
FAM177B	family with sequence similarity 177, member B	6.37	7.61	-2.38	0.0011
SLC25A27	solute carrier family 25, member 27	6.20	7.44	-2.37	0.0006
CDC20B	cell division cycle 20 homolog B (<i>S. cerevisiae</i>)	4.52	5.76	-2.36	0.0006
ZNF788	zinc finger family member 788	5.11	6.33	-2.33	0.0000
ABCA10	ATP-binding cassette, sub-family A (ABC1), member 10	8.21	9.43	-2.33	0.0008
KRT81	keratin 81	7.47	8.69	-2.33	0.0010
LANCL3	LanC lantibiotic synthetase component C-like 3 (bacterial)	7.11	8.32	-2.31	0.0019
DNAH11	dynein, axonemal, heavy chain 11	6.77	7.98	-2.30	0.0006
HPGD	hydroxyprostaglandin dehydrogenase 15-(NAD)	10.47	11.67	-2.30	0.0005
ZNF117	zinc finger protein 117	3.97	5.17	-2.30	0.0017
CCDC146	coiled-coil domain containing 146	5.41	6.60	-2.29	0.0039
ZNF528	zinc finger protein 528	5.88	7.08	-2.29	0.0005
CFH	complement factor H	8.35	9.54	-2.28	0.0006
CGNL1	cingulin-like 1	6.10	7.29	-2.28	0.0009
C2orf66	chromosome 2 open reading frame 66	3.77	4.95	-2.27	0.0012
XAF1	XIAP associated factor 1	4.34	5.52	-2.27	0.0042
MUC15	mucin 15, cell surface associated	7.83	9.01	-2.27	0.0016
SATB1	SATB homeobox 1	5.51	6.69	-2.27	0.0003
TMEM45A	transmembrane protein 45A	8.29	9.47	-2.26	0.0024
KIAA1244	KIAA1244	7.54	8.72	-2.26	0.0001
TNFSF10	tumor necrosis factor (ligand) superfamily, member 10	6.52	7.69	-2.25	0.0026
ZNF253	zinc finger protein 253	5.29	6.45	-2.24	0.0064
APOD	apolipoprotein D	8.35	9.50	-2.22	0.0029
PARP14	poly (ADP-ribose) polymerase family, member 14	7.03	8.18	-2.22	0.0005
ZNF91	zinc finger protein 91	7.39	8.53	-2.21	0.0106
STC2	stanniocalcin 2	7.33	8.46	-2.19	0.0006
TBC1D8B	TBC1 domain family, member 8B (with GRAM domain)	7.36	8.48	-2.18	0.0076
KIAA1370	KIAA1370	7.23	8.34	-2.16	0.0021
FER1L4	fer-1-like 4 (<i>C. elegans</i>)	7.15	8.26	-2.16	0.0005
PGAP1	post-GPI attachment to proteins 1	8.45	9.55	-2.15	0.0035
IFIT1	interferon-induced protein with tetratricopeptide repeats 1	5.59	6.68	-2.14	0.0042
MUC5B	mucin 5B, oligomeric mucus	8.33	9.43	-2.13	0.0018
EHF	ets homologous factor	5.22	6.31	-2.13	0.0021
ELOVL2	elongation of very long chain fatty acids (FEN1)	6.16	7.25	-2.13	0.0014
FCGR2A	Fc fragment of IgG, low affinity IIa, receptor (CD32)	10.81	11.89	-2.11	0.0003

ZNF841	zinc finger protein 841	9.06	10.14	-2.11	0.0004
PPP4R1L	protein phosphatase 4, regulatory subunit 1-like	7.61	8.69	-2.11	0.0011
IFIT2	interferon-induced protein with tetratricopeptide repeats 2	7.10	8.17	-2.10	0.0031
ZNF83	zinc finger protein 83	8.49	9.56	-2.10	0.0026
DDX60	DEAD (Asp-Glu-Ala-Asp) box polypeptide 60	6.68	7.75	-2.10	0.0098
ZNF625	zinc finger protein 625	8.17	9.23	-2.09	0.0003
C5	complement component 5	8.55	9.61	-2.09	0.0012
C10orf10	chromosome 10 open reading frame 10	7.10	8.16	-2.08	0.0234
LGR5	leucine-rich repeat-containing G protein-coupled receptor 5	9.60	10.66	-2.08	0.0066
STAT4	signal transducer and activator of transcription 4	9.06	10.11	-2.07	0.0003
PCDHB9	protocadherin beta 9	6.45	7.50	-2.07	0.0010
LOX	lysyl oxidase	8.10	9.14	-2.06	0.0028
SRGN	serglycin	6.21	7.25	-2.06	0.0024
VAV3	vav 3 guanine nucleotide exchange factor	7.01	8.05	-2.06	0.0002
ZNF439	zinc finger protein 439	4.72	5.76	-2.05	0.0008
LAMA4	laminin, alpha 4	6.41	7.44	-2.04	0.0011
CDH1	cadherin 1, type 1, E-cadherin (epithelial)	5.99	7.02	-2.04	0.0010
TTC18	tetratricopeptide repeat domain 18	5.51	6.54	-2.03	0.0005
FRK	fyn-related kinase	6.93	7.95	-2.03	0.0053
TSPAN1	tetraspanin 1	7.40	8.42	-2.02	0.0020
COL3A1	collagen, type III, alpha 1	7.35	8.36	-2.02	0.0009
GBP2	guanylate binding protein 2, interferon-inducible	4.86	5.87	-2.02	0.0048
DDX60L	DEAD (Asp-Glu-Ala-Asp) box polypeptide 60-like	7.35	8.36	-2.02	0.0006
RNF144B	ring finger 144B	6.91	7.92	-2.01	0.0000
HIST1H4H	histone cluster 1, H4h	6.35	7.35	-2.01	0.0003
KRTAP12-2	keratin associated protein 12-2	8.72	9.73	-2.01	0.0004
SKIL	SKI-like oncogene	7.42	8.43	-2.01	0.0100
FLJ20184	hypothetical protein FLJ20184	6.35	7.35	-2.00	0.0085
ZNF585B	zinc finger protein 585B	5.95	6.95	-2.00	0.0005

Table 6: Differentially expressed genes in PC3-A3 versus PC3-wt xenografts (2 fold regulation; T-Test: $p < 0.05$)

Gene_Symbol	Gene_Name	Average PC3-A3	Average PC3-D3	fold change D3 vs A3	t-test/Anova D3 vs A3
PASD1	PAS domain containing 1	5.63	7.70	4.21	0.0000
RP6-213H19.1	serine	5.96	7.36	2.64	0.0005
ZNF711	zinc finger protein 711	5.06	6.42	2.56	0.0065
ESM1	endothelial cell-specific molecule 1	4.84	6.06	2.33	0.0030
ZNF626	zinc finger protein 626	5.62	6.80	2.27	0.0007
CDC20B	cell division cycle 20 homolog B (S. cerevisiae)	4.52	5.61	2.14	0.0017
CDH12	cadherin 12, type 2 (N-cadherin 2)	5.29	6.39	2.14	0.0054
ANKRD30A	ankyrin repeat domain 30A	5.31	6.38	2.10	0.0025
ZNF788	zinc finger family member 788	5.11	6.16	2.07	0.0000
CALB1	calbindin 1, 28kDa	5.50	6.48	1.97	0.0103
MBNL3	muscleblind-like 3 (Drosophila)	5.46	6.43	1.96	0.0074
ZNF117	zinc finger protein 117	3.97	4.94	1.96	0.0003
GPC4	glypican 4	5.54	6.50	1.93	0.0004
SATB1	SATB homeobox 1	5.51	6.45	1.91	0.0006
ZNF486	zinc finger protein 486	5.56	6.49	1.91	0.0002
NCAM2	neural cell adhesion molecule 2	4.36	5.28	1.90	0.0001
RBM35A	RNA binding motif protein 35A	5.85	6.77	1.89	0.0013
ZNF429	zinc finger protein 429	4.57	5.47	1.86	0.0201
MPZL2	myelin protein zero-like 2	5.15	6.04	1.86	0.0012
ZNF66	zinc finger protein 66	5.82	6.71	1.85	0.0001
ZNF492	zinc finger protein 492	5.46	6.32	1.82	0.0118
SLC10A5	solute carrier family 10 (sodium	4.10	4.95	1.81	0.0191
ERV3	endogenous retroviral sequence 3 (includes zinc finger protein H-plk	6.06	6.90	1.79	0.0001

CDH13	cadherin 13, H-cadherin (heart)	8.13	8.96	1.78	0.0001
ZNF257	zinc finger protein 257	4.27	5.10	1.78	0.0370
PROKR1	prokineticin receptor 1	5.97	6.78	1.76	0.0002
BCAT1	branched chain aminotransferase 1, cytosolic	6.73	7.54	1.75	0.0005
ZNF625	zinc finger protein 625	8.17	8.97	1.75	0.0006
TFF1	trefoil factor 1	8.12	8.91	1.73	0.0000
MSTN	myostatin	3.80	4.59	1.72	0.0240
TMEM71	transmembrane protein 71	7.64	8.43	1.72	0.0148
GALNT14	UDP-N-acetyl-alpha-D-galactosamine:polypeptide N-acetylgalactosaminyltransferase 14 (GalNAc-T14)	5.90	6.69	1.72	0.0001
SLC1A3	solute carrier family 1 (glial high affinity glutamate transporter), member 3	6.54	7.30	1.70	0.0000
GLB1L3	galactosidase, beta 1-like 3	5.69	6.45	1.69	0.0011
ZNF91	zinc finger protein 91	7.39	8.14	1.68	0.0893
NTS	neurotensin	9.54	7.48	-4.18	0.0003
MAGEC2	melanoma antigen family C, 2	7.89	6.36	-2.89	0.0007
TCN1	transcobalamin I (vitamin B12 binding protein, R binder family)	9.64	8.34	-2.45	0.0005
PDPN	podoplanin	7.24	6.18	-2.09	0.0000
HCLS1	hematopoietic cell-specific Lyn substrate 1	7.93	6.91	-2.02	0.0007
IL1RAPL1	interleukin 1 receptor accessory protein-like 1	6.88	5.89	-1.97	0.0124
SSX8	synovial sarcoma, X breakpoint 8	7.42	6.47	-1.92	0.0093
SH2D1B	SH2 domain containing 1B	5.56	4.63	-1.91	0.0011
IL13RA2	interleukin 13 receptor, alpha 2	8.70	7.81	-1.86	0.0224
SCN3A	sodium channel, voltage-gated, type III, alpha subunit	5.97	5.10	-1.83	0.0103
SLAMF9	SLAM family member 9	6.82	5.97	-1.81	0.1041
APOL6	apolipoprotein L, 6	6.33	5.53	-1.75	0.0789
BMPR1B	bone morphogenetic protein receptor, type IB	7.71	6.95	-1.69	0.0036

Table 7: Differentially expressed genes in PC3-D3 versus PC3-A3 xenografts (1.6 fold regulation; T-Test: $p < 0.05$)

Gene_Symbol	Gene_Name	Average A3	Average D4	fold change D4 vs A3	t-test/Anova D4 vs A3
F3	coagulation factor III (thromboplastin, tissue factor)	7.01	8.93	3.79	0.0008
PASD1	PAS domain containing 1	5.63	7.51	3.68	0.0001
PRSS35	protease, serine, 35	6.58	7.81	2.35	0.0000
RBM35A	RNA binding motif protein 35A	5.85	6.93	2.10	0.0006
CDH13	cadherin 13, H-cadherin (heart)	8.13	9.19	2.08	0.0001
ZNF626	zinc finger protein 626	5.62	6.61	1.98	0.0007
SATB1	SATB homeobox 1	5.51	6.50	1.98	0.0003
ME1	malic enzyme 1, NADP(+)-dependent, cytosolic	8.23	9.20	1.96	0.0006
STAT1	signal transducer and activator of transcription 1, 91kDa	10.03	10.99	1.94	0.0002
MPZL2	myelin protein zero-like 2	5.15	6.10	1.94	0.0040
ZNF486	zinc finger protein 486	5.56	6.51	1.94	0.0022
CDC20B	cell division cycle 20 homolog B (S. cerevisiae)	4.52	5.47	1.93	0.0010
APOBEC3G	apolipoprotein B mRNA editing enzyme, catalytic polypeptide-like 3G	5.18	6.10	1.90	0.0049
C17orf60	chromosome 17 open reading frame 60	7.85	8.77	1.89	0.0012
CCDC141	coiled-coil domain containing 141	6.69	7.57	1.85	0.0042
ZNF788	zinc finger family member 788	5.11	5.99	1.84	0.0002
MBNL3	muscleblind-like 3 (Drosophila)	5.46	6.32	1.82	0.0006
GLB1L3	galactosidase, beta 1-like 3	5.69	6.54	1.80	0.0004
ZNF66	zinc finger protein 66	5.82	6.64	1.76	0.0006
TFF1	trefoil factor 1	8.12	8.93	1.76	0.0014
NOG	noggin	8.60	9.41	1.75	0.0042
ZNF625	zinc finger protein 625	8.17	8.97	1.75	0.0003
MGC9913	hypothetical protein MGC9913	5.87	6.67	1.73	0.0169
ODZ1	odz, odd Oz	6.64	7.43	1.73	0.0008
RP6-213H19.1	serine	5.96	6.75	1.73	0.0007
CDH3	cadherin 3, type 1, P-cadherin (placental)	6.69	7.47	1.71	0.0007

TGFB2	transforming growth factor, beta 2	6.09	6.86	1.70	0.0014
NTS	neurotensin	9.54	6.93	-6.10	0.0002
IL13RA2	interleukin 13 receptor, alpha 2	8.70	7.16	-2.91	0.0009
TCN1	transcobalamin I (vitamin B12 binding protein, R binder family)	9.64	8.17	-2.75	0.0009
SERPINB7	serpin peptidase inhibitor, clade B (ovalbumin), member 7	7.82	6.42	-2.64	0.0010
HCLS1	hematopoietic cell-specific Lyn substrate 1	7.93	6.69	-2.35	0.0000
NAV3	neuron navigator 3	7.53	6.44	-2.13	0.0005
IL1RAPL1	interleukin 1 receptor accessory protein-like 1	6.88	5.79	-2.12	0.0031
BMPR1B	bone morphogenetic protein receptor, type IB	7.71	6.62	-2.12	0.0016
PDE3A	phosphodiesterase 3A, cGMP-inhibited	7.52	6.45	-2.10	0.0003
PARP8	poly (ADP-ribose) polymerase family, member 8	7.48	6.48	-2.00	0.0033
SCN3A	sodium channel, voltage-gated, type III, alpha subunit	5.97	4.99	-1.98	0.0101
CHRM3	cholinergic receptor, muscarinic 3	8.97	7.98	-1.98	0.0001
ELMOD1	ELMO	6.53	5.55	-1.98	0.0023
KCNJ6	potassium inwardly-rectifying channel, subfamily J, member 6	6.98	6.01	-1.97	0.0007
FAM130A2	family with sequence similarity 130, member A2	6.99	6.02	-1.96	0.1060
KITLG	KIT ligand	9.58	8.65	-1.90	0.0481
MX1	myxovirus (influenza virus) resistance 1, interferon-inducible protein p78 (mouse)	8.76	7.84	-1.90	0.0001
S100A2	S100 calcium binding protein A2	8.16	7.27	-1.86	0.0019
PLA2G4A	phospholipase A2, group IVA (cytosolic, calcium-dependent)	6.22	5.32	-1.86	0.0389
MAGEC2	melanoma antigen family C, 2	7.89	7.05	-1.80	0.0037
SCEL	sciellin	6.87	6.04	-1.78	0.0615
ARMCX3	armadillo repeat containing, X-linked 3	6.82	5.99	-1.78	0.0025
SLC14A1	solute carrier family 14 (urea transporter), member 1 (Kidd blood group)	5.42	4.59	-1.78	0.0669
NR2F1	nuclear receptor subfamily 2, group F, member 1	9.25	8.43	-1.76	0.0037
SRPX	sushi-repeat-containing protein, X-linked	7.88	7.08	-1.74	0.0003
ORM2	orosomuroid 2	5.44	4.64	-1.74	0.0416
C13orf18	chromosome 13 open reading frame 18	6.45	5.66	-1.73	0.0006
CALCRL	calcitonin receptor-like	6.43	5.66	-1.71	0.1222
SCN2A	sodium channel, voltage-gated, type II, alpha subunit	5.70	4.93	-1.70	0.0251
HAS2	hyaluronan synthase 2	8.84	8.07	-1.70	0.0064
SSX1	synovial sarcoma, X breakpoint 1	4.83	4.08	-1.69	0.0294

Table 8: Differentially expressed genes in PC3-D4 versus PC3-A3 xenografts (1.6 fold regulation; T-Test: $p < 0.05$)

6.2. *Abbreviations*

2D	twodimensional
2DE	twodimensional electrophoresis
3D	threedimensional
5-FU	5-fluorouracil
ABC	ATP-binding cassette
Bcl-2	B-cell lymphoma 2 protein
Bcl-XL	Bcl-2 like protein 1
BMDC	bone marrow derived cells
COGA-12/G6	5-FU resistant COGA-12 cells
COGA-12/NO	long term passaged COGA-12 cells
CPA	cyclophosphamide
DNA	deoxyribonucleic acid
dTMP	deoxythymidine monophosphate
FdUMP	fluorodeoxyuridine monophosphate
HRPC	hormone resistant prostate cancer
Hsp27	heat shock protein 27
MALDI-TOF	matrix assisted laser desorption-time of flight
Mcl-1	Induced myeloid leukemia cell differentiation protein Mcl-1
MCS	multicellular spheroid
MLH1	MutL homolog 1, colon cancer, nonpolyposis type 2 gene
mRNA	messenger ribonucleic acid
MS	mass spectrometry
MTD	maximum tolerated dose
RNA	ribonucleic acid
rRNA	ribosomal ribonucleic acid
TS	thymidylate synthase
VEGF	vascular growth factor
VEGFR2	vascular growth factor receptor 2
GBM	glioblastoma multiform
CSCs	cancer stem cells
ALDH1	aldehyde dehydrogenase 1

DIGE	differential in gel electrophoresis
LC-MS	liquid chromatography mass spectrometry
SCID	severe combined immuno deficiency
4-HOO-CPA	4-hydroperoxy-cyclophosphamide
PC3	human prostate carcinoma cell line
PC3-wt	wild type PC3 cell
PC3-A3	reisolated in vivo passaged PC3 cells
PC3-D3	reisolated in vivo resistant PC3 cells
PC3-D4	reisolated in vivo resistant PC3 cells
4-HO-CPA	4-hydroxy CPA
CD31	cluster of differentiation 31
siRNA	small interfering ribonucleic acid
TUNEL	Terminal deoxynucleotidyl transferase dUTP nick end labelling
zVAD-fmk	carbobenzoxy-valyl-alanyl-aspartyl-[O-methyl]- fluoromethylketone (pan caspases inhibitor)
zVEID-fmk	carbobenzoxy-valyl-glutamyl -[O-methyl]- isoleucyl- aspartyl -[O-methyl]- fluoromethylketone (caspases 6 inhibitor)
CK18	cytokeratin 18
RT-PCR	reverse transcriptase PCR
MTT	(3-(4,5-Dimethylthiazol-2-yl)-2,5-diphenyltetrazolium bromide
EGF(R)	epidermal growth factor (receptor)
CD71	cluster of differentiation 71 (transferrin receptor)
hEGFR	human epidermal growth factor receptor
MS/MS	tandem mass spectrometry
PMF	peptide mass fingerprint
CK19	cytokeratin 19
MCF-7	breast carcinoma cell line
pI	isoelectric point
CatB	cathepsin B
kDa	kilo Dalton
TXNDC5	thioredoxin domain containing protein 5

ANXA3	Annexin A3
RMA	robust multichip analysis
GABRE	gamma-aminobutyric acid (GABA) A receptor, epsilon
STAT1	signal transducer and activator of transcription-1
SLC7A6	Solute carrier family 7 member 6
MBNL-3	muscleblind-like 3
ZNF468	zinc finger protein 486
TGFB2	transforming growth factor, beta 2
CD274	programmed cell death 1 ligand 1
TNFAIP6	tumor necrosis factor alpha-inducible protein 6
GPR126	G protein-coupled receptor 126
PMAIP1	phorbol-12-myristate-13-acetate-induced protein 1
MPHOSPH6	M-phase phosphoprotein 6
PASD1	PAS domain containing protein 1
GALNT4	UDP-N-acetyl-alpha-D-galactosamine:polypeptide N-acetylgalactosaminyltransferase 4
BMPR1	bone morphogenetic protein receptor type 1
CHRM3	cholinergic receptor, muscarinic 3
KCNJ6	potassium inwardly-rectifying channel, subfamily J, member 6
Mx1	myxovirus (influenza virus) resistance protein 1
PDGFD	platelet derived growth factor D
F3	tissue factor gene symbol
TF	tissue factor protein
P0	acidic ribosomal protein P0
tRNA	transfer ribonucleic acid
15-PGDH	15-hydroxyprostaglandin dehydrogenase
HSF	heatshock transcription factor
dTTP	deoxythymidine triphosphate
DU145	human prostate cancer cell line
HSPD1	heat shock 60kDa protein 1
Trx	thioredoxin
PDI	protein disulfide isomerase
IL13RA2	interleukin 13 receptor, alpha 2

S100A2	S100 calcium binding protein A2
TP53INP1	tumor protein p53 inducible nuclear protein 1
LOX	lysyl oxidase
EMP-2	epithelial membrane protein 2
COX-2	cyclooxygenase-2
Sox-10	SRY (sex determining region Y)-box 10 protein
PLC	phospholipase C
PIP2	phosphatidylinositol-4,5-bisphosphate
OAS3	2'-5'-oligoadenylate synthetase 3

6.3. Publications

6.3.1. Original Papers

L.Gaedtke*, L.Thoenes*, C.Culmsee, B. Mayer, E. Wagner. Proteomic Analysis Reveals Differences in Protein Expression in Spheroid versus Monolayer Cultures of Low-Passage Colon Carcinoma Cells, J. Proteome Res., 6 (11), 4111 -4118, 2007

L.Thoenes, M.Hoehn, R. Kashirin, M.Ogris, G.J.Arnold, E.Wagner, M. Guenther. In vivo chemoresistance of prostate cancer in metronomic cyclophosphamide therapy, resubmitted Manuscript

6.3.2. Review Article

L.Thoenes, M.Guenther. Novel approaches in anti-angiogenic treatment targeting endothelial F-actin: a new anti-angiogenic strategy?, Current Opinion in Molecular Therapeutics, 10 (6), 579-590, 2008

6.3.3. Poster Presentations

L.Thoenes, M.Guenther, M. Ogris, G.J. Arnold, E.Wagner, Escape mechanisms in metronomic cyclophosphamide therapy in vivo (HUPO world congress, Amsterdam, 2008)

M.Guenther*, L.Thoenes*, M.Ogris, G.J. Arnold, E. Wagner, Chemoresistance of prostate cancer cells in metronomic cyclophosphamide therapy in vivo (Integrative cancer genomics Meeting, Munich, 2008)

L.Thoenes*, L.Gaedtke*, C.Culmsee, B. Mayer, E. Wagner. Proteome differences in spheroid versus monolayer cultures of low passage colon carcinoma cells (Capri Science Conference: Cancer therapeutcis-the road ahead, Capri, 2007)

7. References

- (1) Jemal, A.; Siegel, R.; Ward, E.; Hao, Y.; Xu, J.; Murray, T.; Thun, M. J. Cancer Statistics, 2008. *CA Cancer J. Clin.* **2008**, *58*, 71-96.
- (2) Marian, B. In vitro models for the identification and characterization of tumor-promoting and protective factors for colon carcinogenesis. *Food Chem. Toxicol.* **2002**, *40*, 1099-1104.
- (3) Vecsey-Semjen, B.; Becker, K. F.; Sinski, A.; Blennow, E.; Vietor, I.; Zatloukal, K.; Beug, H.; Wagner, E.; Huber, L. A. Novel colon cancer cell lines leading to better understanding of the diversity of respective primary cancers. *Oncogene* **2002**, *21*, 4646-4662.
- (4) Lin, R. Z.; Chang, H. Y. Recent advances in three-dimensional multicellular spheroid culture for biomedical research. *Biotechnol. J.* **2008**, *3*, 1172-1184.
- (5) Friedrich, J.; Ebner, R.; Kunz-Schughart, L. A. Experimental anti-tumor therapy in 3-D: spheroids--old hat or new challenge? *Int. J. Radiat. Biol.* **2007**, *83*, 849-871.
- (6) Mayer, B.; Klement, G.; Kaneko, M.; Man, S.; Jothy, S.; Rak, J.; Kerbel, R. S. Multicellular gastric cancer spheroids recapitulate growth pattern and differentiation phenotype of human gastric carcinomas. *Gastroenterology* **2001**, *121*, 839-852.
- (7) Mueller-Klieser, W. Three-dimensional cell cultures: from molecular mechanisms to clinical applications. *Am. J. Physiol* **1997**, *273*, C1109-C1123.
- (8) Lin, R. Z.; Chou, L. F.; Chien, C. C.; Chang, H. Y. Dynamic analysis of hepatoma spheroid formation: roles of E-cadherin and beta1-integrin. *Cell Tissue Res.* **2006**, *324*, 411-422.
- (9) Curcio, E.; Salerno, S.; Barbieri, G.; De Bartolo, L.; Drioli, E.; Bader, A. Mass transfer and metabolic reactions in hepatocyte spheroids cultured in rotating wall gas-permeable membrane system. *Biomaterials* **2007**, *28*, 5487-5497.
- (10) Alvarez-Perez, J.; Ballesteros, P.; Cerdan, S. Microscopic images of intraspheroidal pH by ¹H magnetic resonance chemical shift imaging of pH sensitive indicators. *MAGMA.* **2005**, *18*, 293-301.
- (11) Weaver, V. M.; Lelievre, S.; Lakins, J. N.; Chrenek, M. A.; Jones, J. C.; Giancotti, F.; Werb, Z.; Bissell, M. J. beta4 integrin-dependent formation of polarized three-dimensional architecture confers resistance to apoptosis in normal and malignant mammary epithelium. *Cancer Cell* **2002**, *2*, 205-216.
- (12) Freyer, J. P.; Schor, P. L.; Jarrett, K. A.; Neeman, M.; Sillerud, L. O. Cellular energetics measured by phosphorous nuclear magnetic resonance spectroscopy are not correlated with chronic nutrient deficiency in multicellular tumor spheroids. *Cancer Res.* **1991**, *51*, 3831-3837.

- (13) Teutsch, H. F.; Goellner, A.; Mueller-Klieser, W. Glucose levels and succinate and lactate dehydrogenase activity in EMT6/Ro tumor spheroids. *Eur. J. Cell Biol.* **1995**, *66*, 302-307.
- (14) Gaedtke, L.; Thoenes, L.; Culmsee, C.; Mayer, B.; Wagner, E. Proteomic analysis reveals differences in protein expression in spheroid versus monolayer cultures of low-passage colon carcinoma cells. *J. Proteome. Res.* **2007**, *6*, 4111-4118.
- (15) Gaedtke, L. Cell culture models and novel gene therapeutic strategies for colorectal cancer. Dissertation. 2006. LMU Munich.
Ref Type: Generic
- (16) Wolpin, B. M.; Mayer, R. J. Systemic treatment of colorectal cancer. *Gastroenterology* **2008**, *134*, 1296-1310.
- (17) Zhang, N.; Yin, Y.; Xu, S. J.; Chen, W. S. 5-Fluorouracil: mechanisms of resistance and reversal strategies. *Molecules.* **2008**, *13*, 1551-1569.
- (18) Parker, W. B.; Cheng, Y. C. Metabolism and mechanism of action of 5-fluorouracil. *Pharmacol. Ther.* **1990**, *48*, 381-395.
- (19) Noordhuis, P.; Holwerda, U.; Van der Wilt, C. L.; Van Groeningen, C. J.; Smid, K.; Meijer, S.; Pinedo, H. M.; Peters, G. J. 5-Fluorouracil incorporation into RNA and DNA in relation to thymidylate synthase inhibition of human colorectal cancers. *Ann. Oncol.* **2004**, *15*, 1025-1032.
- (20) Thomas, D. M.; Zalcborg, J. R. 5-fluorouracil: a pharmacological paradigm in the use of cytotoxics. *Clin. Exp. Pharmacol. Physiol* **1998**, *25*, 887-895.
- (21) An, Q.; Robins, P.; Lindahl, T.; Barnes, D. E. 5-Fluorouracil incorporated into DNA is excised by the Smug1 DNA glycosylase to reduce drug cytotoxicity. *Cancer Res.* **2007**, *67*, 940-945.
- (22) Gustavsson, M.; Ronne, H. Evidence that tRNA modifying enzymes are important in vivo targets for 5-fluorouracil in yeast. *RNA.* **2008**, *14*, 666-674.
- (23) Hoskins, J.; Butler, J. S. RNA-based 5-fluorouracil toxicity requires the pseudouridylation activity of Cbf5p. *Genetics* **2008**, *179*, 323-330.
- (24) Longley, D. B.; Allen, W. L.; Johnston, P. G. Drug resistance, predictive markers and pharmacogenomics in colorectal cancer. *Biochim. Biophys. Acta* **2006**.
- (25) Peters, G. J.; Backus, H. H.; Freemantle, S.; van Triest, B.; Codacci-Pisanelli, G.; Van der Wilt, C. L.; Smid, K.; Lunec, J.; Calvert, A. H.; Marsh, S.; McLeod, H. L.; Bloemena, E.; Meijer, S.; Jansen, G.; Van Groeningen, C. J.; Pinedo, H. M. Induction of thymidylate synthase as a 5-fluorouracil resistance mechanism. *Biochim. Biophys. Acta* **2002**, *1587*, 194-205.
- (26) Grem, J. L. Intratumoral molecular or genetic markers as predictors of clinical outcome with chemotherapy in colorectal cancer. *Semin. Oncol.* **2005**, *32*, 120-127.

- (27) Arnold, C. N.; Goel, A.; Boland, C. R. Role of hMLH1 promoter hypermethylation in drug resistance to 5-fluorouracil in colorectal cancer cell lines. *Int. J. Cancer* **2003**, 106, 66-73.
- (28) Violette, S.; Poulain, L.; Dussaulx, E.; Pepin, D.; Faussat, A. M.; Chambaz, J.; Lacorte, J. M.; Staedel, C.; Lesuffleur, T. Resistance of colon cancer cells to long-term 5-fluorouracil exposure is correlated to the relative level of Bcl-2 and Bcl-X(L) in addition to Bax and p53 status. *Int. J. Cancer* **2002**, 98, 498-504.
- (29) Schulz, W. A.; Hoffmann, M. J. Epigenetic mechanisms in the biology of prostate cancer. *Semin. Cancer Biol.* **2009**, 19, 172-180.
- (30) Oudard, S.; Banu, E.; Beuzeboc, P.; Voog, E.; Dourthe, L. M.; Hardy-Bessard, A. C.; Linassier, C.; Scotte, F.; Banu, A.; Coscas, Y.; Guinet, F.; Poupon, M. F.; Andrieu, J. M. Multicenter randomized phase II study of two schedules of docetaxel, estramustine, and prednisone versus mitoxantrone plus prednisone in patients with metastatic hormone-refractory prostate cancer. *J. Clin. Oncol.* **2005**, 23, 3343-3351.
- (31) Petrylak, D. P.; Tangen, C. M.; Hussain, M. H.; Lara, P. N., Jr.; Jones, J. A.; Taplin, M. E.; Burch, P. A.; Berry, D.; Moinpour, C.; Kohli, M.; Benson, M. C.; Small, E. J.; Raghavan, D.; Crawford, E. D. Docetaxel and estramustine compared with mitoxantrone and prednisone for advanced refractory prostate cancer. *N. Engl. J. Med.* **2004**, 351, 1513-1520.
- (32) Nelius, T.; Klatter, T.; de Riese, W.; Haynes, A.; Filleur, S. Clinical outcome of patients with docetaxel-resistant hormone-refractory prostate cancer treated with second-line cyclophosphamide-based metronomic chemotherapy. *Med. Oncol.* **2009**.
- (33) Morales, C.; Ribas, M.; Aiza, G.; Peinado, M. A. Genetic determinants of methotrexate responsiveness and resistance in colon cancer cells. *Oncogene* **2005**, 24, 6842-6847.
- (34) Browder, T.; Butterfield, C. E.; Kraling, B. M.; Shi, B.; Marshall, B.; O'Reilly, M. S.; Folkman, J. Antiangiogenic scheduling of chemotherapy improves efficacy against experimental drug-resistant cancer. *Cancer Res.* **2000**, 60, 1878-1886.
- (35) Laquente, B.; Vinals, F.; Germa, J. R. Metronomic chemotherapy: an antiangiogenic scheduling. *Clin. Transl. Oncol.* **2007**, 9, 93-98.
- (36) Hanahan, D.; Bergers, G.; Bergsland, E. Less is more, regularly: metronomic dosing of cytotoxic drugs can target tumor angiogenesis in mice. *J. Clin. Invest* **2000**, 105, 1045-1047.
- (37) Miller, K. D.; Sweeney, C. J.; Sledge, G. W., Jr. Redefining the target: chemotherapeutics as antiangiogenics. *J. Clin. Oncol.* **2001**, 19, 1195-1206.
- (38) Asahara, T.; Murohara, T.; Sullivan, A.; Silver, M.; van der, Z. R.; Li, T.; Witzenbichler, B.; Schatteman, G.; Isner, J. M. Isolation of putative progenitor endothelial cells for angiogenesis. *Science* **1997**, 275, 964-967.

- (39) Bertolini, F.; Paul, S.; Mancuso, P.; Monestiroli, S.; Gobbi, A.; Shaked, Y.; Kerbel, R. S. Maximum tolerable dose and low-dose metronomic chemotherapy have opposite effects on the mobilization and viability of circulating endothelial progenitor cells. *Cancer Res.* **2003**, *63*, 4342-4346.
- (40) Bocci, G.; Francia, G.; Man, S.; Lawler, J.; Kerbel, R. S. Thrombospondin 1, a mediator of the antiangiogenic effects of low-dose metronomic chemotherapy. *Proc. Natl. Acad. Sci. U. S. A* **2003**, *100*, 12917-12922.
- (41) Hamano, Y.; Sugimoto, H.; Soubasakos, M. A.; Kieran, M.; Olsen, B. R.; Lawler, J.; Sudhakar, A.; Kalluri, R. Thrombospondin-1 associated with tumor microenvironment contributes to low-dose cyclophosphamide-mediated endothelial cell apoptosis and tumor growth suppression. *Cancer Res.* **2004**, *64*, 1570-1574.
- (42) Kerbel, R. S.; Kamen, B. A. The anti-angiogenic basis of metronomic chemotherapy. *Nat. Rev. Cancer* **2004**, *4*, 423-436.
- (43) Emmenegger, U.; Man, S.; Shaked, Y.; Francia, G.; Wong, J. W.; Hicklin, D. J.; Kerbel, R. S. A comparative analysis of low-dose metronomic cyclophosphamide reveals absent or low-grade toxicity on tissues highly sensitive to the toxic effects of maximum tolerated dose regimens. *Cancer Res.* **2004**, *64*, 3994-4000.
- (44) Gunther, M.; Wagner, E.; Ogris, M. Acrolein: unwanted side product or contribution to antiangiogenic properties of metronomic cyclophosphamide therapy? *J. Cell Mol. Med.* **2008**, *12*, 2704-2716.
- (45) Saltz, L. B.; Rosen, L. S.; Marshall, J. L.; Belt, R. J.; Hurwitz, H. I.; Eckhardt, S. G.; Bergsland, E. K.; Haller, D. G.; Lockhart, A. C.; Rocha Lima, C. M.; Huang, X.; DePrimo, S. E.; Chow-Maneval, E.; Chao, R. C.; Lenz, H. J. Phase II trial of sunitinib in patients with metastatic colorectal cancer after failure of standard therapy. *J. Clin. Oncol.* **2007**, *25*, 4793-4799.
- (46) Shojaei, F.; Ferrara, N. Antiangiogenic therapy for cancer: an update. *Cancer J.* **2007**, *13*, 345-348.
- (47) Si, Z. C.; Liu, J. What "helps" tumors evade vascular targeting treatment? *Chin Med. J. (Engl.)* **2008**, *121*, 844-849.
- (48) van Brussel, J. P.; Mickisch, G. H. Multidrug resistance in prostate cancer. *Onkologie.* **2003**, *26*, 175-181.
- (49) Rak, J.; Yu, J. L. Oncogenes and tumor angiogenesis: the question of vascular "supply" and vascular "demand". *Semin. Cancer Biol.* **2004**, *14*, 93-104.
- (50) Schottelius, A. J.; Dinter, H. Cytokines, NF-kappaB, microenvironment, intestinal inflammation and cancer. *Cancer Treat. Res.* **2006**, *130*, 67-87.
- (51) Bergers, G.; Hanahan, D. Modes of resistance to anti-angiogenic therapy. *Nat. Rev. Cancer* **2008**, *8*, 592-603.

- (52) Folberg, R.; Hendrix, M. J.; Maniotis, A. J. Vasculogenic mimicry and tumor angiogenesis. *Am. J. Pathol.* **2000**, 156, 361-381.
- (53) Hendrix, M. J.; Seftor, E. A.; Hess, A. R.; Seftor, R. E. Vasculogenic mimicry and tumour-cell plasticity: lessons from melanoma. *Nat. Rev. Cancer* **2003**, 3, 411-421.
- (54) Holash, J.; Maisonpierre, P. C.; Compton, D.; Boland, P.; Alexander, C. R.; Zagzag, D.; Yancopoulos, G. D.; Wiegand, S. J. Vessel cooption, regression, and growth in tumors mediated by angiopoietins and VEGF. *Science* **1999**, 284, 1994-1998.
- (55) Kunkel, P.; Ulbricht, U.; Bohlen, P.; Brockmann, M. A.; Fillbrandt, R.; Stavrou, D.; Westphal, M.; Lamszus, K. Inhibition of glioma angiogenesis and growth in vivo by systemic treatment with a monoclonal antibody against vascular endothelial growth factor receptor-2. *Cancer Res.* **2001**, 61, 6624-6628.
- (56) Shaked, Y.; Ciarrocchi, A.; Franco, M.; Lee, C. R.; Man, S.; Cheung, A. M.; Hicklin, D. J.; Chaplin, D.; Foster, F. S.; Benezra, R.; Kerbel, R. S. Therapy-induced acute recruitment of circulating endothelial progenitor cells to tumors. *Science* **2006**, 313, 1785-1787.
- (57) Darland, D. C.; Massingham, L. J.; Smith, S. R.; Piek, E.; Saint-Geniez, M.; D'Amore, P. A. Pericyte production of cell-associated VEGF is differentiation-dependent and is associated with endothelial survival. *Dev. Biol.* **2003**, 264, 275-288.
- (58) Song, S.; Ewald, A. J.; Stallcup, W.; Werb, Z.; Bergers, G. PDGFRbeta+ perivascular progenitor cells in tumours regulate pericyte differentiation and vascular survival. *Nat. Cell Biol.* **2005**, 7, 870-879.
- (59) Warburg, O.; Posener, K.; Negelein, E. On the metabolism of carcinoma cells. *Biochemische Zeitschrift* **1924**, 152, 309-344.
- (60) Visvader, J. E.; Lindeman, G. J. Cancer stem cells in solid tumours: accumulating evidence and unresolved questions. *Nat. Rev. Cancer* **2008**, 8, 755-768.
- (61) Matsui, W.; Huff, C. A.; Wang, Q.; Malehorn, M. T.; Barber, J.; Tanhehco, Y.; Smith, B. D.; Civin, C. I.; Jones, R. J. Characterization of clonogenic multiple myeloma cells. *Blood* **2004**, 103, 2332-2336.
- (62) Clarke, M. F.; Fuller, M. Stem cells and cancer: two faces of eve. *Cell* **2006**, 124, 1111-1115.
- (63) Dean, M.; Fojo, T.; Bates, S. Tumour stem cells and drug resistance. *Nat. Rev. Cancer* **2005**, 5, 275-284.
- (64) Ginestier, C.; Hur, M. H.; Charafe-Jauffret, E.; Monville, F.; Dutcher, J.; Brown, M.; Jacquemier, J.; Viens, P.; Kleer, C. G.; Liu, S.; Schott, A.; Hayes, D.; Birnbaum, D.; Wicha, M. S.; Dontu, G. ALDH1 is a marker of normal and malignant human mammary stem cells and a predictor of poor clinical outcome. *Cell Stem Cell* **2007**, 1, 555-567.

- (65) Bao, S.; Wu, Q.; Sathornsumetee, S.; Hao, Y.; Li, Z.; Hjelmeland, A. B.; Shi, Q.; McLendon, R. E.; Bigner, D. D.; Rich, J. N. Stem cell-like glioma cells promote tumor angiogenesis through vascular endothelial growth factor. *Cancer Res.* **2006**, *66*, 7843-7848.
- (66) Sun, L.; Hui, A. M.; Su, Q.; Vortmeyer, A.; Kotliarov, Y.; Pastorino, S.; Passaniti, A.; Menon, J.; Walling, J.; Bailey, R.; Rosenblum, M.; Mikkelsen, T.; Fine, H. A. Neuronal and glioma-derived stem cell factor induces angiogenesis within the brain. *Cancer Cell* **2006**, *9*, 287-300.
- (67) Tavaluc, R. T.; Hart, L. S.; Dicker, D. T.; El Deiry, W. S. Effects of low confluency, serum starvation and hypoxia on the side population of cancer cell lines. *Cell Cycle* **2007**, *6*, 2554-2562.
- (68) Teicher, B. A. Acute and chronic in vivo therapeutic resistance. *Biochem. Pharmacol.* **2009**, *77*, 1665-1673.
- (69) Righetti, P. G.; Castagna, A.; Antonioli, P.; Cecconi, D.; Campostrini, N.; Righetti, S. C. Proteomic approaches for studying chemoresistance in cancer. *Expert. Rev. Proteomics.* **2005**, *2*, 215-228.
- (70) Zhang, J. T.; Liu, Y. Use of comparative proteomics to identify potential resistance mechanisms in cancer treatment. *Cancer Treat. Rev.* **2007**, *33*, 741-756.
- (71) Di Michele, M.; Della, C. A.; Cicchillitti, L.; Del Boccio, P.; Urbani, A.; Ferlini, C.; Scambia, G.; Donati, M. B.; Rotilio, D. A proteomic approach to paclitaxel chemoresistance in ovarian cancer cell lines. *Biochim. Biophys. Acta* **2009**, *1794*, 225-236.
- (72) Hasegawa, N.; Mizutani, K.; Suzuki, T.; Deguchi, T.; Nozawa, Y. A comparative study of protein profiling by proteomic analysis in camptothecin-resistant PC3 and camptothecin-sensitive LNCaP human prostate cancer cells. *Urol. Int.* **2006**, *77*, 347-354.
- (73) Cooper, C. S.; Campbell, C.; Jhavar, S. Mechanisms of Disease: biomarkers and molecular targets from microarray gene expression studies in prostate cancer. *Nat. Clin. Pract. Urol.* **2007**, *4*, 677-687.
- (74) Shen, Y.; Wu, B. L. Microarray-based genomic DNA profiling technologies in clinical molecular diagnostics. *Clin. Chem.* **2009**, *55*, 659-669.
- (75) Hall, J. A.; Brown, R.; Paul, J. An exploration into study design for biomarker identification: issues and recommendations. *Cancer Genomics Proteomics.* **2007**, *4*, 111-119.
- (76) Goebell, P. J. Outcomes and response to therapy in bladder cancer. Are biomarkers of any help? *Minerva Urol. Nefrol.* **2009**, *61*, 91-107.
- (77) Sutcliffe, P.; Hummel, S.; Simpson, E.; Young, T.; Rees, A.; Wilkinson, A.; Hamdy, F.; Clarke, N.; Staffurth, J. Use of classical and novel biomarkers as prognostic risk factors for localised prostate cancer: a systematic review. *Health Technol. Assess.* **2009**, *13*, iii, xi-iiiixiii.

- (78) Guenther, M. Cancer Therapy with Metronomically Scheduled Cyclophosphamide: Experimental Modalities within GDEPT and Tumor escape mechanisms. 18-12-2006.
Ref Type: Generic
- (79) Hales, B. F. Comparison of the mutagenicity and teratogenicity of cyclophosphamide and its active metabolites, 4-hydroxycyclophosphamide, phosphoramidate mustard, and acrolein. *Cancer Res.* **1982**, 42, 3016-3021.
- (80) Morazzani, M.; de Carvalho, D. D.; Kovacic, H.; Smida-Rezgui, S.; Briand, C.; Penel, C. Monolayer versus aggregate balance in survival process for EGF-induced apoptosis in A431 carcinoma cells: Implication of ROS-P38 MAPK-integrin alpha2beta1 pathway. *Int. J. Cancer* **2004**, 110, 788-799.
- (81) Muir, C. P.; Adams, M. A.; Graham, C. H. Nitric oxide attenuates resistance to doxorubicin in three-dimensional aggregates of human breast carcinoma cells. *Breast Cancer Res. Treat.* **2006**, 96, 169-176.
- (82) Mellor, H. R.; Ferguson, D. J.; Callaghan, R. A model of quiescent tumour microregions for evaluating multicellular resistance to chemotherapeutic drugs. *Br. J. Cancer* **2005**, 93, 302-309.
- (83) Mayer, B.; Klement, G.; Kaneko, M.; Man, S.; Jothy, S.; Rak, J.; Kerbel, R. S. Multicellular gastric cancer spheroids recapitulate growth pattern and differentiation phenotype of human gastric carcinomas. *Gastroenterology* **2001**, 121, 839-852.
- (84) Eisen, M. B.; Spellman, P. T.; Brown, P. O.; Botstein, D. Cluster analysis and display of genome-wide expression patterns. *Proc. Natl. Acad. Sci. U. S. A* **1998**, 95, 14863-14868.
- (85) Mueller-Klieser, W. Tumor biology and experimental therapeutics. *Crit Rev. Oncol. Hematol.* **2000**, 36, 123-139.
- (86) Takahashi, A.; Musy, P. Y.; Martins, L. M.; Poirier, G. G.; Moyer, R. W.; Earnshaw, W. C. CrmA/SPI-2 inhibition of an endogenous ICE-related protease responsible for lamin A cleavage and apoptotic nuclear fragmentation. *J. Biol. Chem.* **1996**, 271, 32487-32490.
- (87) Rocchi, P.; Jugpal, P.; So, A.; Sinneman, S.; Ettinger, S.; Fazli, L.; Nelson, C.; Gleave, M. Small interference RNA targeting heat-shock protein 27 inhibits the growth of prostatic cell lines and induces apoptosis via caspase-3 activation in vitro. *BJU. Int.* **2006**, 98, 1082-1089.
- (88) Chuthapisith, S.; Layfield, R.; Kerr, I. D.; Hughes, C.; Eremin, O. Proteomic profiling of MCF-7 breast cancer cells with chemoresistance to different types of anti-cancer drugs. *Int. J. Oncol.* **2007**, 30, 1545-1551.
- (89) Shi, L.; Jones, W. D.; Jensen, R. V.; Harris, S. C.; Perkins, R. G.; Goodsaid, F. M.; Guo, L.; Croner, L. J.; Boysen, C.; Fang, H.; Qian, F.; Amur, S.; Bao, W.; Barbacioru, C. C.; Bertholet, V.; Cao, X. M.; Chu, T. M.; Collins, P. J.; Fan, X. H.; Frueh, F. W.; Fuscoe, J. C.; Guo, X.; Han, J.; Herman, D.; Hong, H.; Kawasaki, E. S.; Li, Q. Z.; Luo, Y.; Ma, Y.; Mei, N.; Peterson, R. L.; Puri, R. K.;

- Shippy, R.; Su, Z.; Sun, Y. A.; Sun, H.; Thorn, B.; Turpaz, Y.; Wang, C.; Wang, S. J.; Warrington, J. A.; Willey, J. C.; Wu, J.; Xie, Q.; Zhang, L.; Zhang, L.; Zhong, S.; Wolfinger, R. D.; Tong, W. The balance of reproducibility, sensitivity, and specificity of lists of differentially expressed genes in microarray studies. *BMC. Bioinformatics*. **2008**, 9 Suppl 9, S10.
- (90) Tchorzewski, M.; Boldyreff, B.; Issinger, O. G.; Grankowski, N. Analysis of the protein-protein interactions between the human acidic ribosomal P-proteins: evaluation by the two hybrid system. *Int. J. Biochem. Cell Biol.* **2000**, 32, 737-746.
- (91) Uchiumi, T.; Wahba, A. J.; Traut, R. R. Topography and stoichiometry of acidic proteins in large ribosomal subunits from *Artemia salina* as determined by crosslinking. *Proc. Natl. Acad. Sci. U. S. A* **1987**, 84, 5580-5584.
- (92) Wu, S.; Storey, K. B. Up-regulation of acidic ribosomal phosphoprotein P0 in response to freezing or anoxia in the freeze tolerant wood frog, *Rana sylvatica*. *Cryobiology* **2005**, 50, 71-82.
- (93) Kondoh, N.; Wakatsuki, T.; Ryo, A.; Hada, A.; Aihara, T.; Horiuchi, S.; Goseki, N.; Matsubara, O.; Takenaka, K.; Shichita, M.; Tanaka, K.; Shuda, M.; Yamamoto, M. Identification and characterization of genes associated with human hepatocellular carcinogenesis. *Cancer Res.* **1999**, 59, 4990-4996.
- (94) Barnard, G. F.; Staniunas, R. J.; Bao, S.; Mafune, K.; Steele, G. D., Jr.; Gollan, J. L.; Chen, L. B. Increased expression of human ribosomal phosphoprotein P0 messenger RNA in hepatocellular carcinoma and colon carcinoma. *Cancer Res.* **1992**, 52, 3067-3072.
- (95) Jin, J. P.; Wu, D.; Gao, J.; Nigam, R.; Kwong, S. Expression and purification of the h1 and h2 isoforms of calponin. *Protein Expr. Purif.* **2003**, 31, 231-239.
- (96) Applegate, D.; Feng, W.; Green, R. S.; Taubman, M. B. Cloning and expression of a novel acidic calponin isoform from rat aortic vascular smooth muscle. *J. Biol. Chem.* **1994**, 269, 10683-10690.
- (97) Winder, S. J.; Walsh, M. P. Smooth muscle calponin. Inhibition of actomyosin MgATPase and regulation by phosphorylation. *J. Biol. Chem.* **1990**, 265, 10148-10155.
- (98) Maguchi, M.; Nishida, W.; Kohara, K.; Kuwano, A.; Kondo, I.; Hiwada, K. Molecular cloning and gene mapping of human basic and acidic calponins. *Biochem. Biophys. Res. Commun.* **1995**, 217, 238-244.
- (99) Fujii, T.; Yabe, S.; Nakamura, K.; Koizumi, Y. Functional analysis of rat acidic calponin. *Biol. Pharm. Bull.* **2002**, 25, 573-579.
- (100) Yoshimoto, R.; Hori, M.; Ozaki, H.; Karaki, H. Proteolysis of acidic calponin by mu-calpain. *J. Biochem.* **2000**, 128, 1045-1049.
- (101) Lieubeau-Teillet, B.; Rak, J.; Jothy, S.; Iliopoulos, O.; Kaelin, W.; Kerbel, R. S. von Hippel-Lindau gene-mediated growth suppression and induction of

- differentiation in renal cell carcinoma cells grown as multicellular tumor spheroids. *Cancer Res.* **1998**, 58, 4957-4962.
- (102) Sutherland, R. M. Cell and environment interactions in tumor microregions: the multicell spheroid model. *Science* **1988**, 240, 177-184.
- (103) Hauptmann, S.; Denkert, C.; Lohrke, H.; Tietze, L.; Ott, S.; Klosterhalfen, B.; Mittermayer, C. Integrin expression on colorectal tumor cells growing as monolayers, as multicellular tumor spheroids, or in nude mice. *Int. J. Cancer* **1995**, 61, 819-825.
- (104) Konety, B. R.; Getzenberg, R. H. Nuclear structural proteins as biomarkers of cancer. *J. Cell Biochem.* **1999**, Suppl 32-33, 183-191.
- (105) Tai, H. H.; Ensor, C. M.; Tong, M.; Zhou, H.; Yan, F. Prostaglandin catabolizing enzymes. *Prostaglandins Other Lipid Mediat.* **2002**, 68-69, 483-493.
- (106) Badawi, A. F. The role of prostaglandin synthesis in prostate cancer. *BJU. Int.* **2000**, 85, 451-462.
- (107) Shumaker, D. K.; Kuczmarski, E. R.; Goldman, R. D. The nucleoskeleton: lamins and actin are major players in essential nuclear functions. *Curr. Opin. Cell Biol.* **2003**, 15, 358-366.
- (108) Lammerding, J.; Fong, L. G.; Ji, J. Y.; Reue, K.; Stewart, C. L.; Young, S. G.; Lee, R. T. Lamins A and C but not lamin B1 regulate nuclear mechanics. *J. Biol. Chem.* **2006**, 281, 25768-25780.
- (109) Gruenbaum, Y.; Margalit, A.; Goldman, R. D.; Shumaker, D. K.; Wilson, K. L. The nuclear lamina comes of age. *Nat. Rev. Mol. Cell Biol.* **2005**, 6, 21-31.
- (110) Hutchison, C. J. Lamins: building blocks or regulators of gene expression? *Nat. Rev. Mol. Cell Biol.* **2002**, 3, 848-858.
- (111) Moir, R. D.; Spann, T. P. The structure and function of nuclear lamins: implications for disease. *Cell Mol. Life Sci.* **2001**, 58, 1748-1757.
- (112) Ruchaud, S.; Korfali, N.; Villa, P.; Kottke, T. J.; Dingwall, C.; Kaufmann, S. H.; Earnshaw, W. C. Caspase-6 gene disruption reveals a requirement for lamin A cleavage in apoptotic chromatin condensation. *EMBO J.* **2002**, 21, 1967-1977.
- (113) Rao, L.; Perez, D.; White, E. Lamin proteolysis facilitates nuclear events during apoptosis. *J. Cell Biol.* **1996**, 135, 1441-1455.
- (114) Culmsee, C.; Zhu, C.; Landshamer, S.; Becattini, B.; Wagner, E.; Pellecchia, M.; Blomgren, K.; Plesnila, N. Apoptosis-inducing factor triggered by poly(ADP-ribose) polymerase and Bid mediates neuronal cell death after oxygen-glucose deprivation and focal cerebral ischemia. *J. Neurosci.* **2005**, 25, 10262-10272.

- (115) Lee, S. C.; Chan, J.; Clement, M. V.; Pervaiz, S. Functional proteomics of resveratrol-induced colon cancer cell apoptosis: caspase-6-mediated cleavage of lamin A is a major signaling loop. *Proteomics*. **2006**, *6*, 2386-2394.
- (116) Orth, K.; Chinnaiyan, A. M.; Garg, M.; Froelich, C. J.; Dixit, V. M. The CED-3/ICE-like protease Mch2 is activated during apoptosis and cleaves the death substrate lamin A. *J. Biol. Chem.* **1996**, *271*, 16443-16446.
- (117) Poland, J.; Sinha, P.; Siegert, A.; Schnolzer, M.; Korf, U.; Hauptmann, S. Comparison of protein expression profiles between monolayer and spheroid cell culture of HT-29 cells revealed fragmentation of CK18 in three-dimensional cell culture. *Electrophoresis* **2002**, *23*, 1174-1184.
- (118) Ferns, G.; Shams, S.; Shafi, S. Heat shock protein 27: its potential role in vascular disease. *Int. J. Exp. Pathol.* **2006**, *87*, 253-274.
- (119) Concannon, C. G.; Gorman, A. M.; Samali, A. On the role of Hsp27 in regulating apoptosis. *Apoptosis*. **2003**, *8*, 61-70.
- (120) Tsuruta, M.; Nishibori, H.; Hasegawa, H.; Ishii, Y.; Endo, T.; Kubota, T.; Kitajima, M.; Kitagawa, Y. Heat shock protein 27, a novel regulator of 5-fluorouracil resistance in colon cancer. *Oncol. Rep.* **2008**, *20*, 1165-1172.
- (121) Mader, R. M.; Muller, M.; Steger, G. G. Resistance to 5-fluorouracil. *Gen. Pharmacol.* **1998**, *31*, 661-666.
- (122) Emmenegger, U.; Shaked, Y.; Man, S.; Bocci, G.; Spasojevic, I.; Francia, G.; Kouri, A.; Coke, R.; Cruz-Munoz, W.; Ludeman, S. M.; Colvin, O. M.; Kerbel, R. S. Pharmacodynamic and pharmacokinetic study of chronic low-dose metronomic cyclophosphamide therapy in mice. *Mol. Cancer Ther.* **2007**, *6*, 2280-2289.
- (123) Sharma, N.; Seftor, R. E.; Seftor, E. A.; Gruman, L. M.; Heidger, P. M., Jr.; Cohen, M. B.; Lubaroff, D. M.; Hendrix, M. J. Prostatic tumor cell plasticity involves cooperative interactions of distinct phenotypic subpopulations: role in vasculogenic mimicry. *Prostate* **2002**, *50*, 189-201.
- (124) Mathew, G.; Timm, E. A., Jr.; Sotomayor, P.; Godoy, A.; Montecinos, V. P.; Smith, G. J.; Huss, W. J. ABCG2-mediated DyeCycle Violet efflux defined side population in benign and malignant prostate. *Cell Cycle* **2009**, *8*, 1053-1061.
- (125) Abe, T.; Tada, M.; Shinohara, N.; Okada, F.; Itoh, T.; Hamada, J.; Harabayashi, T.; Chen, Q.; Moriuchi, T.; Nonomura, K. Establishment and characterization of human urothelial cancer xenografts in severe combined immunodeficient mice. *Int. J. Urol.* **2006**, *13*, 47-57.
- (126) Mueller, M. M.; Peter, W.; Mappes, M.; Huelsen, A.; Steinbauer, H.; Boukamp, P.; Vaccariello, M.; Garlick, J.; Fusenig, N. E. Tumor progression of skin carcinoma cells in vivo promoted by clonal selection, mutagenesis, and autocrine growth regulation by granulocyte colony-stimulating factor and granulocyte-macrophage colony-stimulating factor. *Am. J. Pathol.* **2001**, *159*, 1567-1579.

- (127) Giatromanolaki, A.; Koukourakis, M. I.; Kakolyris, S.; Mavroudis, D.; Kouroussis, C.; Mavroudi, C.; Perraki, M.; Sivridis, E.; Georgoulis, V. Assessment of highly angiogenic and disseminated in the peripheral blood disease in breast cancer patients predicts for resistance to adjuvant chemotherapy and early relapse. *Int. J. Cancer* **2004**, 108, 620-627.
- (128) Yuan, C. C.; Huang, H. C.; Tsai, L. C.; Ng, H. T.; Huang, T. S. Cytokeratin-19 associated with apoptosis and chemosensitivity in human cervical cancer cells. *Apoptosis*. **1997**, 2, 101-105.
- (129) Podgorski, I.; Sloane, B. F. Cathepsin B and its role(s) in cancer progression. *Biochem. Soc. Symp.* **2003**, 263-276.
- (130) Mohamed, M. M.; Sloane, B. F. Cysteine cathepsins: multifunctional enzymes in cancer. *Nat. Rev. Cancer* **2006**, 6, 764-775.
- (131) Kehinde, E. O.; Maghrebi, M. A.; Anim, J. T. The importance of determining the aggressiveness of prostate cancer using serum and tissue molecular markers. *Can. J. Urol.* **2008**, 15, 3967-3974.
- (132) Yan, S.; Sloane, B. F. Molecular regulation of human cathepsin B: implication in pathologies. *Biol. Chem.* **2003**, 384, 845-854.
- (133) Mehtani, S.; Gong, Q.; Panella, J.; Subbiah, S.; Peffley, D. M.; Frankfater, A. In vivo expression of an alternatively spliced human tumor message that encodes a truncated form of cathepsin B. Subcellular distribution of the truncated enzyme in COS cells. *J. Biol. Chem.* **1998**, 273, 13236-13244.
- (134) Baici, A.; Muntener, K.; Willmann, A.; Zwicky, R. Regulation of human cathepsin B by alternative mRNA splicing: homeostasis, fatal errors and cell death. *Biol. Chem.* **2006**, 387, 1017-1021.
- (135) Muntener, K.; Zwicky, R.; Csucs, G.; Rohrer, J.; Baici, A. Exon skipping of cathepsin B: mitochondrial targeting of a lysosomal peptidase provokes cell death. *J. Biol. Chem.* **2004**, 279, 41012-41017.
- (136) Arner, E. S.; Holmgren, A. The thioredoxin system in cancer. *Semin. Cancer Biol.* **2006**, 16, 420-426.
- (137) Powis, G.; Kirkpatrick, D. L. Thioredoxin signaling as a target for cancer therapy. *Curr. Opin. Pharmacol.* **2007**, 7, 392-397.
- (138) Knoblach, B.; Keller, B. O.; Groenendyk, J.; Aldred, S.; Zheng, J.; Lemire, B. D.; Li, L.; Michalak, M. ERp19 and ERp46, new members of the thioredoxin family of endoplasmic reticulum proteins. *Mol. Cell Proteomics.* **2003**, 2, 1104-1119.
- (139) Sullivan, D. C.; Huminiecki, L.; Moore, J. W.; Boyle, J. J.; Poulsom, R.; Creamer, D.; Barker, J.; Bicknell, R. EndoPDI, a novel protein-disulfide isomerase-like protein that is preferentially expressed in endothelial cells acts as a stress survival factor. *J. Biol. Chem.* **2003**, 278, 47079-47088.

- (140) Bruneel, A.; Labas, V.; Mailloux, A.; Sharma, S.; Royer, N.; Vinh, J.; Pernet, P.; Vaubourdolle, M.; Baudin, B. Proteomics of human umbilical vein endothelial cells applied to etoposide-induced apoptosis. *Proteomics*. **2005**, *5*, 3876-3884.
- (141) Wang, Y.; Ma, Y.; Lu, B.; Xu, E.; Huang, Q.; Lai, M. Differential expression of mimecan and thioredoxin domain-containing protein 5 in colorectal adenoma and cancer: a proteomic study. *Exp. Biol. Med. (Maywood.)* **2007**, *232*, 1152-1159.
- (142) Nissom, P. M.; Lo, S. L.; Lo, J. C.; Ong, P. F.; Lim, J. W.; Ou, K.; Liang, R. C.; Seow, T. K.; Chung, M. C. Hcc-2, a novel mammalian ER thioredoxin that is differentially expressed in hepatocellular carcinoma. *FEBS Lett.* **2006**, *580*, 2216-2226.
- (143) Puig, A.; Gilbert, H. F. Protein disulfide isomerase exhibits chaperone and anti-chaperone activity in the oxidative refolding of lysozyme. *J. Biol. Chem.* **1994**, *269*, 7764-7771.
- (144) Ahamed, J.; Versteeg, H. H.; Kerver, M.; Chen, V. M.; Mueller, B. M.; Hogg, P. J.; Ruf, W. Disulfide isomerization switches tissue factor from coagulation to cell signaling. *Proc. Natl. Acad. Sci. U. S. A* **2006**, *103*, 13932-13937.
- (145) Moss, S. E.; Morgan, R. O. The annexins. *Genome Biol.* **2004**, *5*, 219.
- (146) Blackwood, R. A.; Ernst, J. D. Characterization of Ca²⁺(+)-dependent phospholipid binding, vesicle aggregation and membrane fusion by annexins. *Biochem. J.* **1990**, *266*, 195-200.
- (147) Wang, X. M.; Wu, T. X.; Hamza, M.; Ramsay, E. S.; Wahl, S. M.; Dionne, R. A. Rofecoxib modulates multiple gene expression pathways in a clinical model of acute inflammatory pain. *Pain* **2007**, *128*, 136-147.
- (148) Namikawa, K.; Okamoto, T.; Suzuki, A.; Konishi, H.; Kiyama, H. Pancreatitis-associated protein-III is a novel macrophage chemoattractant implicated in nerve regeneration. *J. Neurosci.* **2006**, *26*, 7460-7467.
- (149) Tan, Y. H.; Lee, K. H.; Lin, T.; Sun, Y. C.; Hsieh-Li, H. M.; Juan, H. F.; Wang, Y. C. Cytotoxicity and proteomics analyses of OSU03013 in lung cancer. *Clin. Cancer Res.* **2008**, *14*, 1823-1830.
- (150) Yan, X. D.; Pan, L. Y.; Yuan, Y.; Lang, J. H.; Mao, N. Identification of platinum-resistance associated proteins through proteomic analysis of human ovarian cancer cells and their platinum-resistant sublines. *J. Proteome. Res.* **2007**, *6*, 772-780.
- (151) Park, J. E.; Lee, D. H.; Lee, J. A.; Park, S. G.; Kim, N. S.; Park, B. C.; Cho, S. Annexin A3 is a potential angiogenic mediator. *Biochem. Biophys. Res. Commun.* **2005**, *337*, 1283-1287.
- (152) Mueller, M. M.; Fusenig, N. E. Tumor-stroma interactions directing phenotype and progression of epithelial skin tumor cells. *Differentiation* **2002**, *70*, 486-497.

- (153) Xi, Y.; Riker, A.; Shevde-Samant, L.; Samant, R.; Morris, C.; Gavin, E.; Fodstad, O.; Ju, J. Global comparative gene expression analysis of melanoma patient samples, derived cell lines and corresponding tumor xenografts. *Cancer Genomics Proteomics*. **2008**, *5*, 1-35.
- (154) Raica, M.; Cimpean, A. M.; Ribatti, D. The role of podoplanin in tumor progression and metastasis. *Anticancer Res*. **2008**, *28*, 2997-3006.
- (155) Marie, S. K.; Okamoto, O. K.; Uno, M.; Hasegawa, A. P.; Oba-Shinjo, S. M.; Cohen, T.; Camargo, A. A.; Kosoy, A.; Carlotti, C. G., Jr.; Toledo, S.; Moreira-Filho, C. A.; Zago, M. A.; Simpson, A. J.; Caballero, O. L. Maternal embryonic leucine zipper kinase transcript abundance correlates with malignancy grade in human astrocytomas. *Int. J. Cancer* **2008**, *122*, 807-815.
- (156) Bulk, E.; Sargin, B.; Krug, U.; Hascher, A.; Jun, Y.; Knop, M.; Kerkhoff, C.; Gerke, V.; Liersch, R.; Mesters, R. M.; Hotfilder, M.; Marra, A.; Koschmieder, S.; Dugas, M.; Berdel, W. E.; Serve, H.; Muller-Tidow, C. S100A2 induces metastasis in non-small cell lung cancer. *Clin. Cancer Res*. **2009**, *15*, 22-29.
- (157) Jiang, P. H.; Motoo, Y.; Garcia, S.; Iovanna, J. L.; Pebusque, M. J.; Sawabu, N. Down-expression of tumor protein p53-induced nuclear protein 1 in human gastric cancer. *World J. Gastroenterol*. **2006**, *12*, 691-696.
- (158) Kaneda, A.; Wakazono, K.; Tsukamoto, T.; Watanabe, N.; Yagi, Y.; Tatematsu, M.; Kaminishi, M.; Sugimura, T.; Ushijima, T. Lysyl oxidase is a tumor suppressor gene inactivated by methylation and loss of heterozygosity in human gastric cancers. *Cancer Res*. **2004**, *64*, 6410-6415.
- (159) Lehen'kyi, V.; Flourakis, M.; Skryma, R.; Prevarskaya, N. TRPV6 channel controls prostate cancer cell proliferation via Ca²⁺/NFAT-dependent pathways. *Oncogene* **2007**, *26*, 7380-7385.
- (160) Eckstein, L. A.; Van Quill, K. R.; Bui, S. K.; Uusitalo, M. S.; O'Brien, J. M. Cyclosporin a inhibits calcineurin/nuclear factor of activated T-cells signaling and induces apoptosis in retinoblastoma cells. *Invest Ophthalmol. Vis. Sci*. **2005**, *46*, 782-790.
- (161) Hui, Z.; Tretiakova, M.; Zhang, Z.; Li, Y.; Wang, X.; Zhu, J. X.; Gao, Y.; Mai, W.; Furge, K.; Qian, C. N.; Amato, R.; Butler, E. B.; Teh, B. T.; Teh, B. S. Radiosensitization by inhibiting STAT1 in renal cell carcinoma. *Int. J. Radiat. Oncol. Biol. Phys*. **2009**, *73*, 288-295.
- (162) Efimova, E. V.; Liang, H.; Pitroda, S. P.; Labay, E.; Darga, T. E.; Levina, V.; Lokshin, A.; Roizman, B.; Weichselbaum, R. R.; Khodarev, N. N. Radioresistance of Stat1 over-expressing tumour cells is associated with suppressed apoptotic response to cytotoxic agents and increased IL6-IL8 signalling. *Int. J. Radiat. Biol*. **2009**, *85*, 421-431.
- (163) Hebenstreit, D.; Horejs-Hoeck, J.; Duschl, A. JAK/STAT-dependent gene regulation by cytokines. *Drug News Perspect*. **2005**, *18*, 243-249.
- (164) Nair, J. S.; DaFonseca, C. J.; Tjernberg, A.; Sun, W.; Darnell, J. E., Jr.; Chait, B. T.; Zhang, J. J. Requirement of Ca²⁺ and CaMKII for Stat1 Ser-727

- phosphorylation in response to IFN-gamma. *Proc. Natl. Acad. Sci. U. S. A* **2002**, 99, 5971-5976.
- (165) Rosales, J. L.; Ernst, J. D. Calcium-dependent neutrophil secretion: characterization and regulation by annexins. *J. Immunol.* **1997**, 159, 6195-6202.
- (166) Morris, A. G. Interferons. *Immunol. Suppl* **1988**, 1, 43-45.
- (167) Wadehra, M.; Forbes, A.; Pushkarna, N.; Goodglick, L.; Gordon, L. K.; Williams, C. J.; Braun, J. Epithelial membrane protein-2 regulates surface expression of alphavbeta3 integrin in the endometrium. *Dev. Biol.* **2005**, 287, 336-345.
- (168) Wadehra, M.; Natarajan, S.; Seligson, D. B.; Williams, C. J.; Hummer, A. J.; Hedvat, C.; Braun, J.; Soslow, R. A. Expression of epithelial membrane protein-2 is associated with endometrial adenocarcinoma of unfavorable outcome. *Cancer* **2006**, 107, 90-98.
- (169) Shimazaki, K.; Chan, A. M.; Moniz, R. J.; Wadehra, M.; Nagy, A.; Coulam, C. P.; Mareninov, S.; Lepin, E. M.; Wu, A. M.; Kelly, K. A.; Braun, J.; Gordon, L. K. Blockade of epithelial membrane protein 2 (EMP2) abrogates infection of *Chlamydia muridarum* murine genital infection model. *FEMS Immunol. Med. Microbiol.* **2009**, 55, 240-249.
- (170) Govinden, R.; Bhoola, K. D. Genealogy, expression, and cellular function of transforming growth factor-beta. *Pharmacol. Ther.* **2003**, 98, 257-265.
- (171) Solimando, D. A. Overview of hypercalcemia of malignancy. *Am. J. Health Syst. Pharm.* **2001**, 58 Suppl 3, S4-S7.
- (172) Lu, T.; Burdelya, L. G.; Swiatkowski, S. M.; Boiko, A. D.; Howe, P. H.; Stark, G. R.; Gudkov, A. V. Secreted transforming growth factor beta2 activates NF-kappaB, blocks apoptosis, and is essential for the survival of some tumor cells. *Proc. Natl. Acad. Sci. U. S. A* **2004**, 101, 7112-7117.
- (173) Starke, A.; Wuthrich, R. P.; Waeckerle-Men, Y. TGF-beta treatment modulates PD-L1 and CD40 expression in proximal renal tubular epithelial cells and enhances CD8 cytotoxic T-cell responses. *Nephron Exp. Nephrol.* **2007**, 107, e22-e29.
- (174) Dong, H.; Zhu, G.; Tamada, K.; Chen, L. B7-H1, a third member of the B7 family, co-stimulates T-cell proliferation and interleukin-10 secretion. *Nat. Med.* **1999**, 5, 1365-1369.
- (175) Okazaki, T.; Honjo, T. PD-1 and PD-1 ligands: from discovery to clinical application. *Int. Immunol.* **2007**, 19, 813-824.
- (176) Routh, J. C.; Ashley, R. A.; Sebo, T. J.; Lohse, C. M.; Husmann, D. A.; Kramer, S. A.; Kwon, E. D. B7-H1 expression in Wilms tumor: correlation with tumor biology and disease recurrence. *J. Urol.* **2008**, 179, 1954-1959.

- (177) Stehlik, C.; Kroismayr, R.; Dorfleutner, A.; Binder, B. R.; Lipp, J. VIGR--a novel inducible adhesion family G-protein coupled receptor in endothelial cells. *FEBS Lett.* **2004**, 569, 149-155.
- (178) Wisniewski, H. G.; Vilcek, J. TSG-6: an IL-1/TNF-inducible protein with anti-inflammatory activity. *Cytokine Growth Factor Rev.* **1997**, 8, 143-156.
- (179) Mindrescu, C.; Le, J.; Wisniewski, H. G.; Vilcek, J. Up-regulation of cyclooxygenase-2 expression by TSG-6 protein in macrophage cell line. *Biochem. Biophys. Res. Commun.* **2005**, 330, 737-745.
- (180) Tsukahara, S.; Ikeda, R.; Goto, S.; Yoshida, K.; Mitsumori, R.; Sakamoto, Y.; Tajima, A.; Yokoyama, T.; Toh, S.; Furukawa, K.; Inoue, I. Tumour necrosis factor alpha-stimulated gene-6 inhibits osteoblastic differentiation of human mesenchymal stem cells induced by osteogenic differentiation medium and BMP-2. *Biochem. J.* **2006**, 398, 595-603.
- (181) Liggins, A. P.; Brown, P. J.; Asker, K.; Pulford, K.; Banham, A. H. A novel diffuse large B-cell lymphoma-associated cancer testis antigen encoding a PAS domain protein. *Br. J. Cancer* **2004**, 91, 141-149.
- (182) Herr, P.; Korniyuchuk, G.; Yamamoto, Y.; Grubisic, K.; Oelgeschlager, M. Regulation of TGF-(beta) signalling by N-acetylgalactosaminyltransferase-like 1. *Development* **2008**, 135, 1813-1822.
- (183) Miyazaki, H.; Watabe, T.; Kitamura, T.; Miyazono, K. BMP signals inhibit proliferation and in vivo tumor growth of androgen-insensitive prostate carcinoma cells. *Oncogene* **2004**, 23, 9326-9335.
- (184) Mou, Z.; Tapper, A. R.; Gardner, P. D. The Armadillo Repeat-containing Protein, ARMCX3, Physically and Functionally Interacts with the Developmental Regulatory Factor Sox10. *J. Biol. Chem.* **2009**, 284, 13629-13640.
- (185) Matsui, M.; Araki, Y.; Karasawa, H.; Matsubara, N.; Taketo, M. M.; Seldin, M. F. Mapping of five subtype genes for muscarinic acetylcholine receptor to mouse chromosomes. *Genes Genet. Syst.* **1999**, 74, 15-21.
- (186) Lei, Q.; Jones, M. B.; Talley, E. M.; Garrison, J. C.; Bayliss, D. A. Molecular mechanisms mediating inhibition of G protein-coupled inwardly-rectifying K⁺ channels. *Mol. Cells* **2003**, 15, 1-9.
- (187) Locklin, R. M.; Riggs, B. L.; Hicok, K. C.; Horton, H. F.; Byrne, M. C.; Khosla, S. Assessment of gene regulation by bone morphogenetic protein 2 in human marrow stromal cells using gene array technology. *J. Bone Miner. Res.* **2001**, 16, 2192-2204.
- (188) von Bubnoff, A.; Cho, K. W. Intracellular BMP signaling regulation in vertebrates: pathway or network? *Dev. Biol.* **2001**, 239, 1-14.
- (189) Sarkar, S. N.; Sen, G. C. Novel functions of proteins encoded by viral stress-inducible genes. *Pharmacol. Ther.* **2004**, 103, 245-259.

- (190) Justesen, J.; Hartmann, R.; Kjeldgaard, N. O. Gene structure and function of the 2'-5'-oligoadenylate synthetase family. *Cell Mol. Life Sci.* **2000**, *57*, 1593-1612.
- (191) Numajiri, A.; Mibayashi, M.; Nagata, K. Stimulus-dependent and domain-dependent cell death acceleration by an IFN-inducible protein, human MxA. *J. Interferon Cytokine Res.* **2006**, *26*, 214-219.
- (192) Meroni, G.; Diez-Roux, G. TRIM/RBCC, a novel class of 'single protein RING finger' E3 ubiquitin ligases. *Bioessays* **2005**, *27*, 1147-1157.
- (193) Pfaffenbach, G. M.; Uehara, H.; Geliebter, J.; Nathenson, S. G.; Schulze, D. H. Analysis of the H-2Kbm8 mutant: correlation of structure with function. *Mol. Immunol.* **1991**, *28*, 697-701.
- (194) Kong, D.; Wang, Z.; Sarkar, S. H.; Li, Y.; Banerjee, S.; Saliganan, A.; Kim, H. R.; Cher, M. L.; Sarkar, F. H. Platelet-derived growth factor-D overexpression contributes to epithelial-mesenchymal transition of PC3 prostate cancer cells. *Stem Cells* **2008**, *26*, 1425-1435.
- (195) Prevarskaya, N.; Skryma, R.; Shuba, Y. Ca²⁺ homeostasis in apoptotic resistance of prostate cancer cells. *Biochem. Biophys. Res. Commun.* **2004**, *322*, 1326-1335.
- (196) Roznovanu, S. L.; Amalinci, C.; Radulescu, D. Molecular mechanisms in hormone-resistant prostate cancer. *Rev. Med. Chir Soc. Med. Nat. Iasi* **2005**, *109*, 577-583.
- (197) Patterson, S. G.; Wei, S.; Chen, X.; Sallman, D. A.; Gilvary, D. L.; Zhong, B.; Pow-Sang, J.; Yeatman, T.; Djeu, J. Y. Novel role of Stat1 in the development of docetaxel resistance in prostate tumor cells. *Oncogene* **2006**, *25*, 6113-6122.
- (198) Niknami, M.; Patel, M.; Witting, P. K.; Dong, Q. Molecules in focus: cytosolic phospholipase A2-alpha. *Int. J. Biochem. Cell Biol.* **2009**, *41*, 994-997.
- (199) Yang, L.; Moses, H. L. Transforming growth factor beta: tumor suppressor or promoter? Are host immune cells the answer? *Cancer Res.* **2008**, *68*, 9107-9111.
- (200) Gonzalez-Gronow, M.; Gawdi, G.; Pizzo, S. V. Tissue factor is the receptor for plasminogen type 1 on 1-LN human prostate cancer cells. *Blood* **2002**, *99*, 4562-4567.
- (201) Milsom, C.; Rak, J. Tissue factor and cancer. *Pathophysiol. Haemost. Thromb.* **2008**, *36*, 160-176.
- (202) Bogdanov, V. Y.; Kirk, R. I.; Miller, C.; Hathcock, J. J.; Vele, S.; Gazdoiu, M.; Nemerson, Y.; Taubman, M. B. Identification and characterization of murine alternatively spliced tissue factor. *J. Thromb. Haemost.* **2006**, *4*, 158-167.

-
- (203) Chand, H. S.; Ness, S. A.; Kisiel, W. Identification of a novel human tissue factor splice variant that is upregulated in tumor cells. *Int. J. Cancer* **2006**, 118, 1713-1720.
- (204) Chand, H. S.; Kisiel, W. Quantitative real-time reverse transcription polymerase chain reaction analysis of a novel tissue factor splice variant in select human solid tumors. *J. Thromb. Haemost.* **2007**, 5, 640-641.
- (205) O'Connor, R. A review of mechanisms of circumvention and modulation of chemotherapeutic drug resistance. *Curr. Cancer Drug Targets.* **2009**, 9, 273-280.
- (206) Loges, S.; Mazzone, M.; Hohensinner, P.; Carmeliet, P. Silencing or fueling metastasis with VEGF inhibitors: antiangiogenesis revisited. *Cancer Cell* **2009**, 15, 167-170.

8. Acknowledgements

The best and worst moments of my thesis have been shared with many people and I would like to thank all of them for their particular contribution to this work.

Especially, I would like to thank all my colleagues for the great working atmosphere during the last three years. Lots of fun, helpful discussions, 24/7 assistance and open ears for frustrations as well as cheerful afterwork and holiday events on and of the campus made this time unforgettable for me. Without your input this work would not have been possible.

Foremost I would like to thank Prof. Dr. Ernst Wagner for scientific and financial support to realize this work and for providing me the opportunity to improve my professional skills under his supervision. I would like to thank for helpful discussions and for giving me the chance to broaden my horizon during a guest research stay in Prof. Maitland's laboratory and by attending international meetings.

Special thanks go to Prof. Dr. Carsten Culmsee and Dr. Michael Guenther my two direct supervisors. I would like to thank Carsten for providing me a great start-up help with his traditional Monday morning meetings (even if the time point was a challenge every week) and his always open door. Thank you for your guidance with my first project plans, presentations, posters, master student supervision and my first publication as well as for introduction into your scientific network. In the same breath I would like to thank Michael for his support during the second part of my thesis and during the finale countdown. Thank you for all your creative ideas when projects got stuck, for great team work in "murder projects", for breakfast after sleepless nights at the FACS machine, and for continuation of the "Spitzenforschungsgruppe". Furthermore I owe you my life which I would have lost otherwise in the left-hand traffic of York. Finally, lots of fruitful discussions with you during the last months only enabled this work in its actual version.

Initial helpful skill adaption training and introduction into the colon cancer project made thing a lot easier in the beginning. Therefore I would like to thank Dr. Lars Gaedtke, who introduced me into the subject of 3D cell culture and who provided a lot of preliminary work on colon cancer chemoresistance and proteomics of 3D culture of low passage colon cancer cells.

A big thank you goes to all technicians Anna Kulinyak, Markus Kovac, Melinda Kiss, Miriam Höhn, Ursula Biebl and Wolfgang Roedl, who are all part of the fantastic

“Brownie-Team” which keeps things running in the lab and make life so much easier. My special thanks go to Miriam for the great collaboration during the last years. How would I have met any deadline without you, performing the most perfect last minute experiments I have ever seen? What would I have done without your “magic blotting fingers” and your dry sense of humor? Thank you Ursula, for being my best substitute mom providing me with the best cakes, great lunch meals, afternoon SOS-chocolate and aspirin whenever needed and for your bright “good morning” every day, which was the best start into a new working day I could imagine. This work would have still been stuck between broken lab chairs, balances, scanners etc. without Wolfgang, the “rescue-rödl”. I would have never received any of my late parcels without Markus and I do not know what I will do with runs in my tight in the future without Anna’s perfect tight patching skills. I will not forget Melidas fantastic curd cheese with fruits, the highlights of Friday morning meetings.

In addition I would like to thank Dr. Martina Rüffer for her help with the organization of student courses and exams as well as for being the head of the coffee kitty.

Good collaborations are of huge value and I would like to express my gratitude to my collaboration partners from LAFUGA at this point. Dr. Georg Arnold, Dr. Thomas Fröhlich and Roman Kashirin from the proteomics facility as well as Dr. Helmut Blum, Dr. Stefan Krebs and Andrea Klanner all contributed to this work and had always an open ear for questions.

I would like to thank Alexander Philipp for helping with siRNA experiments as well as Dr. Andreas Roidl for his help with the Spotfire software.

How to write a thesis without being cheered up by jokes and procrastination conversations with the best entertaining “Karawanken-Bär”. Fortunately lab life was a lot more than sitting at the bench and I like to thank all people you did their contribution to that. Thank you Omis and Caro for diverse “Mädelsabende”, mountain excursions and for “kidnapping me to the serail” during the writing! Special thanks also go to Clemens, who shared with me the first year of “beginners” including bureaucratic hurdles, first practical courses, cell culture service Friday afternoon hours as well as cheerfull lunch and coffee breaks. I would like to thank Stefan for havin much fun at work and during biochemical student courses as well as for his organization of Wies’n tables even after he left the group. Furtheron, I would like to thank Nicole and Gelja, my salad and fitness team, who motivated me for running many times. As an “inbetweener” I would like to thank the old team for still keeping

contact even over the ocean (Alenka, Verena, Clemens) as well as the “new team” (Kevin, Christian M., Christian D., Arzu, Edith, Thomas, David) for integrating me, the “oldie”, into their friday afternoon sessions and I will not forget Terese’s fantastic Swedish muffins.

However life was much more than just science and would like to thank all my other friends for their support and distraction. I would like express my biggest thanks to Dodo, my and Dodo’s family, who supported me with their love and faith which gave me the power to accomplish this work. Especially I would like to thank Dodo for giving me unfailing support with everything.

9. Curriculum Vitae

Personal data

Date of birth: 23.07.1980
Place of birth: Starnberg, Germany

Education

03/2006-to present Ph.D., Pharmaceutical Biotechnology, Ludwig-Maximilians-Universität, Munich, Germany, supervisor Prof. Dr. Ernst Wagner

10/2005 M.Sc. degree in Molecular Biotechnology, Technische Universität, Munich, Germany

03/2005-08/2005 Master thesis: "Peptide targeted gene delivery to tumor cells and tumor vasculature", Pharmaceutical Biotechnology, Ludwig-Maximilians-Universität, Munich, Germany, supervisor Prof. Dr. Ernst Wagner

10/2003-10/2005 Master of Molecular Biotechnology, Technische Universität, Munich, Germany

09/2003-02/2004 Erasmus fellowship (Maîtrise de Biochemistry, Université de Montpellier II, France)

10/2000- 07/2003 Bachelor of Molecular Biotechnology, Technische Universität, Munich, Germany

08/2001-09/2001 Studies of Spanish at the Instituto Cervantes, Salamanca, Spain

06/2000 Graduation (Abitur), Kurt-Huber-Gymnasium Gräfelfing, Germany

Vocational Training

02/2008-03/2008 guest research stay at the laboratory of Prof. Maitland, York, Great Britain

08/2002-09/2002 Internship at TopLab GmbH, Martinsried, Germany

03/2001-04/2001 Internship at Rubikon AG, Munich, Germany

07/2000-08/2000 Internship at snDiagnostics GmbH, Munich, Germany